UNUSUAL ISOMERIZATION BEHAVIOR OF ORGANIC SOLUTES

AT THE AQUEOUS-SILICA INTERFACE

by

Grace Elizabeth Purnell

A dissertation submitted in partial fulfillment
of the requirements for the degree

of

Doctor of Philosophy

in

Chemistry

MONTANA STATE UNIVERSITY
Bozeman, Montana

November 2019

DEDICATION

This thesis is dedicated to my family. To my parents for putting up with my endless questions and to my sisters for being my first and favorite friends. And to Addie-dog—thanks for keeping me alive and laughing as I did the work for this thesis. I love you.

ACKNOWLEDGEMENTS

The work in this thesis would not have been possible without the advice and support of my advisor, Dr. Robert Walker. He embodies everything I needed in an advisor for my graduate research and I am so grateful for his kind and gracious approach to leading his students. I wouldn't be here without his support. I also want to thank my graduate committee: Dr. Erik Grumstrup, Dr. Mary Cloninger, Dr. Tim Minton and Dr. Patrik Callis. I'm so grateful for their assistance with research questions and their guidance throughout my graduate career.

I also want to thank the members of the Walker Research Group—past and present. In particular, I want to thank Dr. Katie Link for 5 years of excellent conversations about science and otherwise. She was crucial in filling in the gaps in my knowledge and without her perspective I wouldn't be the scientist I am today.

I'm also grateful to the people who helped me get to grad school and encouraged me when making that choice. Particularly, I want to acknowledge my undergraduate advisor Dr. Elizabeth Harbron. Her love of science and molecules that turn colors was my first glimpse that this future was possible. Her consistent and kind advice during my years in her research group, both professional and personal, was instrumental in helping me survive the struggles of my undergraduate years.

TABLE OF CONTENTS

TABLE OF CONTENTS CONTINUED

TABLE OF CONTENTS CONTINUED

LIST OF TABLES

LIST OF FIGURES

LIST OF FIGURES CONTINUED

LIST OF FIGURES CONTINUED

ABSTRACT

Experiments described in this thesis address the question of how strong association between water molecules and the silica surface alter the solvation and isomerization behavior of adsorbed organic molecules from bulk solution limits. The work was motivated by the hypothesis that the ice-like structure induced by strong hydrogen bonding with the surface silanol groups would restrict solute isomerization. This hypothesis was tested using 2 surface-specific spectroscopic techniques: second harmonic generation (SHG) and time-correlated single photon counting in a total internal reflection geometry (TIR-TCSPC). This work examined two different 7-aminocoumarin dyes (Coumarin 151 and Coumarin 152) and dimethylaminobenzonitrile (DMABN). Coumarin 152 and DMABN both isomerize to form a twisted intramolecular charge transfer (TICT) state upon photoexcitation, whereas Coumarin 151 forms a simple (planar) intramolecular charge transfer state. SHG studies characterized the local solvation environment surrounding adsorbed molecules by providing electronic excitation energies that were compared to bulk excitation energies in different representative solvents. TIR-TCSPC measured the time-resolved emission of adsorbed molecules and quantified a solute's tendency to form TICT (or ICT) isomers at the aqueous-silica interface. Together, SHG and TIR-TCSPC provide a cohesive description of the local polarity across an aqueous-silica interface and how restricted solvent dynamics change a solute's photophysical chemistry.

TIR-TCSPC studies reported that both C152 and DMABN are unable to isomerize to TICT states at the aqueous-silica interface, acting as if they were solvated in a nonpolar solvent or in a confined geometry. SHG studies confirm that the aqueous-silica interface is, in fact, more polar than the bulk aqueous limit, strongly implying that the observed effects are dynamic in origin rather than polarity driven. In contrast, studies of C151 show that this solute is largely insensitive to anisotropic, restrictive surface effects. Together results from these three molecules lead us to conclude that adsorption to the strongly associating aqueous-silica interface restricts large amplitude isomerization in organic molecules. Adsorption to less strongly associating interfaces does not cause this restriction. In the event that photo-induced isomerization *does not* require large amplitude motion, interfacial solvation has little effect on adsorbed solute behavior.

CHAPTER ONE

INTRODUCTION

1.1 Motivation

Every source of reflected light is a surface that creates a distinctive, anisotropic environment where molecular organization and reactivity differ from bulk limits. The unique environment at interfaces is responsible for changing properties such as solvent polarity,[1-4] solvent viscosity,[5-7] and solute adsorption[8-9] dramatically from their bulk solution limits. Because solvent structure and properties are so different at interfaces relative to the isotropic bulk, interfaces can facilitate a variety of chemical reactions and rearrangements. Simple chemical substitutions and additions, such as the Diels-Alder reaction, can see a rate increase by as much as five orders of magnitude at the interface.[10-12] Solvent properties induced by the interface are also responsible for enhancing structural rearrangements,[13-16] mediating biological recognition processes,[17-20] enabling photocatalysis,[21-22] and even allowing reactions to occur that are not possible in bulk solution.[23]

Despite the knowledge that the interfacial solvation properties differ so significantly from the bulk and are enormously consequential for a variety of chemical processes, buried interfaces between a solid and a liquid or two immiscible liquids have proven quite difficult to study. Even when the properties of both bulk phases composing the interface are known, anticipating surface effects on interfacial structure and organization is not trivial. At the surface, a variety of competing factors including the

affintiy of the solute, solvent and surface for each other, the energetics of adsorption and the hydrogen bonding ability or the surface and solvent will determine the final structure of interfacial solvent layers as well as that of adsorbed solutes.

For example, at the strongly associating silica-alcohol interface, strong hydrogen bonding between surface silanols and the solvent alcohol group creates a layer with a nonpolar solvation environment due to the arrangement of the solvent alkyl tails in an ordered monolayer adjacent to the interface.[7, 24-26] Silica surfaces affect nitrile solvent adsorption similarly, but with opposite effects on interfacial polarity. Acetonitrile at the silica interface forms a bilayer-like structure that repeats, extending as much as 4 nm into the surrounding bulk liquid. In contrast to methanol and similar alcohols, however, this creates a solvation environment even more polar than the bulk solvent alone.[27]

It is worth an interlude here to specify what is meant when polarity and the bulk static dielectric constant are discussed in this thesis. Polarity is a qualitative descriptor of the extent of dielectric polarization in a material, where the bulk static dielectric constant is a descriptor of the average degree of dielectric polarization in a bulk dielectric material. The dielectric constant is not constant under the influence of an external electric field, as is true in all of the experiments discussed in this thesis. In this case, the frequency-dependent dielectric function is given by:

$$\varepsilon = 1 + \frac{Ne^2}{\varepsilon_0 m} \sum \frac{f_i}{\omega_{i0}^2 - \omega^2 - i\omega\gamma_i} \qquad (1.1)$$

Additionally, the dielectric function of water is complicated by its significant hydrogen bonding network holding neighboring molecules together. It has been shown that the influence of this hydrogen bonding network is to increase the static dielectric constant of

liquid water.[28] The experiments described in this thesis describe the importance of the hydrogen bonding network formed between water molecules and the adjacent silica surface, as well as the molecular response to the dielectric environment of this interface. However, from this point forward, I will only refer to the "bulk static dielectic constant", which for bulk water is known to be $\varepsilon=80$, and disregard the possible effects of the frequency depenence of the dielectric function.

Silica-solvent interfaces have been the subject of intense study and scientific debate, and few buried interfaces have received more attention than the silica-aqueous interface. 71% of the Earth's surface is water, and 59% of the solid crust is made up of silica, or silicon dioxide (SiO_2). Together, these statistics mean that approximately 42% of the planet's surface is an aqueous-silica interface. Additionally, fused silica glassware and the use of silica gel chromatography columns mean that solute behavior at silica-liquid interfaces has important consequences for many areas of chemical functionality. Despite the ubiquity of this interface and its importance in a variety of fields, almost none of the work studying this interface has looked at anything other than the structure of the surface-associated water molecules. While understanding this interfacial structure is certainly important, understanding how surface-altered solvent structure and organization change the solvation properties of water is more important. In this context, solvation describes the noncovalent interactions that a solute experiences with its surroundings, and these solvation properties will control solute orientation, conformation and reactivity. Water's unique hydrogen bonding ability makes it nature's solvent of choice; since surfaces can affect solvation properties, sometimes in nonintuitive ways, understanding

how the solvation properties of interfacial water differ from those in bulk solution is critical for understanding solution phase surface chemistry.

Work described in this thesis examined how surface induced changes at the aqueous-silica interface dramatically altered the isomerization tendencies of adsorbed solutes. Specifically, time-resolved emission and resonance enhanced second harmonic generation (SHG) were used to measure whether or not solutes known to isomerize in bulk aqueous solution isomerized in the same manner when adsorbed to the aqueous-silica interface *and* to characterize the local solvation environment sampled by the adsorbed solutes. Results show that while the silica-aqueous interface is polar, molecules with large amplitdue excited state isomerizations experience a solvation environment that cannot stabilize this isomerization, leading to spectroscopic results that make the interface appear nonpolar.

1.2 Techniques

Buried interfaces are difficult to study because any response from molecules at the surface is overwhelmed by that from those in the adjacent bulk solution. Thus, in order to see signal from surface molecules experimental methods must be able to discriminate signals arising from the bulk molecules from those coming from surface species.

1.2.1 TIR-TCSPC

Total internal reflection (TIR) spectroscopy is one of the most common methods used to study surface chemistry. TIR geometries can be used for most optical

spectroscopy techniques including fluorescence, infrared absorption, and Raman

scattering by exploiting the total internal reflection that occurs when a light propagating

through a medium with a higher refractive index reflects off of a surface at an angle

greater than the critical angle. When light is incident on such an interface at an angle

greater than its critical angle, all of the light will be reflected back on itself, rather than

propagating along the path of its incident vector.[29] This property derives from Snell's law

for the reflection of light that states:

$$n_1 \sin \theta_1 = n_2 \sin \theta_2 \qquad (1.2)$$

where n_1 and n_2 are the refractive indices for the materials at the interface and θ_1 and θ_2

are the angles of incidence and transmission of the light beam incident on the surface. In

order to create a TIR condition, n_1 must be greater than n_2. In this case, we can solve for

the critical angle by setting:

$$\sin \theta_1 = \frac{n_2}{n_1} \sin \theta_2 \qquad (1.3)$$

As the angle of reflection, θ_2, reaches 90°, $\sin \theta_2 = 1$, and we solve for the critical angle,

θ_c:[30]

$$\sin \theta_c = \frac{n_2}{n_1} \qquad (1.4)$$

While TIR spectroscopy is selectively sensitive to surface species, TIR techniques

are not *uniquely* surface sensitive. Even at angles above the critical angle, light

impinging on a surface creates a local electric field, also known as an evanescent wave,

propagates into the adjacent medium with its field strength decaying exponentially as a

function of distance.[31] Depending on the system's critical angle and the wavelength of the

incident light, the evanescent wave in a TIR geometry will propagate into the adjacent

bulk material ~50-500 nm. Although this condition does not confer absolute surface specificity to any TIR technique, any experiment carried out under total internal reflection conditions will necessarily be more sensitive to surface species than any bulk measurement. This sensitivity is enhanced further if TIR methods are being used to study surface active species.

In the experiments described in this work, I have coupled a TIR experimental geometry with a time-resolved fluorescence technique known as time-correlated single photon counting (TCSPC). TCSPC experiments use an ultrafast laser pulse to excite a material, and then count the fluorescent photons that are emitted as a function of time after excitation. This procedure creates a histogram of photons per unit time which can be fit to a sum of exponential decays (equation 1.4) to determine the fluorescence lifetimes of the molecules being excited:

$$I(t) = \sum_{i=1}^{n} A_i e^{\frac{-t}{\tau_i}} \tag{1.5}$$

where A_i is the amplitude of the ith fluorescent lifetime, t is time since excitation and τ_i is the ith fluorescent lifetime. Fitting parameters are optimized with a least squares fit. Knowledge of the fluorescence lifetimes of a molecule gives information about that molecule's environment and photophysical properties.[32]

To perform the TCSPC experiments described in this work, a Coherent Chameleon mode-locked, tunable Ti:sapphire oscillator with a wavelength range of 680-1080 nm and an 80 MHz repetition rate and ~2W average power was coupled to an APE autotracker to convert the fundamental beam into the necessary wavelength using either a second or third harmonic crystal. The second harmonic output was in the range of 350-

520 nm and the third harmonic output was between 230-350 nm, with 50-200 mW power

dependent on wavelength. The beam out of the autotracker was sent into an optoacoustic

modulator (Conoptics Model 350) to reduce the repetition rate from 80 to 4 MHz.

Fluorescent photons were collected with a Picoquant PicoHarp 300 detector with a

FluoTime 200 software interface.
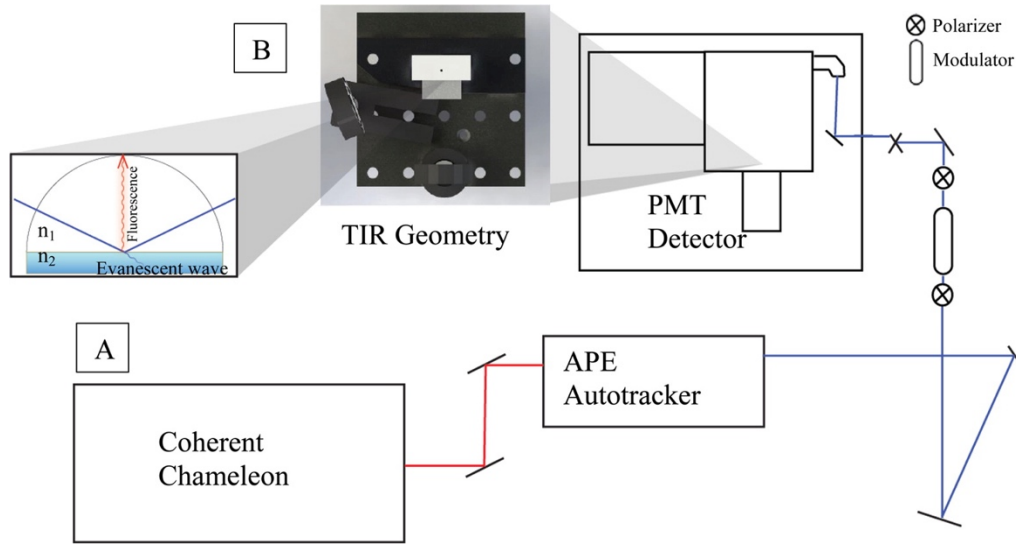
Figure 1.1: Experimental geometry of the TCSPC instrument

1.2.2 Second Harmonic Generation

      The second technique used in the experiments in this work is resonance enhanced

second harmonic generation or SHG spectroscopy. As a second order nonlinear optical

spectroscopy, SHG is inherently surface specific.

      Nonlinear optical effects were first reported in 1961, soon after the discovery of

the first ruby laser.[33] The effects were explained by expanding the expression for the

linear optical polarization, $P(t) = \varepsilon_0 \chi^{(1)} E(t)$, in a power series in electric field strength,

as linear polarization could no longer account for the consequences of illumination with intense, coherent optical radiation, like a laser:

$$P(t) = \varepsilon_0 \left[\chi^{(1)} E(t) + \chi^{(2)} E(t)^2 + \chi^{(3)} E(t)^3 + \cdots \right] \tag{1.6}$$

The second order nonlinear optical polarization, $P^{(2)}$, is the origin of second order nonlinear optical effects, and from the expansion above is equal to the second order nonlinear optical susceptibility times the incident electric field squared: $P^{(2)}(t) = \varepsilon_0 \chi^{(2)} E(t)^2$. The second order nonlinear optical susceptibility, $\chi^{(2)}$, is a third rank tensor so by definition, $\chi^{(2)}_{ijk} = -\chi^{(2)}_{-i-j-k}$, a statement which can only be true in a spatially isotropic material if $\chi^{(2)} = 0$. Thus, the only systems which will have a nonzero second order nonlinear optical susceptibility are those with an inherent anisotropy, such as interfaces. This property of $\chi^{(2)}$ enables detection of signal from molecules at intrinsically anisotropic interfaces to the exclusion of signal arising from the adjacent centrosymmetric bulk materials.

When two laser beams having different frequencies (i.e. $E(t) = E_1 e^{-i\omega_1 t} + E_2 e^{-i\omega_2 t} + c.c$) are incident on a medium with a non-zero nonlinear susceptibility, substitution into the expression for the second order nonlinear polarization, assuming real-valued field amplitudes (i.e. $E_1 E_1^* = E_1^2$), gives:

$$P^{(2)}(t) = \varepsilon_0 \chi^{(2)} \left[\left(E_1^2 e^{-i(2\omega_1)t} + E_2^2 e^{-i(2\omega_2)t} + c.c. \right) + 2E_1 E_2 \left(e^{-i(\omega_1+\omega_2)t} + \right.\right.$$

$$\left.\left. e^{-i(\omega_1-\omega_2)t} + c.c. \right) + 2(E_1^2 + E_2^2) \right] \tag{1.7}$$

The frequency components in the equation above comprise the signals from 3 different second order nonlinear optical techniques: SHG, sum frequency generation (SFG) and

difference frequency generation (DFG). The static electric fields produced are another second order nonlinear polarization effect known as optical rectification.[34-35]

Of these second order optical nonlinear effects, two are the most useful for interface spectroscopy: second harmonic generation and sum frequency generation. Second harmonic generation spectroscopy (SHG) uses two incident photons of frequency ω to generate a single resultant second harmonic (SH) photon of frequency 2ω, and is typically performed with incident photons in the visible region, generating photons in the ultraviolet. When either the incident or the generated second harmonic light is resonant with an electronic transition of the interfacial molecules, the SH signal experiences a large resonant enhancement, making SHG well-suited to study the electronic structure of interfacial molecules and materials.

Sum frequency generation (SFG) is similar in principle to SHG. In SFG, 2 photons of frequencies ω_1 and ω_2 combine to give a single photon of frequency ω_3, where $\omega_3 = \omega_1 + \omega_2$. A typical SFG experiment uses incident beams in the visible and infrared (IR) regions to generate a sum frequency (SF) photon. When the IR frequency is resonant with a vibrational transition of the interfacial molecules, enhancement of the SF signal will occur, allowing detailed structural information about the interfacial molecules to be gathered. SFG requires that 2 pulsed laser beams overlap at the sample in both time and space, as well as necessitating that at least one medium making up the interface be transparent to both visible and IR light. These technical constraints limit the utility of SFG when studying buried interfaces. As the experiments in this thesis were interested exclusively in the buried silica-aqueous interface, and SHG provides a complementary

electronic spectroscopy technique to fluorescence, SHG was used preferentially to vibrational SFG.

Not only is $\chi^{(2)}$ surface specific due to its behavior with respect to inversion, elements in the $\chi^{(2)}$ tensor are also molecularly specific. The $\chi^{(2)}$ tensor has 2 components, a resonant (R) and a nonresonant (NR) piece:

$$\chi^{(2)} = \chi_{NR}^{(2)} + \chi_R^{(2)} \tag{1.8}$$

The nonresonant part of this tensor in the experiments described in this thesis was simple and could be fit to a constant. The resonant portion of $\chi^{(2)}$ is the orientational average over the molecular hyperpolarizability multiplied by the total number of surface molecules:

$$\chi_R^{(2)} = N\langle\beta_{i,j,k}\rangle \tag{1.9}$$

where β is given by: $\beta = \frac{A}{\omega_0 - \omega - i\Gamma}$. In this equation, A is a constant related to the one- and two-photon absorption resonances of the surface molecules,[36] ω_0 is the resonant frequency of the transition, ω is the frequency of the incident light, and Γ is the linewidth associated with the transition. When collecting SHG spectra, the data is fit with equations 1.8 and 1.9 in order to determine the linewidth and central wavelength of the resonance.

In order to collect SHG spectra, a Coherent Libra-HE Ti:sapphire chirped pulse regenerative amplifier (1 kHz repetition rate, 3.3 W average power, 801 nm, 85 fs pulses) was used, coupled to an optical parametric amplifier (Coherent OPerA Solo, FWHM 10 nm) to create the wavelengths needed to perform SHG experiments. If necessary, neutral density filters were used to reduce the intensity of the light to less than 4 mW. The beam from the OPA was focused on the sample, then the fundamental beam was filtered out of

the reflected light and the SH photons were collected by a photomultiplier tube (PMT), coupled to a monochrometer to discriminate the relevant wavelengths.
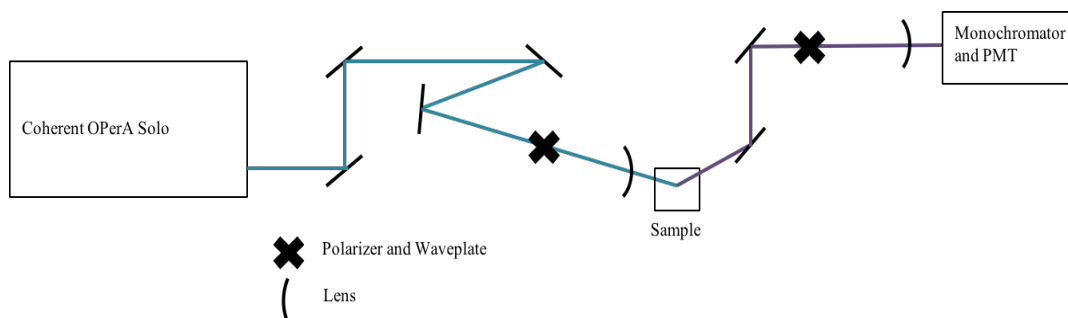
Figure 1.2: Experimental geometry of the SHG instrument

1.3 Description of the Aqueous-Silica Interface

In 1994, the first spectroscopic description of the structure of the aqueous-silica interface was published by Ron Shen's group at Berkeley. This description was based on SFG experiments that probed the OH stretches of interfacial water molecules.[37] This study reported 2 prominent peaks in the SFG spectrum of the aqueous-silica interface: one at 3200 cm^{-1}, which corresponds to the coupled OH stretch of a tetrahedrally coordinated water molecule, indicating ordered (ice-like) water molecules, and one at 3400 cm^{-1}, which is an asymmetric stretch whose intensity correlates with the degree of disorder in the water layers. The relative intensities of these two peaks can give a rough approximation of ordering in the water molecules being studied. The 1994 study concluded that at all pH values, interfacial water layers at the silica surface have bonds that correspond to both ordered and disordered water structures. This result was consistent with findings from molecular dynamics simulations available at the time.[38]

As more accurate and specific surface spectroscopy methods became available

and the ability to analyze complex spectroscopic data became routine, there were several

groups that disagreed with Shen's original assignment of the silica-aqueous spectrum to

bulk water-like and ice-like components.[39-41] These comments led to a controversy about

the structure of the interfacial water layers at the aqueous-silica interface that continues to

this day.[42-45] While there remains no consensus on the absolute assignment of the

vibrational SFG bands at the aqueous-silica interface, all researchers agree that the

presence of a charged silica interface leads to a high degree of anisotropy across the

interfacial region.[44, 46]
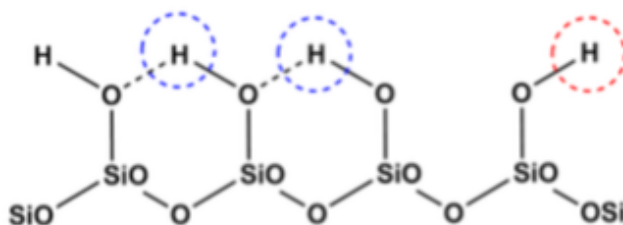
Figure 1.3 Structure of the silica surface. Nonlinear optical studies[47] suggest that the silica surface has 2 different types of silanols. One is isolated (red) with a pKa of approximately 8.5, The other is hydrogen bonded to its neighbors (blue) with a lower pKa of approximately 4.5.

The surface layer of fused, amorphous silica is characterized by silanol and

siloxide groups, with a density of approximately 5 groups per nm^2 although this number

will vary depending on how a sample has been processed and its exposure history.[48-49]

The surface chemistry of the aqueous-silica interface is dominated by the dissociation

reaction:

$$SiOH + OH^- \rightarrow SiO^- + H_2O \hspace{4cm} (1.10)$$

The point of zero charge (PZC) at the silica surface falls between pH 2 and 3.[47, 50-51]

When the silica surface is in contact with an aqueous solution at a higher pH, some

surface silanols will be deprotonated to form siloxides. Above a pH of approximately 10,

no more silanols will be deprotonated. When the silica surface has a higher concentration

of negative charges and therefore a greater surface electric field, it is known to orient

water molecules more strongly. However, even at neutral or weakly charged surfaces,

strong hydrogen bonding interactions between water molecules and the silica surface

aligns water dipoles for as much as 15 Å into the bulk.[46, 51-54] There is also consensus that

this strong association between the silica and its associated interfacial molecules

significantly slows water reorientation dynamics,[44, 46] and a single study that suggested

the same is true for solutes adsorbed at the interface.[55]

1.4 Molecular Isomerization and Twisted Intramolecular Charge Transfer (TICT) States

Work described in this thesis examines how the anisotropy found at silica interfaces

changes a solute's photoisomerization properties. Following photon absorption, an excited

solute will be surrounded by solvent organized in a way to minimize the solute's ground

state energy. Solvent reorganization to stabilize the solute's new excited state electronic

structure will require $10^{-14} – 10^{-11}$ seconds depending on the solvent.[56-58] During this time,

a solute's emission red-shifts and – depending on details of solute structure and

surrounding environment – the photo-excited solute may isomerize. While there are many

different forms of excited state geometries, a particularly common structure is the charge

transfer (CT) state, where an electron is transferred from an electron donating part of the

molecule to an electron accepting part of the molecule or supramolecular structure. This

photoinitiated electron transfer process is the fundamental basis of photosynthesis and a host of technological innovations, particularly in the area of solar energy conversion.[59]

A particularly interesting case of photoexcited electron transfer is that of the twisted intramolecular charge transfer or TICT state. In the creation of a TICT state, an electron donor and an electron acceptor within the same molecule fully separate a set of radical ion pairs across the molecule by twisting some portion of that molecule by 90° relative to the plane of the molecule. In all of the cases discussed in this thesis, this involves an amine group shifting from a pyramidal geometry in the ground state to a 90° twisted structure in the excited TICT state.
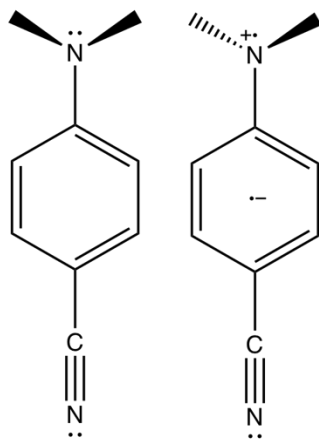
Figure 1.4: The structure of DMABN in its ground state (left) and in its excited TICT state (right)

The first reports of TICT state formation were for a push-pull aromatic solute, 4-dimethylaminobenzonitrile (DMABN), the subject of chapter 4 of this thesis. In 1962, a paper was published describing DMABN's anomalous dual fluorescence in polar solvents.[60] This discovery spawned a host of theories about the origins of DMABN's behavior,[61-68] but in 1973 the first of a series of papers was published describing what became known as the TICT hypothesis for DMABN's fluorescence signature.[69-71] On the

basis of strong experimental and computational evidence, the TICT hypothesis has become the accepted explanation for DMABN's dual fluorescence, and the solute remains the prototypical donor-acceptor TICT compound due to its simple structure and well-understood photophysics.[59]

In the years since the discovery of the TICT state in DMABN, the existence of TICT states in several classes of well-known fluorescent dyes has been postulated on the basis of their photophysical behavior and the highly dipolar nature of their excited states. In particular, the existence of a TICT state in the set of 7-aminocoumarin dyes has been the subject of much debate.[72-79] The generally accepted conclusion is that in coumarin dyes with strong electron donors (e.g. alkyl amines) in the 7-position and strong electron acceptors on the opposing ring, polar solvents can stabilize a charge transfer state following photoexcitation.[80] The CT state can be either planar – described as a simple intramolecular charge transfer or ICT conformation – or twisted (TICT). Two different 7-aminocoumarin solutes are studied in this thesis. Coumarin 152 (7-(Dimethylamino)-4-(trifluoromethyl)-1-benzopyran-2-one) has a tertiary amine in the 7- position and is thought to form a TICT state in polar solvents. Coumarin 151 (7-amino-4-(trifluoromethyl)-1-benzopyran-2-one) is the closely related primary amine and forms a simple planar ICT state. These different pathways have important consequences for each solute's excited state photophysical behavior.

Coumarin 152 (C152), the subject of chapters 2 and 3 of this work, is a member of the 7-aminocoumarin family with a dimethylamino group in the 7-position and a $-CF_3$

group and an ester on the opposing ring, which provide optimal charge transfer

characteristics for the formation of a TICT state. Because the coumarin TICT state is

non-fluorescent, it changes the photophysical behavior of C152 in noticeable and distinct

ways. As C152 is dissolved in solvents of greater polarity, formation of the TICT state

becomes more allowed. With increased TICT character in the excited state, more

molecules decay through the non-fluorescent decay pathway opened by the TICT state.

This effect shortens the fluorescence lifetime and causes the fluorescence to red-shift

relative to dye molecules solvated in less polar environments.[73] The solvatochromism

caused by the TICT state in C152 allows the dye to be used as a fluorescent indicator of

the polarity of its solvation environment.
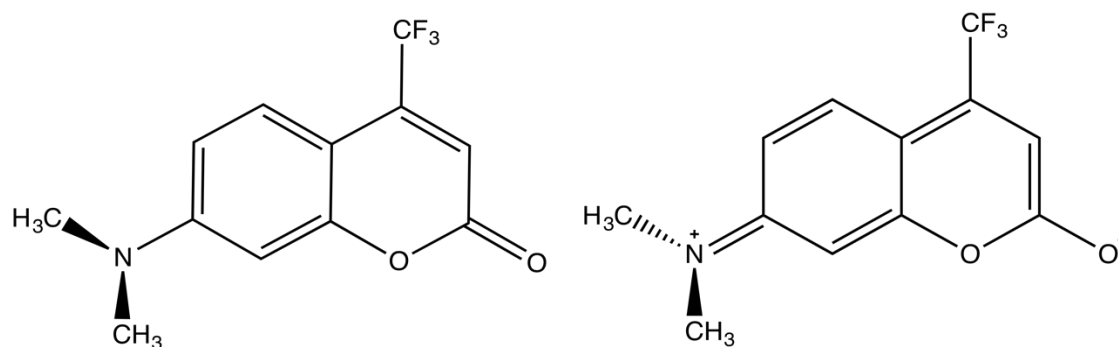
Figure 1.5: The structure of C152 in its ground state configuration (left) and proposed structure of the excited TICT state (right)

1.5 Organization of Thesis

Chapter 2: Hindered Isomerization at the Silica-
Aqueous Interface: Surface Polarity or
Restricted Solvation

     Chapter 2 presents data from TIR-TCSPC studies of Coumarin 152 dye at the

aqueous-silica interface. At this interface, the solvatochromic C152 dye molecule shows

a fluorescent spectral signature reminiscent of the molecule dissolved in a nonpolar bulk solution. This result is unexpected given that the polarity of water is high, as is that of silica. These results are discussed in the context of C152's excited state photoisomerization into a TICT state. A nonpolar solvent's inability to solvate this highly dipolar state is the basis for the spectral signatures in that medium, so we conclude that some aspect of C152's solvation at the aqueous-silica interface is preventing this isomerization following photoexcitation. Since a truly nonpolar region at the aqueous silica interface is unlikely, we hypothesized that possibly the strong association of the water molecules to the silica surface was creating a solvent cage restricting C152 isomerization.

This hypothesis was supported with TCSPC data from C152 dissolved in an ice matrix, which displayed a similar fluorescence signature to C152 at the aqueous-silica interface, despite having a bulk static dielectric constant greater than that of bulk water.

Chapter 3: Surface Solvation and Hindered
Isomerization at the Water-Silica Interface
Explored with Second Harmonic Generation

Chapter 3 continues the line of inquiry begun in Chapter 2. SHG spectra of C152 at the aqueous-silica interface show that in its ground state C152 experiences a polar environment, lending support to the theory that the unusual fluorescence results observed at the same interface are the result of confined water structure and not that of a genuine interfacial nonpolar region.

To test if the strong association between water and the silica surface was, in fact, responsible for C152's unexpected behavior, we disrupted hydrogen bonding at the

interface by rendering the silica surface hydrophobic through reaction with

dichlorodimethylsilane. At this hydrophobic silica-aqueous interface, C152 molecules

showed a lifetime similar to C152 dissolved in a polar organic solvent like methanol.

SHG results confirm that this hydrophobic interface is less polar than that made by

unmodified hydrophilic silica; the hydrophobic silica-aqueous interface also shows a

spectral signature reminiscent of C152 dissolved in a polar organic solvent in SHG

spectra. These results implicate the strong, ordered hydrogen bonding network between

water and silica as the instigator of C152's hindered photoisomerization to a TICT state

at the aqueous-silica interface.

Chapter 4: Buried Liquid Interfaces as a Form
of Chemistry in Confinement: The Case of 4-
dimethylaminobenzonitrile (DMABN) at the
Silica-Aqueous Interface

Chapter 4 presents data that tests the generality of the hypothesis set out in

Chapters 2 and 3, namely that hydrogen bonding networks at the aqueous-silica interface

impede TICT formation. The new solute that is the subject of these experiments, 4-

dimethylaminobenzonitrile or DMABN, is the earliest and classic example of TICT

chemistry as noted in Section 1.4. TIR-TCSPC data from DMABN at the aqueous-silica

interface are consistent with C152 studies and indicate the DMABN is unable to

isomerize into its TICT at this interface. Both TIR-TCSPC and SHG spectra at the

hydrophobic silica-aqueous interface with DMABN show that removing the hydrogen

bonding network enables the solute to once again form a TICT state following

photoisomerization. SHG studies show that at this hydrophobic interface DMABN, like

C152, samples a slightly less polar environment than molecules at the hydrophilic interface.

SHG studies of DMABN at the hydrophilic aqueous-silica interface confirm that DMABN in its ground state is experiencing a bulk static dielectric constant consistent with that of water. However, SHG spectra show the presence of an unexpected and large peak that is not seen in bulk absorbance spectra. With the help of semi-empirical computations, this feature is assigned to the $S_0 \rightarrow S_1$ transition of DMABN. In order for a transition to have a strong $\chi^{(2)}$ response, the transition in question must be both 1- and 2-photon absorption allowed. In the case of DMABN, the S_0-S_1 transition is only very weakly allowed in 1-photon absorption experiments, although its 2-photon absorption cross section is more significant. However, semi-empirical and DFT calculations predict that in the presence of strong electric fields at the surface, the relative oscillator strengths of the S_1 and S_2 transitions can flip, explaining the dramatic intensity seen for this transition in the surface SHG spectra. These studies also lend a generality to the theory that we posited about surface association via hydrogen bond networks restricting TICT formation.

Chapter 5: Isomerization in Coumarin 152 and
Coumarin 151 at the Water-Silica Interface:
Effect of Primary vs. Tertiary Amines

Chapter 5 is a comparative study of Coumarin 151 and 152 at the aqueous-silica interface. C151 has the same molecular structure as C152, except in the 7-position it has a primary amine instead of the tertiary dimethyl amine found in C152. This change in structure means that C151 does not form an excited TICT state because its primary amine

is not a strong enough electron donor. Instead, C151 forms a planar ICT state which involves an isomerization of a much smaller magnitude than that required to form the TICT state in C152. These studies showed that even though C151 forms an excited state with a significant dipole, its spectral response is unchanged from those in bulk water by adsorption at the aqueous-silica interface. This led us to conclude that it is the large-amplitude isomerization in C152 and DMABN that is hindered at the silica-aqueous interface.

1.6 References

1.   Zenasni, O.; Marquez, M. D.; Jamison, A. C.; Lee, H. J.; Czader, A.; Lee, T. R., Inverted Surface Dipoles in Fluorinated Self-Assembled Monolayers. *Chem Mater* **2015,** *27* (21), 7433-7446.

2.   Steel, W. H.; Walker, R. A., Measuring dipolar width across liquid-liquid interfaces with 'molecular rulers'. *Nature* **2003,** *424* (6946), 296-299.

3.   Zhang, X. Y.; Esenturk, O.; Walker, R. A., Reduced polarity in protic solvents near hydrophobic solid surfaces. *J Am Chem Soc* **2001,** *123* (43), 10768-10769.

4.   Zhong, J.; Carignano, M. A.; Kais, S.; Zeng, X. C.; Francisco, J. S.; Gladich, I., Tuning the Stereoselectivity and Solvation Selectivity at Interfacial and Bulk Environments by Changing Solvent Polarity: Isomerization of Glyoxal in Different Solvent Environments. *J Am Chem Soc* **2018,** *140* (16), 5535-5543.

5.   Gobrogge, E. A.; Walker, R. A., Binary Solvent Organization at Silica/Liquid Interfaces: Preferential Ordering in Acetonitrile-Methanol Mixtures. *J Phys Chem Lett* **2014,** *5* (15), 2688-2693.

6.   Gobrogge, E. A.; Woods, B. L.; Walker, R. A., Liquid organization and solvation properties at polar solid/liquid interfaces. *Faraday Discuss* **2013,** *167*, 309-327.

7.   Roy, D.; Liu, S. L.; Woods, B. L.; Siler, A. R.; Fourkas, J. T.; Weeks, J. D.; Walker, R. A., Nonpolar Adsorption at the Silica/Methanol Interface: Surface Mediated Polarity and Solvent Density across a Strongly Associating Solid/Liquid Boundary. *J Phys Chem C* **2013,** *117* (51), 27052-27061.

8.   Woods, B. L.; Walker, R. A., pH Effects on Molecular Adsorption and Solvation of p-Nitrophenol at Silica/Aqueous Interfaces. *J Phys Chem A* **2013,** *117* (29), 6224-6233.

9.   Woods, B. L.; George, J. K.; Sherman, A. M.; Callis, P. R.; Walker, R. A., Adsorption and Aggregation at Silica/Methanol Interfaces: The Role of Solute Structure. *J Phys Chem C* **2015,** *119* (25), 14230-14238.

10.   Beniwal, V.; Manna, A.; Kumar, A., Spectacular Rate Enhancement of the Diels-Alder Reaction at the Ionic Liquid/n-Hexane Interface. *Chemphyschem* **2016,** *17* (13), 1969-1972.

11.   Dong, R. H.; Zhang, T.; Feng, X. L., Interface-Assisted Synthesis of 2D Materials: Trend and Challenges. *Chem Rev* **2018,** *118* (13), 6189-6235.

12.   Arnold, W. A.; Roberts, A. L., Pathways and kinetics of chlorinated ethylene and chlorinated acetylene reaction with Fe(O) particles. *Environ Sci Technol* **2000,** *34* (9), 1794-1805.

13.   Tseng, T. C.; Urban, C.; Wang, Y.; Otero, R.; Tait, S. L.; Alcami, M.; Ecija, D.; Trelka, M.; Gallego, J. M.; Lin, N.; Konuma, M.; Starke, U.; Nefedov, A.; Langner, A.; Woll, C.; Herranz, M. A.; Martin, F.; Martin, N.; Kern, K.; Miranda, R., Charge-transfer-induced structural rearrangements at both sides of organic/metal interfaces. *Nat Chem* **2010,** *2* (5), 374-379.

14.   Munninghoff, J. A. W.; Elemans, J. A. A. W., Chemistry at the square nanometer: reactivity at liquid/solid interfaces revealed with an STM. *Chem Commun* **2017,** *53* (11), 1769-1788.

15.   Shibukawa, M.; Miyake, A.; Eda, S.; Saito, S., Determination of the cis-trans lsomerization Barriers of L-Alanyl-L-proline in Aqueous Solutions and at Water/Hydrophobic Interfaces by On-Line Temperature-Jump Relaxation HPLC and Dynamic On-Column Reaction HPLC. *Anal Chem* **2015,** *87* (18), 9280-9287.

16.   Chen, H.; Zou, H. B.; Hao, Y. J.; Yang, H. Q., Flow Pickering Emulsion Interfaces Enhance Catalysis Efficiency and Selectivity for Cyclization of Citronellal. *Chemsuschem* **2017,** *10* (9), 1989-1995.

17.   Guo, L. W.; Cesari, S.; de Guillen, K.; Chalvon, V.; Mammri, L.; Ma, M. Q.; Meusnier, I.; Bonnot, F.; Padilla, A.; Peng, Y. L.; Liu, J. F.; Kroj, T., Specific recognition of two MAX effectors by integrated HMA domains in plant immune receptors involves distinct binding surfaces. *P Natl Acad Sci USA* **2018,** *115* (45), 11637-11642.

18.   Fukuda, T., Biological recognition at interfaces involving dendritic molecules. *Polym J* **2019,** *51* (6), 535-546.

19.   Neal, J. F.; Zhao, W.; Grooms, A. J.; Smeltzer, M. A.; Shook, B. M.; Flood, A. H.; Allen, H. C., Interfacial Supramolecular Structures of Amphiphilic Receptors Drive Aqueous Phosphate Recognition. *J Am Chem Soc* **2019,** *141* (19), 7876-7886.

20.   Dubacheva, G. V.; Curk, T.; Frenkel, D.; Richter, R. P., Multivalent Recognition at Fluid Surfaces: The Interplay of Receptor Clustering and Superselectivity. *J Am Chem Soc* **2019,** *141* (6), 2577-2588.

21.   Lin, J. F.; Liu, Y.; Liu, Y. P.; Huang, C.; Liu, W. H.; Mi, X. H.; Fan, D. Y.; Fan, F. T.; Lu, H. D.; Chen, X. B., SnS2 Nanosheets/H-TiO2 Nanotube Arrays as a Type II Heterojunctioned Photoanode for Photoelectrochemical Water Splitting. *Chemsuschem* **2019,** *12* (5), 961-967.

22.   Zang, S. H.; Zhang, G. G.; Lan, Z. A.; Zheng, D. D.; Wang, X. C., Enhancement of photocatalytic H-2 evolution on pyrene-based polymer promoted by MoS2 and visible light. *Appl Catal B-Environ* **2019,** *251*, 102-111.

23.   Urban, C.; Wang, Y.; Rodriguez-Fernandez, J.; Garcia, R.; Herranz, M. A.; Alcami, M.; Martin, N.; Martin, F.; Gallego, J. M.; Miranda, R.; Otero, R., Charge transfer-assisted self-limited decyanation reaction of TCNQ-type electron acceptors on Cu(100). *Chem Commun* **2014,** *50* (7), 833-835.

24.   Zhang, X.; Steel, W. H.; Walker, R. A., Probing solvent polarity across strongly associating solid/liquid interfaces using molecular rulers. *J Phys Chem B* **2003,** *107* (16), 3829-3836.

25.   Karnes, J. J.; Gobrogge, E. A.; Walker, R. A.; Benjamin, I., Unusual Structure and Dynamics at Silica/Methanol and Silica/Ethanol Interfaces-A Molecular Dynamics and Nonlinear Optical Study. *J Phys Chem B* **2016,** *120* (8), 1569-1578.

26.   Shang, X. M.; Benderskii, A. V.; Eisenthal, K. B., Ultrafast solvation dynamics at silica/liquid interfaces probed by time-resolved second harmonic generation. *J Phys Chem B* **2001,** *105* (47), 11578-11585.

27.   Ding, F.; Hu, Z. H.; Zhong, Q.; Manfred, K.; Gattass, R. R.; Brindza, M. R.; Fourkas, J. T.; Walker, R. A.; Weeks, J. D., Interfacial Organization of Acetonitrile: Simulation and Experiment. *J Phys Chem C* **2010,** *114* (41), 17651-17659.

28.   Kirkwood, J. G., The dielectric polarization of polar liquids. *J Chem Phys* **1939,** *7* (10), 911-919.

29.   Axelrod, D.; Burghardt, T. P.; Thompson, N. L., Total Internal-Reflection Fluorescence. *Annu Rev Biophys Bio* **1984,** *13*, 247-268.

30.   Hecht, E., *Optics*. Fourth ed.; Addison Wesley: San Francisco, CA, 2002.

31.   Martin-Fernandez, M. L.; Tynan, C. J.; Webb, S. E. D., A 'pocket guide' to total internal reflection fluorescence. *J Microsc-Oxford* **2013,** *252* (1), 16-22.

32.   Birch, D. J. S.; Imhof, R. E., Time-Domain Fluorescence Spectroscopy Using Time-Correlated Single-Photon Counting. In *Topics in Fluorescence Spectroscopy, Volume 1: Techniques*, Lakowicz, J. R., Ed. Plenum Press: New York, 1991.

33.   Franken, P. A.; Weinreich, G.; Peters, C. W.; Hill, A. E., Generation of Optical Harmonics. *Phys Rev Lett* **1961,** *7* (4), 118-&.

34.   Boyd, R. W., Nonlinear Optics, 3rd Edition. *Nonlinear Optics, 3rd Edition* **2008**, 1-613.

35.   He, G. S., *Nonlinear Optics and Photonics*. First ed.; Oxford University Press: Oxford, UK, 2015.

36.   Moad, A. J.; Simpson, G. J., A unified treatment of selection rules and symmetry relations for sum-frequency and second harmonic spectroscopies. *J Phys Chem B* **2004,** *108* (11), 3548-3562.

37.   Du, Q.; Freysz, E.; Shen, Y. R., Vibrational-Spectra of Water-Molecules at Quartz Water Interfaces. *Phys Rev Lett* **1994,** *72* (2), 238-241.

38.   Klier, K.; Zettlemoyer, A. C., Water at Interfaces - Molecular-Structure and Dynamics. *J Colloid Interf Sci* **1977,** *58* (2), 216-229.

39.   Sovago, M.; Campen, R. K.; Bakker, H. J.; Bonn, M., Hydrogen bonding strength of interfacial water determined with surface sum-frequency generation. *Chem Phys Lett* **2009,** *470* (1-3), 7-12.

40.   Sovago, M.; Campen, R. K.; Wurpel, G. W. H.; Muller, M.; Bakker, H. J.; Bonn, M., Vibrational response of hydrogen-bonded interfacial water is dominated by intramolecular coupling. *Phys Rev Lett* **2008,** *100* (17).

41.   Nihonyanagi, S.; Yamaguchi, S.; Tahara, T., Water Hydrogen Bond Structure near Highly Charged Interfaces Is Not Like Ice. *J Am Chem Soc* **2010,** *132* (20), 6867-+.

42.   Tian, C. S.; Shen, Y. R., Comment on "Vibrational Response of Hydrogen-Bonded Interfacial Water is Dominated by Intramolecular Coupling". *Phys Rev Lett* **2008,** *101* (13).

43.   Sovago, M.; Campen, R. K.; Wurpel, G. W. H.; Muller, M.; Bakker, H. J.; Bonn, M., Comment on "Vibrational Response of Hydrogen-Bonded Interfacial Water is Dominated by Intramolecular Coupling" - Reply. *Phys Rev Lett* **2008,** *101* (13).

44.   Nihonyanagi, S.; Mondal, J. A.; Yamaguchi, S.; Tahara, T., Structure and Dynamics of Interfacial Water Studied by Heterodyne-Detected Vibrational Sum-Frequency Generation. *Annu Rev Phys Chem* **2013,** *64*, 579-603.

45.   de Beer, A. G. F.; Roke, S., What interactions can distort the orientational distribution of interfacial water molecules as probed by second harmonic and sum frequency generation? *J Chem Phys* **2016,** *145* (4).

46.   Gupta, P. K.; Meuwly, M., Dynamics and vibrational spectroscopy of water at hydroxylated silica surfaces. *Faraday Discuss* **2013,** *167*, 329-346.

47.   Ong, S. W.; Zhao, X. L.; Eisenthal, K. B., Polarization of Water-Molecules at a Charged Interface - 2nd Harmonic Studies of the Silica Water Interface. *Chem Phys Lett* **1992,** *191* (3-4), 327-335.

48.   Zhuravlev, L. T., Concentration of Hydroxyl-Groups on the Surface of Amorphous Silicas. *Langmuir* **1987,** *3* (3), 316-318.

49.   Iler, R. K., *Chemistry of Silica*. John Wiley & Sons: 1979.

50.   Yeganeh, M. S.; Dougal, S. M.; Pink, H. S., Vibrational spectroscopy of water at liquid/solid interfaces: Crossing the isoelectric point of a solid surface. *Phys Rev Lett* **1999,** *83* (6), 1179-1182.

51.   Sulpizi, M.; Gaigeot, M. P.; Sprik, M., The Silica-Water Interface: How the Silanols Determine the Surface Acidity and Modulate the Water Properties. *J Chem Theory Comput* **2012,** *8* (3), 1037-1047.

52.   Argyris, D.; Cole, D. R.; Striolo, A., Dynamic Behavior of Interfacial Water at the Silica Surface. *J Phys Chem C* **2009,** *113* (45), 19591-19600.

53.   Kjellander, R.; Marcelja, S., Perturbation of Hydrogen-Bonding in Water near Polar Surfaces. *Chem Phys Lett* **1985,** *120* (4-5), 393-396.

54.   Shen, Y. R.; Ostroverkhov, V., Sum-frequency vibrational spectroscopy on water interfaces: Polar orientation of water molecules at interfaces. *Chem Rev* **2006,** *106* (4), 1140-1154.

55.   Shi, X.; Borguet, E.; Tarnovsky, A. N.; Eisenthal, K. B., Ultrafast dynamics and structure at aqueous interfaces by second harmonic generation. *Chem Phys* **1996,** *205* (1-2), 167-178.

56.   Shirota, H.; Castner, E. W., Solvation in highly nonideal solutions: A study of aqueous 1-propanol using the coumarin 153 probe. *J Chem Phys* **2000,** *112* (5), 2367-2376.

57.   Barbara, P. F., Ultrafast Studies on Intramolecular Charge-Transfer and Solvation. *Springer Series Chem* **1990,** *53*, 393-396.

58.   Nagarajan, V.; Brearley, A. M.; Kang, T. J.; Barbara, P. F., Time-Resolved Spectroscopic Measurements on Microscopic Solvation Dynamics. *J Chem Phys* **1987,** *86* (6), 3183-3196.

59.   Grabowski, Z. R.; Rotkiewicz, K.; Rettig, W., Structural changes accompanying intramolecular electron transfer: Focus on twisted intramolecular charge-transfer states and structures. *Chem Rev* **2003,** *103* (10), 3899-4031.

60.   Lippert, E.; Lüder, W.; Boos, H., Fluoreszenzspektrum und Frank-Condon-Prinzip in Lösungen aroma-tischer Verbindungen. In *Advances in Molecular Spectroscopy*, Mangini, A., Ed. Pergamon Press: Oxford, 1962; Vol. 1, pp 442-456.

61.   Visser, R. J.; Varma, C. A. G. O., Source of Anomalous Fluorescence from Solutions of 4-N,N-Dimethylaminobenzonitrile in Polar-Solvents. *J Chem Soc Farad T 2* **1980,** *76*, 453-471.

62.   Chandross, E. A.; Thomas, H. T., The interaction of amine-hydrocarbon exciplexes with small dipolar molecules - stoichiometric complex formation. *Chem Phys Lett* **1971,** *9* (5), 397-400.

63.   Khalil, O. S., Excimer Model of N,N-Dialkyl-Para-Cyanoanilines Fluorescence in Polar-Solvents. *Chem Phys Lett* **1975,** *35* (2), 172-174.

64.   Zachariasse, K. A., Comment on "Pseudo-Jahn-Teller and TICT-models: a photophysical comparison of meta-and para-DMABN derivatives" [Chem. Phys. Lett. 305(1999)8] - The PICT model for dual fluorescence of aminobenzonitriles. *Chem Phys Lett* **2000,** *320* (1-2), 8-13.

65.   Zachariasse, K. A.; Grobys, M.; vonderHaar, T.; Hebecker, A.; Ilichev, Y. V.; Morawski, O.; Ruckert, I.; Kuhnle, W., Photoinduced intramolecular charge transfer and internal conversion in molecules with a small energy gap between S-1 and S-2. Dynamics and structure. *J Photoch Photobio A* **1997,** *105* (2-3), 373-383.

66.   Lewis, F. D.; Holman, B., Singlet-States of Benzonitrile and Para-Dimethylaminobenzonitrile. *J Phys Chem-Us* **1980,** *84* (18), 2326-2328.

67.   Sobolewski, A. L.; Domcke, W., Promotion of intramolecular charge transfer in dimethylamino derivatives: Twisting versus acceptor-group rehybridization. *Chem Phys Lett* **1996,** *259* (1-2), 119-127.

68.   Sobolewski, A. L.; Domcke, W., Charge transfer in aminobenzonitriles: Do they twist? *Chem Phys Lett* **1996,** *250* (3-4), 428-436.

69.   Rotkiewicz, K.; Grellmann, K. H.; Grabowski, Z. R., Reinterpretation of Anomalous Fluorescence of "Para-N,N-Dimethylamino-Benzonitrile. *Chem Phys Lett* **1973,** *19* (3), 315-318.

70.   Siemiarczuk, A.; Grabowski, Z. R.; Krowczynski, A., 2 Emitting States of Excited Para-(9-Anthryl)-N,N-Dimethylaniline Derivatives in Polar-Solvents. *Chem Phys Lett* **1977,** *51* (2), 315-320.

71.   Grabowski, Z. R.; Rotkiewicz, K.; Siemiarczuk, A., Dual Fluorescence of Donor-Acceptor Molecules and the Twisted Intra-Molecular Charge-Transfer (Tict) States. *J Lumin* **1979,** *18-9* (Jan), 420-424.

72.   Dahiya, P.; Kumbhakar, M.; Mukherjee, T.; Pal, H., Effect of protic solvents on twisted intramolecular charge transfer state formation in coumarin-152 and coumarin-481 dyes. *Chem Phys Lett* **2005,** *414* (1-3), 148-154.

73.   Nad, S.; Kumbhakar, M.; Pal, H., Photophysical properties of coumarin-152 and coumarin-481 dyes: Unusual behavior in nonpolar and in higher polarity solvents. *Journal of Physical Chemistry A* **2003,** *107* (24), 4808-4816.

74.   Arbeloa, T. L.; Arbeloa, F. L.; Estevez, M. J. T.; Arbeloa, I. L., Binary Solvent Effects on the Absorption and Emission of 7-Aminocoumarins. *J Lumin* **1994,** *59* (6), 369-375.

75.   Arbeloa, T. L.; Arbeloa, F. L.; Tapia, M. J.; Arbeloa, I. L., Hydrogen-Bonding Effect on the Photophysical Properties of 7-Aminocoumarin Derivatives. *J Phys Chem-Us* **1993,** *97* (18), 4704-4707.

76.   Cave, R. J.; Burke, K.; Castner, E. W., Theoretical Investigation of the Ground and Excited States of Coumarin 151 and Coumarin 120. *The Journal of Physical Chemistry A* **2002,** *106* (40), 9294-9305.

77.   Cave, R. J.; Castner, E. W., Time-Dependent Density Functional Theory Investigation of the Ground and Excited States of Coumarins 102, 152, 153, and 343. *The Journal of Physical Chemistry A* **2002,** *106* (50), 12117-12123.

78.   Rettig, W.; Klock, A., Intramolecular Fluorescence Quenching in Aminocoumarines - Identification of an Excited-State with Full Charge Separation. *Can J Chem* **1985,** *63* (7), 1649-1653.

79.   Rechthaler, K.; Kohler, G., Excited-State Properties and Deactivation Pathways of 7-Aminocoumarins. *Chem Phys* **1994,** *189* (1), 99-116.

80.   Corrie, J. E. T.; Munasinghe, V. R. N.; Rettig, W., Synthesis and fluorescence properties of substituted 7-aminocoumarin-3-carboxylate derivatives. *J Heterocyclic Chem* **2000,** *37* (6), 1447-1455.

CHAPTER TWO

HINDERED ISOMERIZATION AT THE SILICA/AQUEOUS

INTERFACE: SURFACE POLARITY OR

RESTRICTED SOLVATION?

<u>Contribution of Authors and Co-Authors</u>

Manuscript in Chapter 2:

Author: Grace E. Purnell

Contributions: Collected and analyzed all experimental data and authored manuscript

Co-Author: Robert A. Walker

Contributions: Assisted with data analysis and edited manuscript

Manuscript Information

Grace E. Purnell and Robert A. Walker

Langmuir

Status of Manuscript:
____ Prepared for submission to a peer-reviewed journal
____ Officially submitted to a peer-reviewed journal
____ Accepted by a peer-reviewed journal
 _X_ Published in a peer-reviewed journal

CHAPTER TWO

HINDERED ISOMERIZATION AT THE SILICA/AQUEOUS

INTERFACE: SURFACE POLARITY OR

RESTRICTED SOLVATION?

2.1 Introduction

Water's complicated interfacial properties have motivated innumerable studies

and sparked considerable debate ever since the first surface-specific, nonlinear

vibrational spectrum of water's aqueous/vapor interface was reported more than two

decades ago.[54, 81-82] With its broad features and characteristic sharp 'free–OH' band,

water's vibrational structures at aqueous/vapor, liquid/liquid and solid/liquid interfaces

have led researchers to describe surface water as 'liquid-like'[83], 'ice-like'[37], and/or

propose models that identify interfacial populations having specific hydrogen bonding

configurations.[54, 84] Complementing these discoveries, theory and simulations have

provided nuanced insight into how surface-altered hydrogen bonding changes water's

properties from bulk limits.[46, 82] Despite these concerted efforts, however, very few

studies[55, 85] have explored how changes in water structure and dynamics impact the

water's ability to solvate solutes adsorbed to aqueous interfaces.

Interfacial solvation often differs from a solvent's bulk solution limit. In this

context, interfacial solvation describes the surface-modified, non-covalent interactions a

solute experiences with its surroundings. Eisenthal and coworkers first addressed

questions about interfacial polarity, using surface specific second harmonic generation

(SHG) to record effective excitation wavelengths of solutes adsorbed to different

liquid/liquid and liquid/vapor interfaces.[86] Shifts in SHG spectra led the authors to

describe interfacial polarity as an average between polarities of the two adjacent phases.

Subsequent work by Steel, et al. reported that an interface's local dielectric environment

depends sensitively on solvent structure, and polarity across strongly associating

interfaces (such as water/1-octanol) is characterized by a low polarity region having an

effective dielectric constant of ≤ 2.[2, 87] Similar results have been reported from

silica/*n*-alcohol interfaces where strong hydrogen bonding between surface silanol groups

and the first solvent layer effectively transforms the silica surface into a hydrophobic,

alkyl terminated substrate.[7, 26]

2.2 Experimental

Experiments were carried out using a locally-constructed TCSPC fluorometer that

has been described previously.[9] The output of a Ti:sapphire oscillator (Chameleon,

Coherent) was frequency doubled (APE Autotracker) and the 80 MHz repetition rate was

attenuated to 4 MHz using an electro-optic modulator (Conoptics Model 350-105).

Fluorescence emission was collected using a Picoquant 200 time-to-amplitude converter

and the instrument response function was measured using a non-emissive Ludox

scattering solution. For bulk solution measurements, the IRF was between 20 and 50 ps.

For TIR measurements, a custom-built assembly enabled the excitation pulse to irradiate

the interface formed between a hemispherical prism and aqueous solution at angles

beyond the critical angle (61° at 400 nm). Emission was detected at 90° relative to the

silica/aqueous interface. The TIR assembly's IRF was ~200 ps. For every experiment the IRF was deconvoluted from the time-resolved emission histogram and the resulting trace was then fit to one or more single exponential decays. The minimum number of lifetimes required to accurately fit the data was determined using the Akaike information criterion.

For all experiments, cuvettes and experimental assemblies were rinsed with methanol and DI water (Millipore, 18.2Ω), then soaked in a bath of 50/50 sulfuric/nitric acid for no less than an hour, and rinsed with DI water before use. TIR-TCSPC spectra used fused silica hemispheres from SPI Optics, and bulk TCSPC spectra were taken in quartz Starna cuvettes.
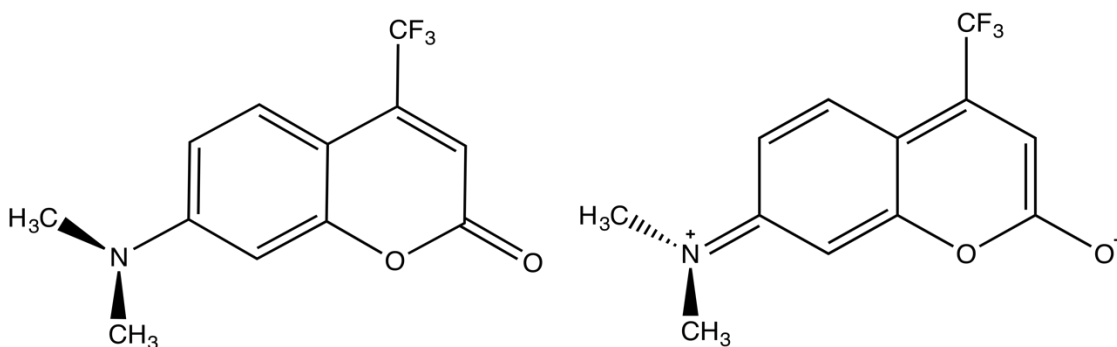
Figure 2.1: The structure of C152 in its ground state configuration (left) and proposed structure of the excited TICT state (right)

Most experiments in this work used saturated aqueous solutions of Coumarin 152 (C152). (Figure 2.1) Coumarin 152 was purchased from Exciton and used as received. C152's photophysical behavior has been examined in detail both experimentally and computationally.[73, 88] Several properties of this solute make it an attractive probe of local solvation environment: well-defined absorption/emission behavior, photostability, and an

insensitivity to local viscosity. In most solvents, C152 emission is characterized by a single exponential decay, simplifying interpretation of C152 fluorescence in chemically complex environments. In polar, protic solvents, C152 photoexcitation leads to rapid formation of a nonradiative, twisted intramolecular charge transfer (TICT) state and a correspondingly short (≤ 1 ns) emission lifetime. Structures of C152's ground state and excited TICT state are shown in Figure 2.1. Less polar solvents such as alkanes cannot stabilize the TICT state. As a result, C152 has a longer fluorescence lifetime (~3.5-4 ns) in these low dielectric environments.
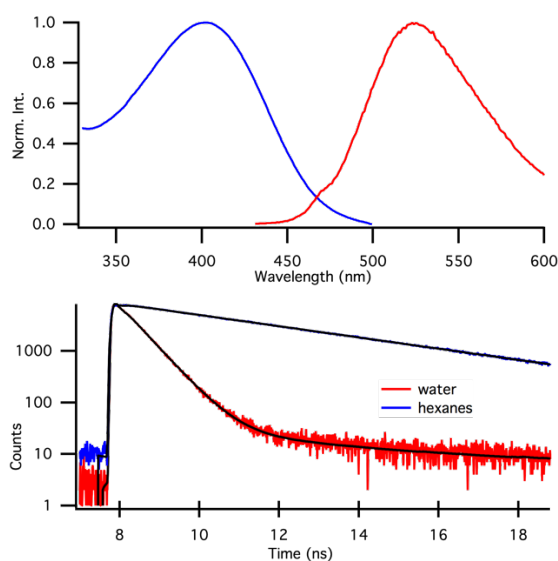
Figure 2.2: Top: Absorbance (blue) and fluorescence (red) spectra of a saturated solution of C152 in water. Bottom: TCSPC decay curves for C152 in water and in hexanes.

Saturated solutions were made by allowing DI water and excess C152 to equilibrate with stirring at 50°C overnight and then filtering excess dye from the solution before use. At room temperature, the concentration of an aqueous solution saturated with C152 is approximately 6 μM. In the experiments presented here, molecules were excited at 396 nm, the peak absorption wavelength of C152 in aqueous solution, and the emission

monochromator was set to collect at either 525 nm, the peak fluorescence emission

wavelength in room temperature water, or 505 nm, the fluorescence emission peak of

C152 in ice. In aqueous solution, C152's emission is characterized by a short, sub-ns

lifetime (0.47 ns), while in nonpolar solvents, C152's emission lifetime is markedly

longer (3.5 ns in alkanes). (Figure 2.2)

For time-resolved fluorescence experiments conducted in a TIR geometry, the

incident beam passes through the higher index fused silica prism at an angle of

approximately 65.5° relative to surface normal; the resulting evanescent wave propagates

~150 nm into the aqueous solvent conferring pseudo-surface specificity to the

measurements.

2.3 Results

2.3.1 Time-Resolved Fluorescence at Silica
<u>Interface</u>

Experiments used time correlated single photon counting in a total internal

reflection (TIR) geometry to measure the time-resolved emission of a coumarin solute

adsorbed to a silica/aqueous (pH = 5.9) interface. In bulk water, >98% of the time-

resolved fluorescence signal from C152 can be fit to a lifetime of 0.47 ns. A small but

measurable fraction of C152's emission fits to a much longer lifetime – 4.02 ns – that has

been assigned previously to dimers in solution.[9] For TIR measurements carried out at the

silica/aqueous interface, the fluorescence decay from a saturated C152 solution is best fit

with 2 lifetimes: a short, 0.47 ns lifetime assigned to C152 in bulk solution and a longer

lifetime of 3.52 ns assigned to C152 adsorbed to the surface. (Figure 2.3) Normalized

amplitudes for the short and long lifetimes are 0.87 and 0.13, respectively. Repeating the

same experiment with a C152 solution that has been diluted by a factor of two (~3 μM)

leads to no change in lifetimes but the longer lifetime contributes twice as much (0.27) to

the overall emission decay data. This result supports assignment of the long-lived

monomers adsorbed to the silica/aqueous interface.[85]
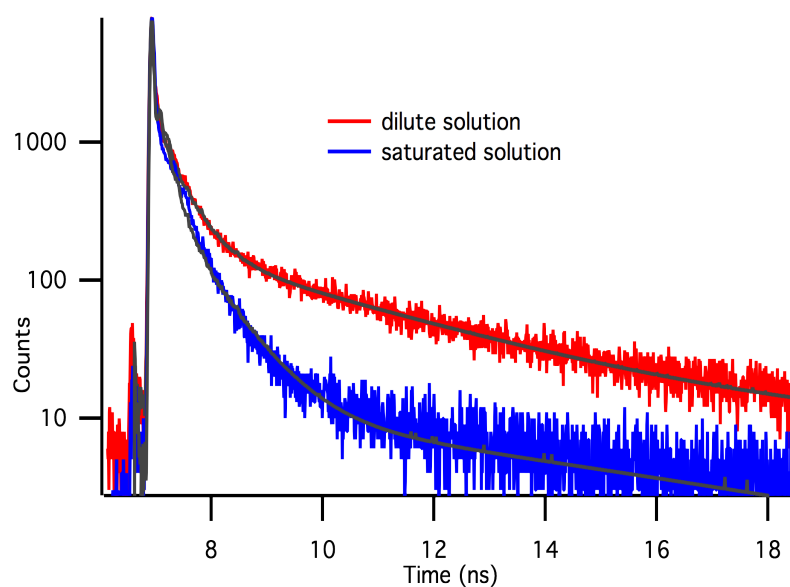
Figure 2.3: TIR TCSPC traces of saturated (blue) and dilute (red) aqueous solutions of
C152. The tail from the 3.52 ns lifetime represents a greater proportional amplitude of the
dilute trace, which is evidence for the idea that the cause of that lifetime is an effect that
is amplified by the surface.

Data in Figure 2.3 imply that the interfacial solvation environment cannot readily

stabilize C152's nonradiative TICT state, effectively making the interfacial region appear

nonpolar. Two possible explanations can rationalize this result: 1) the local dielectric

constant at the silica/aqueous interface is significantly less than $\varepsilon = 78.0$ experienced in

bulk solution, and/or 2) water's restricted motion or 'ice-like' character at the

silica/aqueous interface prevents interfacial solvent from stabilizing C152's TICT state thus inhibiting isomerization. Comparison of TIR data with results from C152 solvated in bulk ice suggests that both effects contribute to the observed behavior although restricted solvent motion appears to play a more important role.   More importantly, findings presented here are among the first reported examples of how surface-mediated solvation in aqueous systems changes solute reactivity from bulk solution limits.

A longer emission lifetime from C152 adsorbed to the silica-aqueous interface is consistent with the solute being solvated in solvents less polar than water and might suggest that the silica-aqueous interface has a local dielectric constant approaching that of alkanes ($\varepsilon \sim 2$). While interfacial polarity is expected to be less than that of bulk water based on prior experiments,[86, 89-90] alkane-like properties at a hydrophilic silica/aqueous interface are not expected. Unlike strongly associating organic solvents such as methanol, 1-butanol, and others, water does not have a 'hydrophobic piece' that can organize at a surface to form a locally non-polar region with alkane-like solvation.[7, 24, 85] Radial distribution functions describing water adjacent to silica surfaces show enhanced densities and well-defined long range ordering that extends up to 2 nm into the liquid.[46, 91] Such a high density of aligned dipoles would be expected to enhance, not diminish, water's permittivity. These arguments are bolstered by surface wetting and electrokinetic measurements that calculate surface potentials at the silica/aqueous (pH ~6) interface > 75 mV in the low ionic strength limit.[92-93] Over a distance of 2 nm, this surface potential will create fields > 10^6 V/cm.

In contrast, water's restricted mobility at a silica surface – also apparent in simulations – would limit the solvent's ability to promote C152 photoisomerization. Such behavior is similar to what one expects in solid matrices composed of polar materials and would be consistent with reports of 'ice-like' water at silica-aqueous interfaces.[94] Experiments and simulations create conflicting narratives about ice's static dielectric constant relative to bulk water,[95-96] but both theory and experiment show unequivocally that water reorientation dynamics at hydrophilic surfaces slow significantly from bulk limits.[97] In vibrational spectroscopy experiments, highly structured water at a silica/aqueous interface is observed as a single broad feature centered at relatively low frequency (3100 cm^{-1}), very similar to the vibrational Raman spectrum of bulk ice.[54]

	A_1[a]	τ_1 (ns)[b]	A_2[a]	τ_2 (ns)[b]
Bulk water	≥ 0.98	.50	≤ 0.02	4.02
TIR water (saturated)	0.87	.47	0.13	3.52
TIR water (dilute)	0.73	.47	0.27	3.52
ice	0.85	.71	0.15	7.47

[a]Amplitude uncertainties are ± 0.02.   [b]Lifetime uncertainties are ± 0.15 ns.

Table 2.1: Lifetimes and amplitudes for C152

2.3.2 Fluorescence of C152 in Frozen Water

To test the viability of these explanations for C152's long emission lifetime at the silica aqueous interface - reduced polarity vs. slow solvation dynamics – we measured the steady state fluorescence excitation and emission and the time-resolved fluorescence

from solutions of C152 in frozen water. (Figure 2.4) While the structure of the ice matrix

was not characterized explicitly in this work, we assumed that ice had an I-h structure

given temperature and ambient pressure considerations.
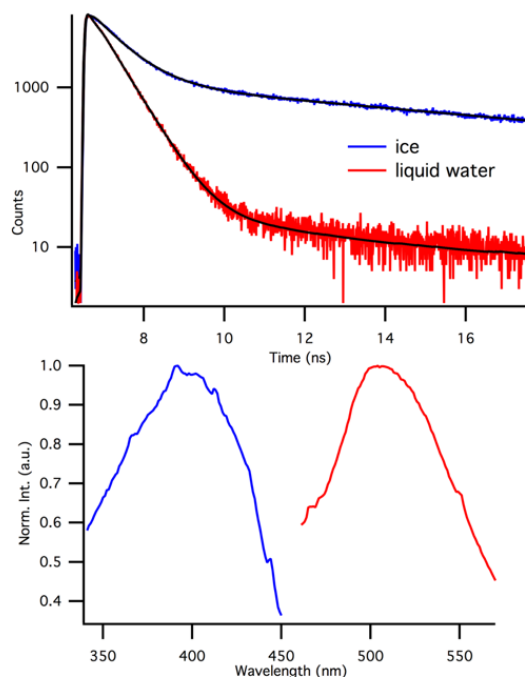
Figure 2.4: Time-resolved fluorescence spectra of C152 in ice and liquid water at room
temperature (top). Excitation (blue) and emission (red) spectra of C152 in ice (bottom)

Approximately 85% of the fluorescence emission from C152 in ice can be fit to a

lifetime assigned to cold, bulk water (.71 ns) in coexistence with ice, with the remaining

decay intensity described by a fluorescence lifetime of 7.47 ns. We assign this long-lived

contribution to the total fluorescence decay to coumarin solutes unable to form the TICT

state. Interestingly, the steady state fluorescence spectrum of C152 also changes when

trapped in ice, with the peak emission wavelength shifting from 525 nm in liquid water to

504 nm in ice. C152's fluorescence excitation maximum in ice (396 nm) remains

unchanged from that in liquid water.

Comparing data from the C152 time resolved emission at the silica/water

interface to C152 behavior in bulk ice shows that although the C152 molecules adsorbed

to the silica surface experience an environment that appears more non-polar based on

comparison to bulk solvent studies,[12,14] in fact, the results are consistent with solutes

'trapped' in a local environment unable to accommodate changes in properties associated

with photoexcitation. What remains to be determined is whether or not complementary

behavior is observed in excitation spectra of adsorbed C152. This question is currently

being addressed with surface-specific SHG measurements and will be the subject of a

future report.

<div align="center">2.4 Conclusions</div>

Time resolved fluorescence measurements of C152 adsorbed to the silica/aqueous

(pH = 5.9), solid/liquid interface show the emergence of a 3.52 ns lifetime that is

significantly longer than the C152's emission lifetime in bulk aqueous solution (0.47 ns).

Concentration dependent amplitudes for these long and short lifetimes support the long

lifetime emission originating from adsorbed monomers that are unable to rapidly

isomerize and form a TICT state. The origin of this behavior may result from a local

dielectric environment at the silica/aqueous interface that is less polar than bulk water *or*

from interfacial water's restricted motion caused by strong solvent-substrate interactions.

Comparative time-resolved fluorescence experiments performed with C152 solvated in

bulk ice imply that slower water reorientation dynamics at the silica/aqueous interface are

more likely responsible for C152's unusual behavior at the strongly associating, silica/aqueous interface.

Regardless of the origin of C152's behavior at the silica/water interface, results described in this communication represent one of the first reported examples of how surface modified solvent properties affect surface isomerization/reactivity. Given the importance of silica-water interfaces in chemical techniques such as chromatography as well as in environmental applications, this result motivates further study to understand the response of organic solutes that are influenced by interfacial asymmetry.

2.5 References

2.   Steel, W. H.; Walker, R. A., Measuring dipolar width across liquid-liquid interfaces with 'molecular rulers'. *Nature* **2003,** *424* (6946), 296-299.

7.   Roy, D.; Liu, S. L.; Woods, B. L.; Siler, A. R.; Fourkas, J. T.; Weeks, J. D.; Walker, R. A., Nonpolar Adsorption at the Silica/Methanol Interface: Surface Mediated Polarity and Solvent Density across a Strongly Associating Solid/Liquid Boundary. *J Phys Chem C* **2013,** *117* (51), 27052-27061.

9.   Woods, B. L.; George, J. K.; Sherman, A. M.; Callis, P. R.; Walker, R. A., Adsorption and Aggregation at Silica/Methanol Interfaces: The Role of Solute Structure. *J Phys Chem C* **2015,** *119* (25), 14230-14238.

24.   Zhang, X.; Steel, W. H.; Walker, R. A., Probing solvent polarity across strongly associating solid/liquid interfaces using molecular rulers. *J Phys Chem B* **2003,** *107* (16), 3829-3836.

26.   Shang, X. M.; Benderskii, A. V.; Eisenthal, K. B., Ultrafast solvation dynamics at silica/liquid interfaces probed by time-resolved second harmonic generation. *J Phys Chem B* **2001,** *105* (47), 11578-11585.

37.   Du, Q.; Freysz, E.; Shen, Y. R., Vibrational-Spectra of Water-Molecules at Quartz Water Interfaces. *Phys Rev Lett* **1994,** *72* (2), 238-241.

46.   Gupta, P. K.; Meuwly, M., Dynamics and vibrational spectroscopy of water at hydroxylated silica surfaces. *Faraday Discuss* **2013,** *167*, 329-346.

54.   Shen, Y. R.; Ostroverkhov, V., Sum-frequency vibrational spectroscopy on water interfaces: Polar orientation of water molecules at interfaces. *Chem Rev* **2006,** *106* (4), 1140-1154.

55.   Shi, X.; Borguet, E.; Tarnovsky, A. N.; Eisenthal, K. B., Ultrafast dynamics and structure at aqueous interfaces by second harmonic generation. *Chem Phys* **1996,** *205* (1-2), 167-178.

73.   Nad, S.; Kumbhakar, M.; Pal, H., Photophysical properties of coumarin-152 and coumarin-481 dyes: Unusual behavior in nonpolar and in higher polarity solvents. *Journal of Physical Chemistry A* **2003,** *107* (24), 4808-4816.

81.   Du, Q.; Superfine, R.; Freysz, E.; Shen, Y. R., Vibrational Spectroscopy of Water at the Vapor Water Interface. *Phys Rev Lett* **1993,** *70* (15), 2313-2316.

82.   Richmond, G. L., Molecular bonding and interactions at aqueous surfaces as probed by vibrational sum frequency spectroscopy. *Chem Rev* **2002,** *102* (8), 2693-2724.

83.   Mondal, J. A.; Nihonyanagi, S.; Yamaguchi, S.; Tahara, T., Structure and Orientation of Water at Charged Lipid Monolayer/Water Interfaces Probed by Heterodyne-Detected Vibrational Sum Frequency Generation Spectroscopy. *J Am Chem Soc* **2010,** *132* (31), 10656-10657.

84.   Leung, K.; Nielsen, I. M. B.; Criscenti, L., Elucidating the bimodal acid-base behavior of the water-silica interface from first principles. *Geochim Cosmochim Ac* **2010,** *74* (12), A584-A584.

85.   Shang, X. M.; Benderskii, A. V.; Eisenthal, K. B., Ultrafast solvation dynamics at silica/liquid interfaces probed by time-resolved second harmonic generation (vol 150B, pg 11578, 2001). *J Phys Chem B* **2001,** *105* (47), 11928-11928.

86.   Wang, H. F.; Borguet, E.; Eisenthal, K. B., Polarity of liquid interfaces by second harmonic generation spectroscopy. *J Phys Chem A* **1997,** *101* (4), 713-718.

87.   Steel, W. H.; Beildeck, C. L.; Walker, R. A., Solvent polarity across strongly associating interfaces. *J Phys Chem B* **2004,** *108* (41), 16107-16116.

88.   Cave, R. J.; Castner, E. W., Time-dependent density functional theory investigation of the ground and excited states of coumarins 102, 152, 153, and 343. *Journal of Physical Chemistry A* **2002,** *106* (50), 12117-12123.

89.   Boamah, M. D.; Ohno, P. E.; Geiger, F. M.; Eisenthal, K. B., Relative permittivity in the electrical double layer from nonlinear optics. *J Chem Phys* **2018,** *148* (22).

90.   Fumagalli, L.; Esfandiar, A.; Fabregas, R.; Hu, S.; Ares, P.; Janardanan, A.; Yang, Q.; Radha, B.; Taniguchi, T.; Watanabe, K.; Gomila, G.; Novoselov, K. S.; Geim, A. K., Anomalously low dielectric constant of confined water. *Science* **2018,** *360* (6395), 1339-+.

91.   Skelton, A. A.; Fenter, P.; Kubicki, J. D.; Wesolowski, D. J.; Cummings, P. T., Simulations of the Quartz(10(1)over-bar1)/Water Interface: A Comparison of Classical Force Fields, Ab Initio Molecular Dynamics, and X-ray Reflectivity Experiments. *J Phys Chem C* **2011,** *115* (5), 2076-2088.

92.   Scales, P. J.; Grieser, F.; Healy, T. W.; White, L. R.; Chan, D. Y. C., Electrokinetics of the Silica Solution Interface - a Flat-Plate Streaming Potential Study. *Langmuir* **1992,** *8* (3), 965-974.

93.   Horiuchi, H.; Nikolov, A.; Wasan, D. T., Calculation of the surface potential and surface charge density by measurement of the three-phase contact angle. *J Colloid Interf Sci* **2012,** *385*, 218-224.

94.   Shishkin, I.; Alon, T.; Dagan, R.; Ginzburg, P., Temperature and Phase Transition Sensing in Liquids with Fluorescent Probes. *Mrs Adv* **2017,** *2* (44), 2391-2399.

95.   Rick, S. W.; Haymet, A. D. J., Dielectric constant and proton order and disorder in ice Ih: Monte Carlo computer simulations. *J Chem Phys* **2003,** *118* (20), 9291-9296.

96.   Johari, G. P.; Whalley, E., The Dielectric-Properties of Ice Ih in the Range 272-133-K. *J Chem Phys* **1981,** *75* (3), 1333-1340.

97.   Eftekhari-Bafrooei, A.; Borguet, E., Effect of Electric Fields on the Ultrafast Vibrational Relaxation of Water at a Charged Solid-Liquid Interface as Probed by Vibrational Sum Frequency Generation. *J Phys Chem Lett* **2011,** *2* (12), 1353-1358.

CHAPTER THREE

SURFACE SOLVATION AND HINDERED ISOMERIZATION AT THE

WATER/SILICA INTERFACE EXPLORED WITH

SECOND HARMONIC GENERATION

<u>Contribution of Authors and Co-Authors</u>

Manuscript in Chapter 3:

Author: Grace E. Purnell

Contributions: Collected and analyzed all experimental data and authored manuscript

Co-Author: Robert A. Walker

Contributions: Assisted with data analysis and edited manuscript

Manuscript Information

Grace E. Purnell and Robert A. Walker

The Journal of Chemical Physics

CHAPTER THREE

SURFACE SOLVATION AND HINDERED ISOMERIZATION AT THE

WATER/SILICA INTERFACE EXPLORED WITH

SECOND HARMONIC GENERATION

3.1. Introduction

Water's complicated behavior at surfaces has attracted significant attention since the first nonlinear spectroscopic study of water's interfacial vibrational structure was published in the early 1990s.[81] In parallel, numerous studies of organic solvents at interfaces have shown that surfaces can significantly change the organization and properties of adjacent liquids from bulk solution limits.[2, 86-87, 98-99] For example, nonlinear optical experiments examining the silica-methanol interface showed conclusively that this interface is characterized by a distinctly nonpolar solvation region where the effective dielectric constant is ~2 (compared to methanol's bulk static dielectric constant $\varepsilon = 32.7$). Molecular dynamics simulations and complementary vibrational studies suggest that at the silica-methanol interface, solvent density is significantly reduced within ~1 nm of the interface, and the interfacial methanol solvent molecules create a bilayer-type structure where methyl groups in adjacent methanol solvent layers adopt anti-parallel orientation.[7] This organization creates an alkane-like sheet adjacent to the interface with a correspondingly low dielectric environment. Analogous results have been reported for the silica-acetonitrile interface.[100]

Water's extended long range ordering at surfaces and strong, directional hydrogen bonding raise similar questions about how anisotropic water structure impacts water's ability to solvate solutes at interfaces. Studies of structure and dynamics at water-air and water-quartz interfaces have sparked considerable debate as to the dielectric environment, pH and structural ordering of interfacial water rather than leading to a definitive consensus.[41, 89-90, 101-102] Despite considerable interest in the structure of interfacial water layering, however, surprisingly little work has considered the effect of water's unique structure at silica interfaces on the solvent's ability to solvate adsorbed solutes.[82-83, 103] In this context, the term solvation refers explicitly to noncovalent interactions between an adsorbed solute and its surrounding solvent. These interactions can be either nonspecific such as those described by polarizable continuum models or specific such as the localized, directional interactions including hydrogen bonding and other dipole-dipole attractions.[104-107]

A recent report examining the time resolved emission of Coumarin 152 (C152), a solvatochromic fluorescent dye, adsorbed at the silica-aqueous (pH 5.9) interface suggested that the adsorbed solute sampled a distinctly nonpolar solvation environment.[108] Specifically, fluorescence lifetimes measured from the silica-aqueous interface in a total internal reflection (TIR) geometry showed that C152 had a long-lived contribution more typical of C152 solvated in non-polar solvents such as alkanes or carbon tetrachloride. Coumarin 152 (Figure 3.1) derives its solvatochromic behavior from the +4 D change in dipole[72-73] and the
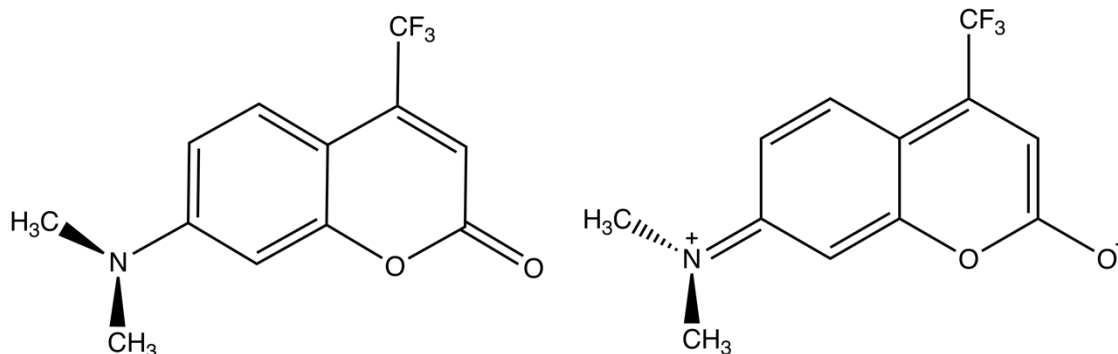
Figure 3.1: The structure of C152 in its ground state (left) and excited TICT state (right)

formation of a twisted intermolecular charge transfer (TICT) state upon

photoexcitation. The TICT state can only be solvated in polar dielectric

environments.[74, 80] Stabilization of the TICT state by polar solvents leads to a

much shorter fluorescence lifetime and a red shift in the fluorescence spectrum

relative to C152's behavior in nonpolar media (Figure 3.2).[73]

Given that water and silica are both polar materials, the existence of a

'nonpolar' fluorescence lifetime at the silica-aqueous interface is surprising. Two

possible explanations for this behavior were proposed: 1) the effective dielectric

permittivity at the aqueous-silica interface was reduced from its value in bulk

water of 80.4, consistent with reports from studies of water in confined spaces[90] or

2) strong hydrogen bonding between water and the silica substrate restricted

interfacial water's mobility so that solvent molecules at the surface could not

reorganize around photoexcited C152 to stabilize the TICT state, leading to a

longer fluorescence lifetime.[109-110]

Additional studies in the same report measured the fluorescence behavior

of C152 frozen in an ice matrix and reported lifetimes consistent with the
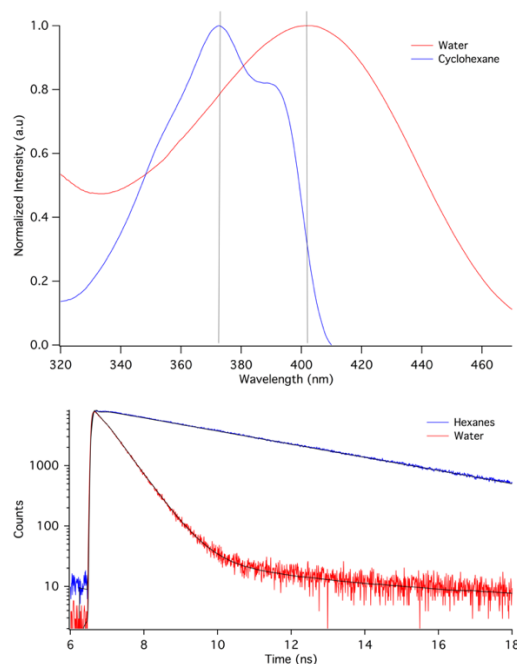
Figure 3.2: Top: Absorbance spectra of C152 in cyclohexane (blue) and water (red). Bottom: TCSPC decay curves for C152 in water (red) and in hexanes (blue)

interfacial TIR measurements. These data implied that either confinement or restricted solvation dynamics prevented C152 from isomerizing into a nonradiative TICT state upon photoexcitation and bolstered an explanation that solvation at silica-aqueous interfaces was controlled largely by immobilized solvent.

Interpretation of TIR time-resolved fluorescence measurements is hampered, however, by ambiguity about the solutes being excited. Given that fluorescence is not intrinsically surface specific *and* that the evanescent field of incident light propagates ~150 nm into the adjacent aqueous phase in the TIR geometry used in previous studies, one cannot definitively correlate observed responses to solutes directly adsorbed to the solid-liquid interface. In order to

resolve whether or not the silica-aqueous interface is truly nonpolar (with a low

effective static dielectric constant) *or* if interfacial solvation is due to restricted

solvent motion, experiments must be able to discriminate responses from solutes

in the interfacial region from those originating in the adjacent, isotropic bulk.

Data presented below report resonance enhanced second harmonic

generation (SHG) spectra from C152 molecules adsorbed to the silica-water

interface. Results show that C152's effective excitation wavelength at the silica-

aqueous interface is similar to that in bulk aqueous solution, supporting the idea

that solvation at the silica-aqueous interface is characterized by a high permittivity

but restricted solvent mobility. SHG is intrinsically sensitive only to molecules

subject to the anisotropy induced by an interface within the electric dipole

limit.[111-113] Furthermore, SHG and time resolved fluorescence data acquired from

C152 molecules adsorbed to a hydrophobic silica-water interface show a local

dielectric environment similar to what one would expect if interfacial solvation

were described by averaged contributions from the adjacent phases. Taken

together, resonance enhanced SHG spectroscopy and time-resolved fluorescence

measurements illustrate that strong solvent-substrate association can conspire to

create conflicting pictures of equilibrium and dynamic solvation.

3.2 Experimental

Laser grade Coumarin 152 was purchased and used as received from

Exciton. Water used in the experiments was nanopure, from a Millipore filtration

system, resistivity of 18.2 MΩ. Silica slides and experimental assemblies were

rinsed with methanol and DI water then soaked in a bath of 50/50 sulfuric/nitric

acid for no less than one hour, and rinsed with DI water and dried under nitrogen

before use. Experiments described in this work used saturated solutions of

Coumarin 152 in water, that were made by combining excess C152 and water and

allowing the solution to equilibrate with stirring overnight at 50°C. The solutions

were filtered to remove excess dye before use. At room temperature, the

concentration of C152 in a saturated aqueous solution is approximately 6 μM.

SHG spectra were collected from Kel-F sample chambers containing saturated

C152 solution in contact with fused silica slides (Structure Probe, Inc.). For TIR-

TCSPC measurements, a custom-built assembly was made from Kel-F sample

chambers containing saturated aqueous C152 solution in contact with fused silica

prisms (ISP Optics, Inc.), which allowed the excitation pulse to irradiate the

interface formed between a hemispherical prism and an aqueous solution at angles

greater than the critical angle (61° at 400 nm). Sample chambers, coumarin

solutions, silica slides and prisms were allowed to equilibrate for at least an hour

before being used in experiments.

Silica slides (Structure Probe, Inc.) and prisms (ISP Optics, Inc.) were

functionalized with a solution of dimethyldichlorosilane in THF to create

hydrophobic surfaces. Silica substrates were cleaned as described above and

allowed to sit in the silane solution at 30°C for 36 hours. Once removed from the

silane solution, silica slides and prisms were first washed with toluene, then

methanol and finally tested with water to verify that the surface was hydrophobic.

To collect TIR-TCSPC spectra, the output of a Ti:Sapphire oscillator (Chameleon, Coherent) was frequency doubled (APE Autotracker) and the 80 MHz repetition rate was attenuated to 4 MHz using an electro-optic modulator (Conoptics Model 350-105). Fluorescence emission was collected using a Picoquant 200 time-to-amplitude converter and the instrument response function (IRF) was measured using a non-emissive Ludox scattering solution. Emission was detected at 90˚ relative to the silica-aqueous interface. The TIR assembly's IRF was ~200 ps. For every experiment, the IRF was deconvoluted from the time-resolved emission histogram and the resulting trace was then fit to one or more single exponential decays. The minimum number of lifetimes required to accurately fit the data was determined using the Akaike information criterion.

In order to collect SHG signal from surface molecules, the coherent output from a tunable, amplified Ti:sapphire pumped optical parametric amplifier (OPA) at frequency ω is focused on the surface and creates a polarization of the surface molecules at 2ω. The intensity of the collected second harmonic signal is proportional to the square of the second order polarizability, denoted as $P^{(2)}$:

$$I(2\omega) \propto \left|P^{(2)}(2\omega)\right|^2 \tag{3.1}$$

where $P^{(2)} = \left|\chi^{(2)}E(\omega_1)E(\omega_2)\right|$. In the case of second harmonic generation, the incident beam is of a single frequency and $\omega_1 = \omega_2$. The surface specificity of SHG, along with all second order nonlinear optical techniques, derives from $\chi^{(2)}$, the second order nonlinear susceptibility. $\chi^{(2)}$ is a rank 3 tensor consisting of 27 matrix elements; in centrosymmetric systems, the requirement that $\chi^{(2)}_{i,j,k} = \chi^{(2)}_{-i,-j,-k}$ means that no second harmonic response will originate from an isotropic

solution within the electric dipole approximation. At an interface where symmetry is broken, elements of the $\chi^{(2)}$ tensor can take on non-zero values, dependent on the identity of the molecules at the interface. $\chi^{(2)}$ is composed of a non-resonant (NR) piece and a resonant (R) piece:

$$\chi^{(2)} = \chi_{NR}^{(2)} + \chi_R^{(2)} \qquad (3.2)$$

The non-resonant portion of the $\chi^{(2)}$ tensor is usually simple and can be fit to a single value whereas the resonant contribution is more complicated. The resonant portion of $\chi^{(2)}$ is equal to the number of molecules on the surface multiplied by the orientational average over the molecular hyperpolarizability (β) of the adsorbed molecules:

$$\chi_R^{(2)} = N\langle\beta_{i,j,k}\rangle, \text{ where } \beta \text{ is given by: } \beta = \frac{A}{\omega_0 - \omega - i\Gamma} \qquad (3.3)$$

In this expression for β, A is a constant related to the transition dipole moment of the electronic resonance being examined, ω_0 is the resonant frequency of the transition, ω is the frequency of the incident light, and Γ is the linewidth associated with the transition.

In cases where the interface under investigation carries a surface charge, the second harmonic spectral lineshape can be influenced by some non-resonant elements of the $\chi^{(3)}$ tensor, which makes equation (3.2) take the form:

$$\chi_{total}^{(2)} \propto \chi^{(2)} + (\chi_1^{(3)} + i\chi_2^{(3)})\Phi(0) \qquad (3.4)$$

where $\Phi(0)$ is the interfacial potential and both elements of the $\chi^{(3)}$ tensor are purely real.[114-115] Collected second harmonic spectra are fit with equations (3.2), (3.3) and (3.4) to determine the linewidth and the center of the resonant peak.

Resonance-enhanced SHG spectra were acquired from an experimental

assembly that has been described previously.[8-9] Briefly, ~3.3W from a Ti:Sapphire

regenerative amplifier (Libra-HE, Coherent, 85 fs pulses, 1 kHz repetition rate,

801 nm) was coupled to a visible optical parametric amplifier (Coherent OPerA

Solo, fwhm 10 nm) and focused on the sample. If necessary, incident visible light

was attenuated to below 4 mW with neutral density filters before it reached the

sample. Second harmonic signal was collected using a photomultiplier tube and

photon counting electronics. Data from each individual wavelength was collected

over 3-5 separate 10s intervals, background corrected and then averaged.

Typically, up to 300 counts were measured on resonance during a 10 sec.

acquisition.

3.3 Results and Discussion

Figure 3.3 shows the second harmonic spectrum of C152 at the

silica/aqueous interface. Also included on the opposite ordinate is C152's

absorbance spectrum in bulk water. The SHG data show clearly that the surface

spectrum experiences a bathochromic shift relative to the spectrum in bulk water,

with the resonance center at the surface measuring 405 nm, 7 nm higher than the

absorbance peak at 398 nm. This result includes the $\chi^{(3)}$ term in Eq. 4 above with

an assumed surface potential of 70-80 mV given an unbuffered, pH = 6 aqueous

solution.[114-116] (Omitting the $\chi^{(3)}$ contribution changes the calculated excitation

wavelength maximum by less than 1.5 nm.)
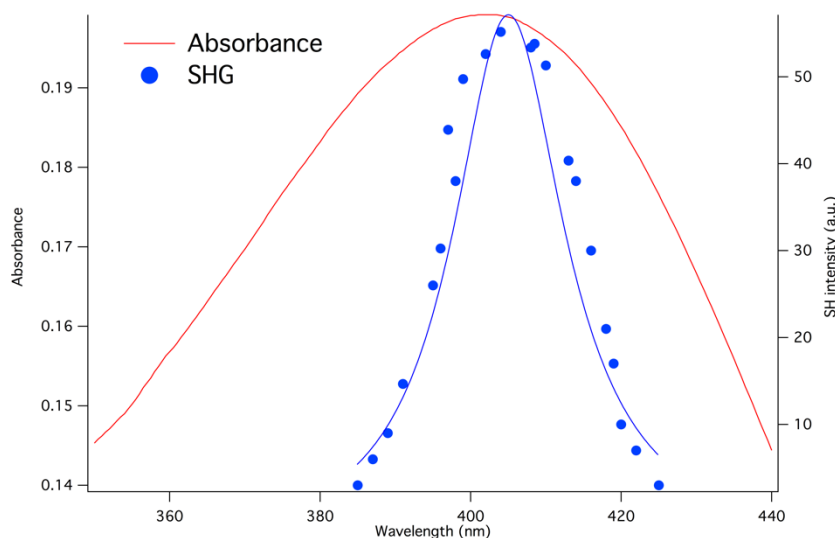
Figure 3.3: Absorbance of C152 in water (red) and the surface second harmonic spectrum of C152 at the water-silica interface (blue)

According to C152's well-characterized solvatochromic behavior, a red-shifted spectrum implies solvation in a more polar dielectric environment.[73] This result at the water-silica interface is consistent with experiments and calculations predicting that water molecules immobilized in a solid ice matrix can also create a more polar dielectric environment than that found in liquid water. Under the influence of dipole ordering introduced by the solid structure, ice's dielectric constant is reported to be between 78.2 and 107, depending on the ice structure and temperature.[95-96, 117] (Pure water has a dielectric constant of 80.4 at room temperature.)

Both experimental and computational results have suggested that water molecules within 10 Å of a silica surface experience a hexagonal ordering analogous to water molecules frozen in a solid state.[37, 54, 118] The alignment of dipoles at the surface induces the coumarin to display spectroscopic evidence of a

more polar *static,* dielectric environment at the surface than in bulk. At the silica-aqueous interface, all of the water dipoles are aligned in the same direction for the first 2-3 solvent layers.[46, 54] We propose that this anisotropic solvent dipole ordering leads to a local permittivity greater than that of an isotropic arrangement of the same solvent in bulk solution. Given these considerations, the fluorescence signatures reported in Chapter 2 are unlikely to originate from any sort of non-polar environment (with an effective alkane-like static dielectric constant). Instead, since the SHG spectrum of the silica-aqueous interface indicates that the molecular dipoles of water are highly arranged under the influence of hydrogen bonds to the silica surface with a high static dielectric constant, a more likely explanation for the long lifetime in C152 fluorescence is that restricted solvent reorientation dynamics are too slow to enable formation of C152's nonradiative TICT state. Taken together, the SHG data imply a very polar static environment but the TIR (and bulk ice) fluorescence measurements suggest slower dynamic solvation than found in bulk solution. These results are not surprising given interfacial water rotational correlation times reported to be as much as 40 times slower at the surface than in bulk solution.[109-110]

At the silica-aqueous interface, time-resolved fluorescence spectra of C152 show a very long fluorescence lifetime, generally resulting from C152 solvated in nonpolar solvents such as alkanes. Since the SHG results presented here confirm that the silica-aqueous interface is indeed polar, we conclude that the fluorescence results derive from restricted solvation at the interface and not from any reduction in the interfacial static

polarity. Furthermore, if this description is accurate, we expect that disrupting the ability of water to hydrogen bond to the silica surface will cause the static solvation environment sampled in SHG experiments and the time-dependent solvation interactions probed by TIR-time resolved fluorescence to be more consistent with each other.

In order to disrupt the strong ordering effects of the silica surface on adjacent water structure and dynamics, we functionalized silica slides with a dimethylsilane to create nonpolar, methyl terminated silica surfaces,[3, 119] and performed SHG and TIR-TCSPC measurements of C152 adsorbed to this hydrophobic silica-water boundary. Figure 3.4 shows the SHG spectrum of C152 adsorbed to the hydrophobic silica-aqueous interface. The same SHG spectrum of C152 adsorbed to the *hydrophilic* silica-aqueous interface first shown in Figure 3.2 is reproduced for comparison. At the hydrophobic-aqueous aqueous interface, C152's SHG spectrum shows strong resonance enhancement with an excitation wavelength maximum of 389 nm, considerably blue-shifted from the 405 nm measured at the unmodified hydrophilic silica-aqueous surface and from the 398 nm measured in bulk aqueous solution. This hydrophobic silica-aqueous excitation wavelength is consistent with a local solvation environment similar to that found in bulk polar organic solvents such as ethyl acetate and acetone.[73] Furthermore, this result is also consistent with expectations that a hydrophobic surface and a polar solvent would create an interfacial solvation environment that reflected averaged contributions from the two phases.[86, 120]
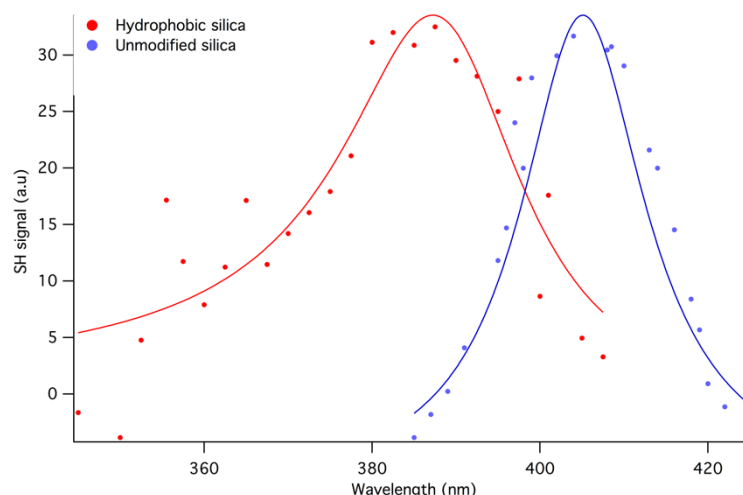
Figure 3.4: SHG spectra of C152 at the hydrophilic (blue) and hydrophobic (red) silica interface

The SHG spectrum acquired from this hydrophobic-aqueous interface is broader than that measured at the unmodified silica-aqueous interface, with a linewidth of 26 nm compared to 19 nm at the hydrophilic interface. This spectral broadening usually indicates a heterogeneous solvation environment.[121] The fact that the linewidth for C152 at the unmodified silica interface is narrower than that at the hydrophobic interface implies that the unmodified silica-water interface exhibits some degree of order that prevents further inhomogeneous broadening relative to what is observed at the hydrophobic interface.

The SHG data show clearly that C152 adsorbed to the hydrophobic silica-aqueous interface samples a less polar environment, indicating that disrupting the strong substrate-solvent interactions diminishes the local polarity. The consequences of this disrupted interfacial solvent structure on C152's

isomerization can also be observed in the TIR-TCSPC measurements shown in Figure 3.5. These experiments were performed using hemispherical silica prisms that had been functionalized with dimethylsilane in the same manner as the silica slides used for SHG experiments. Also shown in Figure 3.5 for comparison is the time-resolved fluorescence from C152 adsorbed to the hydrophilic silica-aqueous interface.
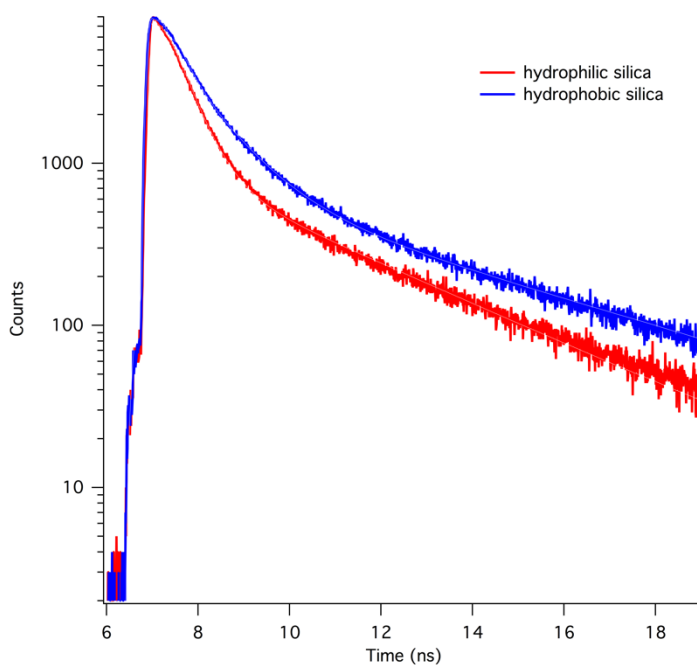
Figure 3.5: TIR-TCSPC traces of C152 at the hydrophobic (blue) and hydrophilic silica-aqueous interface (red)

As previously reported, for a saturated solution of C152 in water at the unmodified silica-aqueous interface, two fluorescence lifetimes are seen—87% of the decay corresponds to C152 solvents in contact with bulk water with a lifetime of .47ns and 13% from solutes in contact with the silica surface with a lifetime of 3.52ns.[108] The longer lifetime is similar to C152's single, ~4 ns lifetime in

nonpolar media. At the hydrophobic silica-aqueous interface, fluorescence decays

cannot be fit with less than 3 lifetimes. 72% of the decay still derives from C152

solutes dissolved in bulk water solution, with a lifetime of .45ns. 4% of the decay

fits to a longer fluorescence lifetime of 4.25ns, either from solutes held by

hydrogen bonds at defects in the hydrophobic surface layer, or from molecules

completely excluded from water by the nonpolar molecules on the silica surface.

The third lifetime seen at this interface composes 24% of the total decay and

corresponds to a new lifetime of .93ns, typically attributed to C152 in a polar,

hydrogen bonding solvent similar to methanol. These results are summarized in

Table 3.1. Considering the structure of the hydrophobic silica-aqueous interface,

this additional lifetime is sensible. The silica surface is composed of a layer of

terminal methyl groups and the interfacial water solvent is expected to diminish in

density and to be considerably less ordered.[122-123]

	A_1	τ_1 (ns)	A_2	τ_2 (ns)	A_3	τ_3 (ns)
Hydrophobic silica	72%	0.45	4%	4.25	24%	0.93
Hydrophilic silica	87%	0.47	13%	3.52	n/a	n/a

Table 3.1 Fluorescence lifetimes and amplitudes of C152 adsorbed to aqueous-hydrophilic and aqueous-hydrophobic interfaces as measured by TIR-TCSPC. Lifetime data assigned to bulk solvated solutes are reported as A_1 and A_2.

The additional lifetime also makes the SHG and TIR-TCSPC results from

the hydrophobic interface much more internally consistent relative to the

apparently conflicting findings from the hydrophilic interface. The SHG results at

the hydrophobic silica interface indicate a dielectric environment similar to that of

bulk acetone (ε=20.7), while the time-resolved fluorescence data indicate a polar, protic solvation environment similar to that of methanol.

3.4 Conclusions

The results presented in this work create a more nuanced picture of water's solvation properties at hydrophilic and hydrophobic silica-aqueous interfaces. Previous results indicated that solute isomerization was impeded at hydrophilic silica-aqueous interfaces and implied that the interface had distinctive nonpolar character. Resonance enhanced SHG spectra of adsorbed C152 show that the hydrophilic silica-aqueous interface is, in fact, characterized by a strong local dielectric constant. The restricted solute isomerization, then, likely reflects slower solvent reorientation dynamics resulting from strong water-silica association. Disrupting these solvent-substrate interactions leads to static and dynamic interfacial solvation properties that more closely mirror each other.

3.5 References

2.   Steel, W. H.; Walker, R. A., Measuring dipolar width across liquid-liquid interfaces with 'molecular rulers'. *Nature* **2003,** *424* (6946), 296-299.

3.   Zhang, X. Y.; Esenturk, O.; Walker, R. A., Reduced polarity in protic solvents near hydrophobic solid surfaces. *J Am Chem Soc* **2001,** *123* (43), 10768-10769.

7.   Roy, D.; Liu, S. L.; Woods, B. L.; Siler, A. R.; Fourkas, J. T.; Weeks, J. D.; Walker, R. A., Nonpolar Adsorption at the Silica/Methanol Interface: Surface Mediated Polarity and Solvent Density across a Strongly Associating Solid/Liquid Boundary. *J Phys Chem C* **2013,** *117* (51), 27052-27061.

8.   Woods, B. L.; Walker, R. A., pH Effects on Molecular Adsorption and Solvation of p-Nitrophenol at Silica/Aqueous Interfaces. *J Phys Chem A* **2013,** *117* (29), 6224-6233.

9.   Woods, B. L.; George, J. K.; Sherman, A. M.; Callis, P. R.; Walker, R. A., Adsorption and Aggregation at Silica/Methanol Interfaces: The Role of Solute Structure. *J Phys Chem C* **2015,** *119* (25), 14230-14238.

37.   Du, Q.; Freysz, E.; Shen, Y. R., Vibrational-Spectra of Water-Molecules at Quartz Water Interfaces. *Phys Rev Lett* **1994,** *72* (2), 238-241.

41.   Nihonyanagi, S.; Yamaguchi, S.; Tahara, T., Water Hydrogen Bond Structure near Highly Charged Interfaces Is Not Like Ice. *J Am Chem Soc* **2010,** *132* (20), 6867-+.

46.   Gupta, P. K.; Meuwly, M., Dynamics and vibrational spectroscopy of water at hydroxylated silica surfaces. *Faraday Discuss* **2013,** *167*, 329-346.

54.   Shen, Y. R.; Ostroverkhov, V., Sum-frequency vibrational spectroscopy on water interfaces: Polar orientation of water molecules at interfaces. *Chem Rev* **2006,** *106* (4), 1140-1154.

72.   Dahiya, P.; Kumbhakar, M.; Mukherjee, T.; Pal, H., Effect of protic solvents on twisted intramolecular charge transfer state formation in coumarin-152 and coumarin-481 dyes. *Chem Phys Lett* **2005,** *414* (1-3), 148-154.

73.   Nad, S.; Kumbhakar, M.; Pal, H., Photophysical properties of coumarin-152 and coumarin-481 dyes: Unusual behavior in nonpolar and in higher polarity solvents. *Journal of Physical Chemistry A* **2003,** *107* (24), 4808-4816.

74.   Arbeloa, T. L.; Arbeloa, F. L.; Estevez, M. J. T.; Arbeloa, I. L., Binary Solvent Effects on the Absorption and Emission of 7-Aminocoumarins. *J Lumin* **1994,** *59* (6), 369-375.

80.   Corrie, J. E. T.; Munasinghe, V. R. N.; Rettig, W., Synthesis and fluorescence properties of substituted 7-aminocoumarin-3-carboxylate derivatives. *J Heterocyclic Chem* **2000,** *37* (6), 1447-1455.

81.   Du, Q.; Superfine, R.; Freysz, E.; Shen, Y. R., Vibrational Spectroscopy of Water at the Vapor Water Interface. *Phys Rev Lett* **1993,** *70* (15), 2313-2316.

82.   Richmond, G. L., Molecular bonding and interactions at aqueous surfaces as probed by vibrational sum frequency spectroscopy. *Chem Rev* **2002,** *102* (8), 2693-2724.

83.   Mondal, J. A.; Nihonyanagi, S.; Yamaguchi, S.; Tahara, T., Structure and Orientation of Water at Charged Lipid Monolayer/Water Interfaces Probed by Heterodyne-Detected Vibrational Sum Frequency Generation Spectroscopy. *J Am Chem Soc* **2010,** *132* (31), 10656-10657.

86.   Wang, H. F.; Borguet, E.; Eisenthal, K. B., Polarity of liquid interfaces by second harmonic generation spectroscopy. *J Phys Chem A* **1997,** *101* (4), 713-718.

87.   Steel, W. H.; Beildeck, C. L.; Walker, R. A., Solvent polarity across strongly associating interfaces. *J Phys Chem B* **2004,** *108* (41), 16107-16116.

89.   Boamah, M. D.; Ohno, P. E.; Geiger, F. M.; Eisenthal, K. B., Relative permittivity in the electrical double layer from nonlinear optics. *J Chem Phys* **2018,** *148* (22).

90.   Fumagalli, L.; Esfandiar, A.; Fabregas, R.; Hu, S.; Ares, P.; Janardanan, A.; Yang, Q.; Radha, B.; Taniguchi, T.; Watanabe, K.; Gomila, G.; Novoselov, K. S.; Geim, A. K., Anomalously low dielectric constant of confined water. *Science* **2018,** *360* (6395), 1339-+.

95.   Rick, S. W.; Haymet, A. D. J., Dielectric constant and proton order and disorder in ice Ih: Monte Carlo computer simulations. *J Chem Phys* **2003,** *118* (20), 9291-9296.

96.   Johari, G. P.; Whalley, E., The Dielectric-Properties of Ice Ih in the Range 272-133-K. *J Chem Phys* **1981,** *75* (3), 1333-1340.

98.   Reymond, F.; Fermin, D.; Lee, H. J.; Girault, H. H., Electrochemistry at liquid/liquid interfaces: methodology and potential applications. *Electrochim Acta* **2000,** *45* (15-16), 2647-2662.

99.   Zhang, X. Y.; Walker, R. A., Discrete partitioning of solvent permittivity at liquid-solid interfaces. *Langmuir* **2001,** *17* (15), 4486-4489.

100.   Berne, B. J.; Fourkas, J. T.; Walker, R. A.; Weeks, J. D., Nitriles at Silica Interfaces Resemble Supported Lipid Bilayers. *Accounts Chem Res* **2016,** *49* (9), 1605-1613.

101.   Leung, K.; Nielsen, I. M. B.; Criscenti, L. J., Elucidating the Bimodal Acid-Base Behavior of the Water-Silica Interface from First Principles. *Journal of the American Chemical Society* **2009,** *131* (51), 18358-18365.

102.   Dalstein, L.; Potapova, E.; Tyrode, E., The elusive silica/water interface: isolated silanols under water as revealed by vibrational sum frequency spectroscopy. *Phys Chem Chem Phys* **2017,** *19* (16), 10343-10349.

103.   Isaienko, O.; Borguet, E., Hydrophobicity of Hydroxylated Amorphous Fused Silica Surfaces. *Langmuir* **2013,** *29* (25), 7885-7895.

104.   Brindza, M. R.; Walker, R. A., Differentiating Solvation Mechanisms at Polar Solid/Liquid Interfaces. *J Am Chem Soc* **2009,** *131* (17), 6207-6214.

105.   Shin, S.; Willard, A. P., Water's Interfacial Hydrogen Bonding Structure Reveals the Effective Strength of Surface-Water Interactions. *Journal of Physical Chemistry B* **2018,** *122* (26), 6781-6789.

106.   Zaera, F., Probing Liquid/Solid Interfaces at the Molecular Level. *Chem Rev* **2012,** *112* (5), 2920-2986.

107.   Sohrabpour, Z.; Kearns, P. M.; Massari, A. M., Vibrational Sum Frequency Generation Spectroscopy of Fullerene at Dielectric Interfaces. *J Phys Chem C* **2016,** *120* (3), 1666-1672.

108.   Purnell, G. E.; Walker, R. A., Hindered Isomerization at the Silica/Aqueous Interface: Surface Polarity or Restricted Solvation? *Langmuir* **2018,** *34* (34), 9946-9949.

109.   Milischuk, A. A.; Ladanyi, B. M., Structure and dynamics of water confined in silica nanopores. *J Chem Phys* **2011,** *135* (17).

110.   Warne, M. R.; Allan, N. L.; Cosgrove, T., Computer simulation of water molecules at kaolinite and silica surfaces. *Phys Chem Chem Phys* **2000,** *2* (16), 3663-3668.

111.   Bloembergen, N., 2nd Harmonic Reflected Light. *Opt Acta* **1966,** *13* (4), 311-+.

112.   Eisenthal, K. B., Second harmonic spectroscopy of aqueous nano- and microparticle interfaces. *Chem Rev* **2006,** *106* (4), 1462-1477.

113.   Heinz, T. F.; Chen, C. K.; Ricard, D.; Shen, Y. R., Spectroscopy of Molecular Monolayers by Resonant 2nd-Harmonic Generation. *Phys Rev Lett* **1982,** *48* (7), 478-481.

114.   Ohno, P. E.; Wang, H. F.; Geiger, F. M., Second-order spectral lineshapes from charged interfaces. *Nat Commun* **2017,** *8*.

115.   Ohno, P. E.; Saslow, S. A.; Wang, H. F.; Geiger, F. M.; Eisenthal, K. B., Phase-referenced nonlinear spectroscopy of the alpha-quartz/water interface. *Nat Commun* **2016,** *7*.

116.   Lowe, B. M.; Skylaris, C. K.; Green, N. G.; Shibuta, Y.; Sakata, T., Calculation of surface potentials at the silica-water interface using molecular dynamics: Challenges and opportunities. *Jpn J Appl Phys* **2018,** *57* (4).

117.   Aragones, J. L.; MacDowell, L. G.; Vega, C., Dielectric Constant of Ices and Water: A Lesson about Water Interactions. *Journal of Physical Chemistry A* **2011,** *115* (23), 5745-5758.

118.   Bouhadja, M.; Skelton, A. A., Dynamical Properties of Water and Ions at the Quartz (101)-Water Interface at a Range of Solution Conditions: A Classical Molecular Dynamics Study. *J Phys Chem C* **2018,** *122* (3), 1535-1546.

119.   Horng, P.; Brindza, M. R.; Walker, R. A.; Fourkas, J. T., Behavior of Organic Liquids at Bare and Modified Silica Interfaces. *J Phys Chem C* **2010,** *114* (1), 394-402.

120.   Wang, H. F.; Borguet, E.; Eisenthal, K. B., Generalized interface polarity scale based on second harmonic spectroscopy. *J Phys Chem B* **1998,** *102* (25), 4927-4932.

121.   Benjamin, I., Inhomogeneous broadening of electronic spectra at liquid interfaces. *Chem Phys Lett* **2011,** *515* (1-3), 56-61.

122.   Tyrode, E.; Liljeblad, J. F. D., Water Structure Next to Ordered and Disordered Hydrophobic Silane Monolayers: A Vibrational Sum Frequency Spectroscopy Study. *J Phys Chem C* **2013,** *117* (4), 1780-1790.

123.   Lee, S. H.; Rossky, P. J., A Comparison of the Structure and Dynamics of Liquid Water at Hydrophobic and Hydrophilic Surfaces - a Molecular-Dynamics Simulation Study. *J Chem Phys* **1994,** *100* (4), 3334-3345.

CHAPTER FOUR

BURIED LIQUID INTERFACES AS A FORM OF CHEMISTRY IN CONFINEMENT:

THE CASE OF 4-DIMETHYLAMINOBENZONITRILE AT THE

SILICA-AQUEOUS INTERFACE

Contribution of Authors and Co-Authors

Manuscript in Chapter 4:

Author: Grace E. Purnell

Contributions: Collected and analyzed experimental data and authored manuscript

Author: Marshall T. McNally

Contributions: Collected second harmonic data

Author: Patrik R. Callis

Contributions: Assisted in performing computational calculations and analysis. Assisted in editing manuscript.

Co-Author: Robert A. Walker

Contributions: Assisted with data analysis and edited manuscript

Manuscript Information

Grace E. Purnell, Marshall T. McNally, Patrik R. Callis and Robert A. Walker

CHAPTER FOUR

BURIED LIQUID INTERFACES AS A FORM OF CHEMISTRY IN CONFINEMENT:

THE CASE OF 4-DIMETHYLAMINOBENZONITRILE AT

THE SILICA-AQUEOUS INTERFACE

4.1 Introduction

Chemical reactivity at buried liquid interfaces differs from bulk solution limits in

ways that affect processes as diverse as biological recognition[17-20] and photocatalysis.[21-22]

These effects arise from a surface's ability to change solvent phase stability criteria,[124-125]

as well as solvent polarity[1-4] and viscosity.[5-7] As a result, chemical transformations such

as simple substitution reactions and Diels-Alder additions can see rate constants change

by as much as five orders of magnitude or more.[10-12] Surface-mediated solvent properties

also facilitate structural rearrangements[13] and enable reactions not possible in bulk

solution.[23]

Of particular interest is solute isomerization at liquid-solid,[14-15] and liquid-liquid[16]

interfaces. Isomerization reactions are important mediators of protein structure-function

relationships, and isomerization also plays an important role controlling conducting

polymer properties and pharmacological activity.[126-128] While surface effects on solution

phase surface-chemistry are clear, anticipating these effects a priori is not trivial. Results

presented in this work show that aqueous-silica interfaces slow photoisomerization of

adsorbed solutes in a way similar to that of solutes in confinement. This effect is

attributed to strong hydrogen bonding between the interfacial solvent and silica substrate,

creating an effective cage-like environment that restricts large amplitude solute motion despite the fact that local dielectric properties should promote isomerization.

Interfacial properties of liquids, especially at strongly associating buried interfaces have proven challenging to categorize. In alcohols, strong hydrogen bonding between surface silanols and the solvent creates a non-polar region that extends a nanometer or more away from the interface due to ordering of the non-polar hydrocarbon tails.[3, 24, 85] This effect is apparent for silica surfaces in contact with methanol where the first two solvent layers adopt an antiparallel structure creating reduced solvent density and an alkane-like static dielectric environment.[7, 9, 25] Silica has similar effects on nitrile solvent organization but with different consequences. At a hydrophilic silica surface, acetonitrile adopts a repeating bilayer type structure that extends more than 4 nm into the bulk liquid and the local solvation environment appears even more polar than bulk solution limits.[27]

Silica's surface properties including its isoelectric point, acidity and surface composition can vary depending on the material's processing and history,[129-131] but in general, silica surfaces are generally quite acidic with a point of zero charge at approximately pH = 2.0[51, 132], and studies have shown that silica functions much more effectively as a hydrogen bond donor rather than a hydrogen bond acceptor.[104] As a result, silica's effect on an adjacent solvent must consider both localized, directional forces (e.g. hydrogen bonding) as well as more general Coulomb and dipolar interactions and the constraints that come with a restricted dynamic surface structure.

Recent studies have reported that the silica-aqueous interface impedes isomerization of a coumarin solute, 7-(dimethylamino)-4-trifluoromethylchromen-2-one, or coumarin 152 (C152).[108, 133] In polar protic solvents, C152 is thought to form a nonradiative twisted, intramolecular charge transfer (TICT) state upon photoexcitation.[73] This isomerization shortens C152's radiative lifetime from ~3.5 ns (in nonpolar solvents) to $\leq$ 1 ns in solvents such as methanol and water. Total internal reflection, time-resolved fluorescence measurements carried out with C152 adsorbed to the silica-aqueous interface show that surface C152 has a lifetime similar to that in alkanes.

Water – unlike methanol – cannot form a nonpolar solvation region at the hydrophilic silica – aqueous interface, and surface specific second harmonic generation experiments showed clearly that the silica-aqueous interface is (slightly) more polar than bulk solution. This paradox was reconciled by proposing that strong hydrogen bonding between water and the silica surface restricts solvent motion and its ability to stabilize C152's TICT state, although the adsorbed solute cavity still experiences strong internal electric fields (i.e. high polarity).

To test this idea that solvent-substrate interactions across the aqueous-silica interface can impede solute isomerization, we applied the methods described above to examine the photophysical behavior of N,N-dimethylaminobenzonitrile (DMABN) adsorbed to the silica-aqueous interface. DMABN was chosen, in part, because of its extensively characterized isomerization following photoexcitation. While some questions linger about the exact nature of C152's solvent-dependent excited state

structure,[76-77] a broad consensus of researchers believe that DMABN forms an emissive

TICT state in protic and aprotic polar solvents.

4-dimethylaminobenzonitrile (DMABN) (Figure 4.1) first attracted attention in

1962 in a report by Lippert et al. that described the solute's anomalous dual fluorescence

in polar solvents.[134] DMABN exhibits 2 fluorescence emission bands; the first, termed

the locally excited (LE) or $1L_b$ fluorescence band, is not sensitive to solvent polarity and

appears around 350 nm in all solvents. The second fluorescence band, the anomalous or

$1L_a$, is strongly solvatochromic and appears between 440 and 520 nm, depending on

solvent polarity (Figure 4.2b). Since the first report of DMABN's dual fluorescence, the

nature of the ^1L_a band has been the subject of intense discussion. Lippert and co-workers

first assigned the ^1L_a fluorescence band of DMABN to a solvent stabilized inversion of

excited state energies that would lower the energy of the excited state producing the long

wavelength fluorescence below the energy of the locally excited state whence the typical

short wavelength emission derives. Given the highly dipolar nature of the excited state,

this inversion can only happen in polar solvents that stabilize charge separation on the

excited molecule.

This explanation was abandoned after further experimental evidence, and other

researchers have since proposed alternate explanations for the dual fluorescence of

DMABN, including a solvent exciplex,[61-62] dimer excitation,[63] a pseudo-Jahn Teller

(PJT) effect,[135] and a twisted intramolecular charge transfer (TICT) state.[69] In recent

years, other geometries of a charge-transfer state, including a planar intramolecular
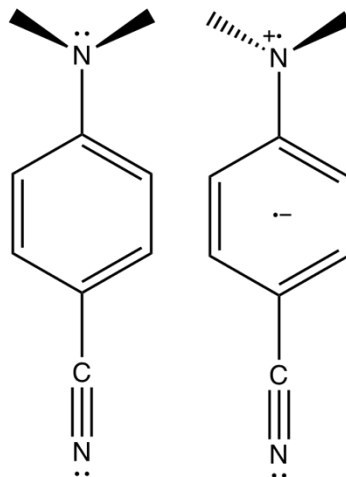
Figure 4.1 Structure of 4-dimethylaminobenzonitrile (left) and proposed structure of its excited TICT state (right)

charge transfer state[64-65] (PICT), a rehybridized intramolecular charge transfer state[66-68] (RICT), and a wagged intramolecular charge transfer state[136] (WICT) have all been proposed on the basis of energy calculations and experiments, but the TICT state explanation has the broadest body of experimental support. DMABN is the prototypical model of the donor-acceptor twisted charge-transfer reaction because its early discovery and simple molecular structure allow its photophysics to be well understood.[59, 69, 137-138]

In the work presented below, we examine the photophysical behavior of DMABN adsorbed to aqueous-silica interfaces. TIR-TCSPC measurements show that photoexcited DMABN at the strongly associating aqueous-silica interface does not decay through its TICT state, as would be expected in bulk aqueous solution. Instead, TIR time-resolved emission measurements show that adsorbed DMABN relaxes with a lifetime more characteristic of the LE state implying a locally nonpolar solvation environment. To test the local dielectric environment at the aqueous-silica interface, we employed resonance enhanced SHG to measure the effective excitation wavelength of adsorbed DMABN.

Interestingly, SHG spectra showed strong resonance enhancement at 340 nm, a wavelength corresponding to the S_0—S_1 transition that is only very weakly observed in absorbance and fluorescence excitation spectra. In contrast, the strongly allowed S_0—S_2 transition
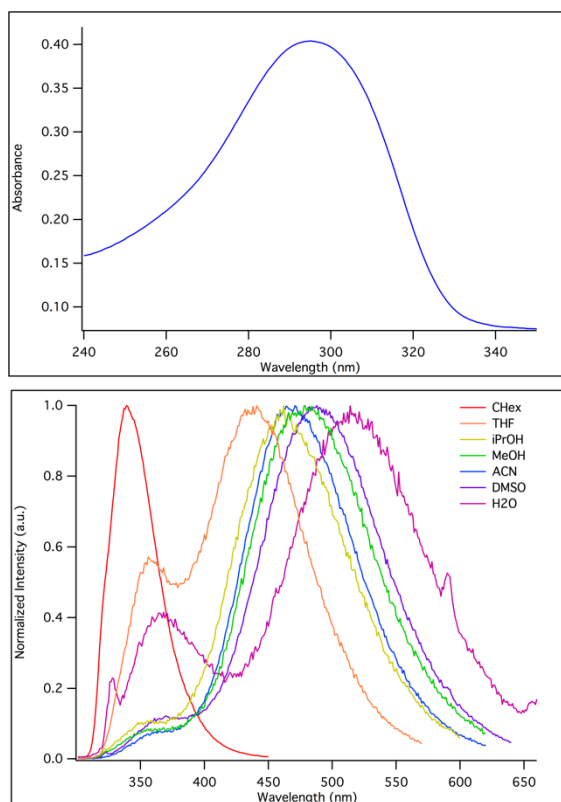
Figure 4.2 Absorbance of DMABN in water (top) and normalized DMABN fluorescence emission spectra (bottom) in selected solvents.

commonly used to photoexcite DMABN (at 290 nm) showed only a very weak NLO response. Electronic structure calculations suggest that these observations are consistent with both a distorted DMABN ground state geometry and strong local electric fields perturbing adsorbed DMABN's ground state electronic structure. Taken together, results

74

from experiments and calculations illustrate how surface induced changes in solvent structure can fundamentally change a solute's reactivity from bulk solution limits.

4.2 Experimental Methods

4-dimethlyaminobenzonitrile was purchased from Sigma Aldrich and used as received. Water used in the experiments was nanopure, from a Millipore filtration system and had a resistivity of 18.2 MΩ. Silica substrates and experimental assemblies were rinsed with methanol and DI water then soaked in a bath of 50/50 sulfuric/nitric acid for no less than one hour, and rinsed with DI water and dried under nitrogen before use. SHG spectra were collected from Kel-F sample chambers containing aqueous DMABN solution in contact with fused silica slides (Structure Probe, Inc.). For TIR-TCSPC measurements, a custom-built assembly was made from Kel-F sample chambers containing aqueous DMABN solution in contact with fused silica hemispheres (ISP Optics, Inc.), that allowed the excitation pulse to irradiate the interface formed between a hemispherical prism and an aqueous solution at angles greater than the critical angle (65° at 290 nm). Sample chambers, DMABN solutions, and silica slides/prisms were allowed to equilibrate for at least an hour before being irradiated.

Silica slides (Structure Probe, Inc.) and prisms (ISP Optics, Inc.) were functionalized according to previously published methods[3, 119] with a solution of dichlorodimethylsilane in toluene to create hydrophobic surfaces. These samples were created to test the role that silica hydrogen bonding played in controlling DMABN isomerization. Fresh silica substrates were cleaned as described above and allowed to sit in a 3% silane solution at 130°C for 36 hours. This procedure reliably leads to water

contact angles of 100˚. Once removed from the silane solution, silica slides and prisms were first washed with toluene, then methanol and finally tested with water to verify that the surface was hydrophobic. Slides were used within 24 hours of silanization to ensure consistency of the monolayer.

To collect TCSPC spectra, the output of a Ti:Sapphire oscillator (Chameleon, Coherent) was frequency doubled (APE Autotracker) and the 80 MHz repetition rate was attenuated to 4 MHz using an electro-optic modulator (Conoptics Model 350-105). Fluorescence emission was collected using a Picoquant 200 time-to-amplitude converter and the instrument response function (IRF) was measured using a non-emissive Ludox scattering solution. In bulk solution, the IRF is between 20-50 ps. For TCSPC in a total internal reflection (TIR) geometry, emission was detected at 90˚ relative to the silica-aqueous interface. The TIR assembly's IRF was < 200 ps. For every experiment, the IRF was deconvoluted from the time-resolved emission histogram and the resulting trace was then fit to one or more single exponential decays:

$$I(t) = \sum_{i=1}^{n} A_i e^{\frac{-t}{\tau_i}} \tag{4.1}$$

where A is the amplitude of the florescence lifetime, t is time since the excitation pulse and τ is the fluorescence lifetime. The minimum number of lifetimes required to accurately fit the data was determined using the Akaike information criterion.[139]

In order to collect SHG signal from surface molecules, the coherent output from a tunable Ti:Sapphire-pumped optical parametric amplifier (OPA) (Coherent, OPerA Solo) at frequency ω is focused on the surface and creates surface polarization at frequency 2ω. SH data were acquired using a $P_{2\omega}P_{\omega}$ polarization scheme. The intensity of the collected

second harmonic signal is proportional to the square of the second order polarizability, denoted as $P^{(2)}$:

$$I(2\omega) \propto \left| P^{(2)}(2\omega) \right|^2 \tag{4.2}$$

where $P^{(2)} = \left| \chi^{(2)} E(\omega_1) E(\omega_2) \right|$ for a generalized second order nonlinear polarization. In the case of second harmonic generation $\omega_1 = \omega_2$. The surface specificity of SHG, along with all second order nonlinear optical techniques, derives from $\chi^{(2)}$, the second order nonlinear susceptibility. $\chi^{(2)}$ is a rank 3 tensor consisting of 27 matrix elements; in centrosymmetric systems, the requirement that $\chi^{(2)}_{i,j,k} = \chi^{(2)}_{-i,-j,-k}$ means that, within the electric dipole approximation, no second harmonic response will originate from an isotropic solution, as the only way to make the equality above true is for $\chi^{(2)}$ to equal zero. At an interface where symmetry is broken, elements of the $\chi^{(2)}$ tensor can take on non-zero values. $\chi^{(2)}$ is composed of a non-resonant (NR) piece and a resonant (R) piece:

$$\chi^{(2)} = \chi^{(2)}_{NR} + \chi^{(2)}_R \tag{4.3}$$

The non-resonant portion of the $\chi^{(2)}$ tensor is often fit to a single value whereas the resonant contribution is more complicated. The resonant portion of $\chi^{(2)}$ is equal to the number of molecules at the surface multiplied by the orientational average over the molecular hyperpolarizability (β) of the adsorbed molecules:

$$\chi^{(2)}_R = N \langle \beta_{i,j,k} \rangle, \tag{4.4}$$

where β is given by: $\beta = \dfrac{A}{\omega_0 - \omega - i\Gamma}$

In this expression for β, A is a constant related to the transition dipole moment and the two photon polarizability[36] of the electronic resonance being examined, ω_0 is the

resonant frequency of the transition, ω is the frequency of the incident light, and Γ is the

linewidth associated with the transition.

When surfaces are charged (as is the case for silica in contact with Millipore

water, pH = 5.8), the second harmonic spectral lineshape can be influenced other

contributions to the nonlinear polarization, namely elements of the $\chi^{(3)}$ tensor, that

modify equation (4.2) take the form:

$$\chi^{(2)}_{total} \propto \chi^{(2)} + (\chi^{(3)}_1 + i\chi^{(3)}_2)\Phi(0) \tag{4.5}$$

Here Φ(0) is the interfacial potential and both elements of the $\chi^{(3)}$ tensor are purely

real.[114-115] Collected second harmonic spectra are fit with equations (4.3), (4.4) and (4.5)

to determine the linewidth and the center of the resonantly enhanced transition

wavelength.

Resonance-enhanced SHG spectra were acquired from an experimental assembly

that has been described previously.[8-9] Briefly, ~3.3W from a Ti:Sapphire regenerative

amplifier (Libra-HE, Coherent, 85 fs pulses, 1 kHz repetition rate, 801 nm) pumped a

visible optical parametric amplifier (Coherent OPerA Solo, fwhm 10 nm) and focused on

the sample. If necessary, incident visible light was attenuated to < 10 mW with neutral

density filters before it reached the sample. Second harmonic data were collected using a

photomultiplier tube and photon counting electronics. Data from each individual

wavelength were collected over 3-5 separate 10s intervals, background corrected and then

averaged. Typically, up to 300 counts were measured on resonance during a 10 sec.

acquisition.

One and two-photon fluorescence excitation spectra were collected using a Horiba Fluorolog-3 fluorescence spectrometer using 50uM aqueous solutions of DMABN. Fluorescence was collected at the LE peak at 355 nm, and the excitation wavelength was scanned from 500nm to 700nm. Excitation and emissions slits were 5nm wide. No additional effort was made to correct the two photon excitation spectrum to account for a quadratic dependence on incident power. Self-absorption may account for anomalously narrow linewidths.

Semiempirical calculations employed the INDO/S program of Ridley and Zerner,[140] which is a spectroscopically calibrated semiempirical MO method, was used in the present study. The program was modified to include the electrostatic effects of surrounding charges and for constant fields, and has been used in numerous studies to provide insight into spectroscopic properties of molecules similar to DMABN.[141-144]The potentials and fields were added to the appropriate elements of the Fock matrix as described by Theiste.[141] The resulting self-consistent field equations were solved, followed by configuration interaction (CI). We have used 196 singly excited configurations for CI, arising from the transitions between the 14 highest occupied and the 14 lowest unoccupied MOs. The Mataga—Nishimoto formula was used to calculate two-center electron-electron repulsion integrals. The overlap weighting factors were 1.267 and 0.585, respectively. Results for relative state energies, intensities, and polarizations were insensitive to changes in the number of configurations.

TD-DFT computations were carried out for the lowest 3 singlet states of DMABN for all 119 functionals listed on the Gaussian.com website using Gaussian 09[145] on a

Colfax CX2450-N4 2U Server with 4 16-core AMD Opteron 6376 CPUs, 256 gb ram, and 12 tb of disk. Geometry optimization of DMABN was carried out with B3LYP/6-31g(dp) with all heavy atoms in a planar configuration. To obtain qualitative behavior, the effect of twisting the DMA group was done by holding the rotating the group rigid. Single point computations were done with constant external fields applied using the "field" keyword.

4.3 Results

This work was motivated by a hypothesis proposing that solutes adsorbed to the strongly associating aqueous-silica interface sample a constrained, polar environment much like what a solute might experience if it were confined in a polar or ionic material with limited opportunity for intramolecular motion.[146]
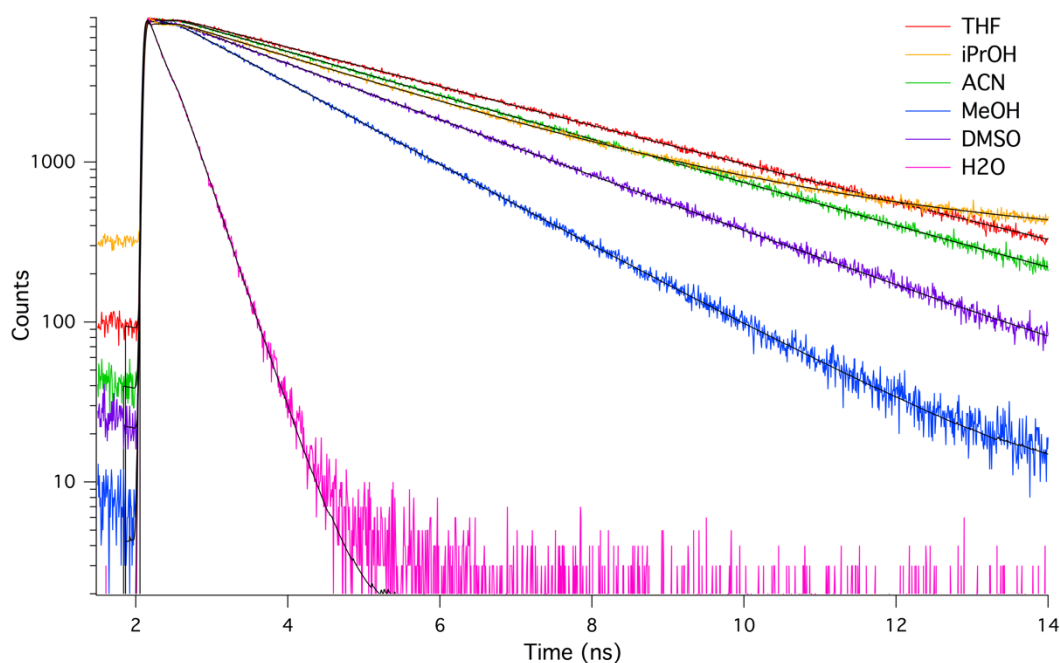
Figure 4.3 TCSPC spectra of DMABN in selected solvents

To test this hypothesis time-resolved emission data were measured from DMABN

adsorbed to an aqueous-silica interface using TIR-TCSPC. Figure 4.3 shows time-

resolved fluorescence from DMABN in bulk solvents. In solvents where the TICT state is

accessible but poorly stabilized, DMABN emission is characterized by a single lifetime

decay that varies between 1.7 ns in methanol and 3.5 ns in less polar, aprotic solvents

such as THF. In aqueous solution, the observed behavior of DMABN emission depends

strongly on the wavelength used to collect the emission. Emission from DMABN's S_1

LE state (collected at shorter wavelengths ($\leq$ 370 nm) shows dual lifetimes with ~85% of

solvent	ε	λ_{exc} (nm)	$\lambda_{em,LE}$ (nm)	$\lambda_{em,TICT}$ (nm)	τ_1 (ns)	A_1	τ_2 (ns)	A_2	χ^2
Chex	2.02	283	340	N/A	< 0.1	0.95			1.09
THF	7.58	290	356	441	3.52	1.00			1.05
i-PrOH	17.9	292	356	462	2.83	1.00			1.07
ACN	37.5	298	356	471	3.15	1.00			1.05
MeOH	32.7	292	356	481	1.71	1.00			1.06
DMSO	46.7	292	365	488	2.47	1.00			1.05
H_2O_{LE}	80.1	293	365		< 0.1	.925	3.19	.085	1.03
H_2O_{TICT}	80.1	293		518	0.31	$\geq$ 0.98	1.74	$\leq$ 0.02	1.05

Table 4.1 DMABN spectroscopic properties in selected bulk solvents
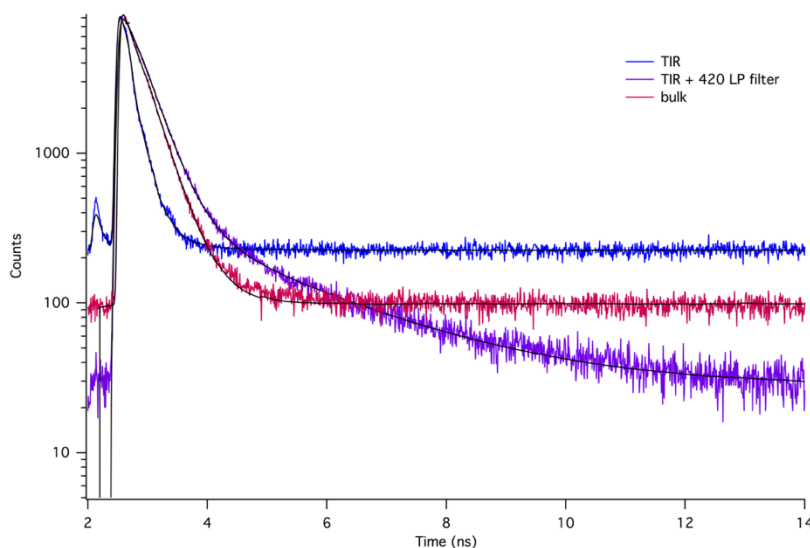
Figure 4.4 TIR-TCSPC spectra of DMABN at the water-silica interface

the emission characterized by a very short lifetime (≤ 0.1 ns) and 15% of the emission

having a much longer, 3.2 ns lifetime. This short lifetime is faster than can be resolved

by our TCSPC assembly and is also consistent with time resolved emission from

nonpolar solvents that cannot stabilize TICT state formation.

At wavelengths corresponding to TICT emission (≥ 450 nm), $\geq 98\%$ of DMABN

emission in water has a lifetime of 0.3 ns. DMABN emission data from the TICT state in

representative solvents are shown in Table 4.1. All bulk solution data measured in this

work compare favorably to values reported previously.[135, 147] Figure 4.4 shows time-

resolved emission from DMABN adsorbed to an aqueous-silica interface acquired using

TIR-TCSPC. The TIR data show emission from adsorbed DMABN decays with a single

exponential lifetime faster than can be resolved unambiguously by our instrument (≤ 0.1

ns, 94%) with only 6% of the emission coming from a putative TICT state ($\tau_{TICT} = 0.3$

ns). (Table 4.2)

	τ_1 (ns)	A_1	τ_2 (ns)	A_2
Water/silica interface	< 0.1	0.96	.31	0.04
Water/silica interface + 420 LP filter	.31	0.96	2.16	0.04
Water/hydrophobic silica interface	.31	0.88	2.05	0.12
Water/hydrophobic silica interface +420 LP filter	.31	0.71	2.04	0.29

Table 4.2 Emission lifetime data from DMABN in water at the silica interface collected in a TIR geometry. Uncertainties in lifetimes are ±0.1 ns and uncertainties in amplitudes are ± 0.04

The longer lifetime component is assigned to those DMABN solutes that are not

adsorbed to the interface but nevertheless excited by the evanescent field that extends

~175 nm into bulk solution. (For reference, DMABN emission in bulk aqueous solution

shown in Figure 4.3 is reproduced in Figure 4.4.) This result suggests that DMABN

adsorbed to the aqueous-silica interface *does not* isomerize after photo-excitation or,

equivalently, that the silica surface and surrounding water impedes TICT state formation.

To test this idea further, we acquired time-resolved spectra using a 420 nm long pass

filter so that only TICT emission was being detected. With the 420 LP filter in place, the

majority (96%) of the measured emission had a 0.31ns lifetime matching the bulk

solution TICT data with 4% of the emission characterized by a 2.16 ns lifetime. Taken

together, TIR results demonstrate clearly that the aqueous-silica interface impedes

DMABN isomerization.

Given that DMABN TICT-state formation appears restricted at the aqueous-silica

interface, questions arise about the local polarity experienced by adsorbed DMABN

solutes. TICT-state formation is less likely in nonpolar solvents such as cyclohexane

where excited state emission is dominated by relaxation from the LE state back to the

ground state. (Figure 4.2) To assess adsorbed DMABN's local dielectric environment, we

measured the solute's resonance-enhanced SHG spectrum. Figure 4.5 shows a surprising

result. SHG data were acquired across the wavelength region 280-370 nm, and the

spectrum shows the expected $S_0 \rightarrow S_2$ excitation peak at 316 nm, red-shifted $\sim$ 10 nm from

its peak in bulk water. More surprisingly, this spectrum is dominated by a strong

resonance at 342 nm that we assign to the $S_0 \rightarrow S_1$ transition. This feature is very weak or

absent in most absorption and fluorescence excitation spectra. When this feature does

appear in bulk solution absorbance spectra, it usually does so at wavelengths between 317

and 321 nm depending on solvent polarity.[148]
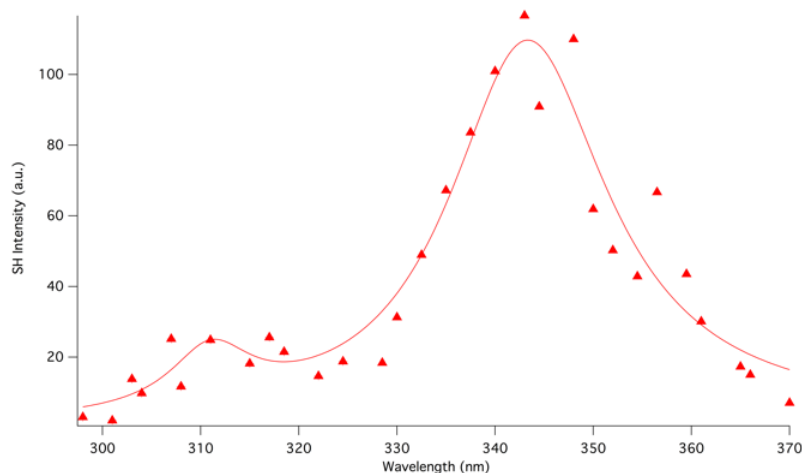
Figure 4.5 SH spectrum of DMABN at the water-silica interface

The red shift of both resonances in the SHG spectrum implies that adsorbed DMABN experience a polar environment, a result that is consistent with previously reported studies of coumarin isomerization. This issue is addressed further in the discussion section where semi-empirical calculations show that DMABN's excitation wavelength depends sensitively on both the magnitude of the electric field inside of the solute cavity *and* structural deformation in the form of a twist about the amine nitrogen-ring carbon bond.

A molecule's second order hyperpolarizability depends on the product of its one and two photon absorption cross sections.[36] To confirm that the observed long wavelength feature in the SH spectrum is consistent with the S_0–S_1 transition, we collected a 2-photon fluorescence excitation spectrum of DMABN dissolved in water. Figure 4.6 shows the 2-photon excitation spectrum of DMABN in aqueous solution. Both the $S_0 \rightarrow S_1$ and the $S_0 \rightarrow S_2$ transitions are clearly visible at (bulk solution) wavelengths of 325 and 280 nm, respectively, confirming the assignment of the $S_0 \rightarrow S_1$ transition
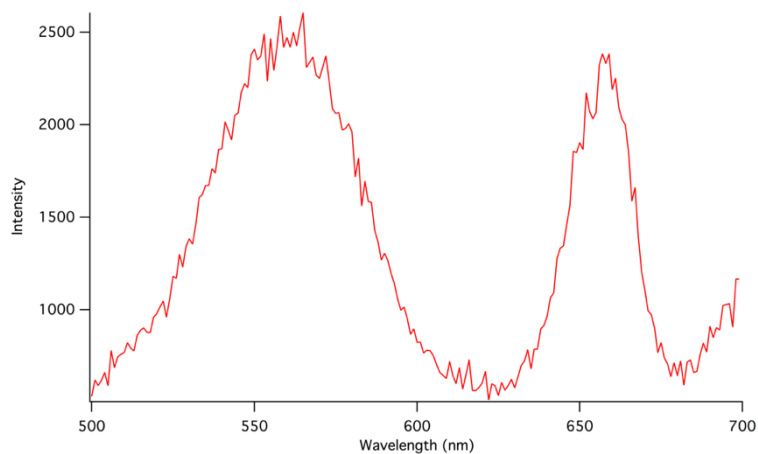
Figure 4.6 Two-photon excitation spectrum of DMABN in aqueous solution. The intensity axis reports DMABN emission recorded at 355 nm.

observed in the SHG spectrum. In order to test strong associations between the silica substrate and adjacent aqueous solvent were responsible for adsorbed DMABN's paradoxical behavior, we functionalized silica slides with dichlorodimethylsilane to create a methyl-terminated surface. Previously reported nonlinear optical studies
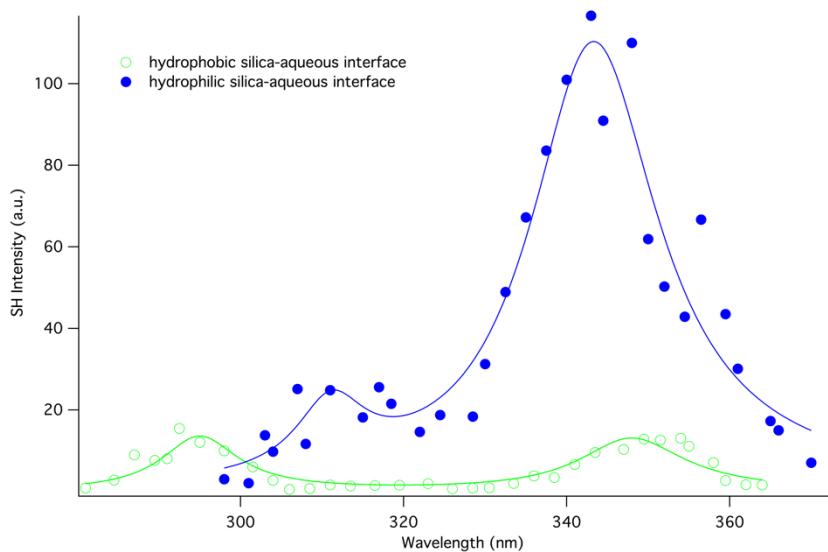
Figure 4.7 SHG spectrum of DMABN at the hydrophobic water-silica interface

proposed that hydrophobic solid surfaces limit the degree of water ordering to only the first solvent layer and that the first layer of water has a significant population of dangling -OH bonds.[149]

Figure 4.7 shows an SHG spectrum of DMABN at the hydrophobic silica-water interface, with data from Figure 4.5 superimposed for comparison. DMABN adsorbed to the aqueous-hydrophobic interface again shows two features, but now both have significantly less intensity and the short wavelength, S_0—S_2 transition has comparable intensity to the longer wavelength S_0—S_1. We attribute the reduced intensity to a smaller number of adsorbed DMABN solutes. Interestingly, the $S_0 \rightarrow S_1$ peak also appears in this spectrum at a slightly longer wavelength (347 nm) relative to the hydrophilic interface (342 nm), while the $S_0 \rightarrow S_2$ resonance peak shifts from 310 nm to 294 nm, similar to its absorbance wavelength in bulk methanol.

Figure 4.8 shows TIR-TCSPC data from the same system (acquired at the aqueous TICT emission wavelength of 520 nm). The time-resolved emission is dominated by a single exponential decay having an emission lifetime of 0.3 ns, consistent with DMABN emitting from a TICT state in bulk aqueous solution. This result stands in marked contrast to results from the aqueous-hydrophilic interface where the dominant contribution to the time resolved emission was assigned to emission from the LE state. (Figure 4.4).

These results are supported by polarization dependent SHG measurements designed to measure the relative orientation of adsorbed solutes. Assuming a single dominant element in the $\chi^{(2)}$ tensor, molecular orientations can be calculated by

measuring second harmonic emission as a function of the incident field polarization.

Fitting these data following previously published methods[150-151] leads to calculated

orientations of 54° for species contributing to the 340 nm transition and 33° for the 310

nm species. These results compare favorably with fluorescence data taken from DMABN

molecules adsorbed in zeolites, that showed DMABN molecules without room to twist

into the TICT excited state still show two spectral bands with different fluorescence

signatures.[146]
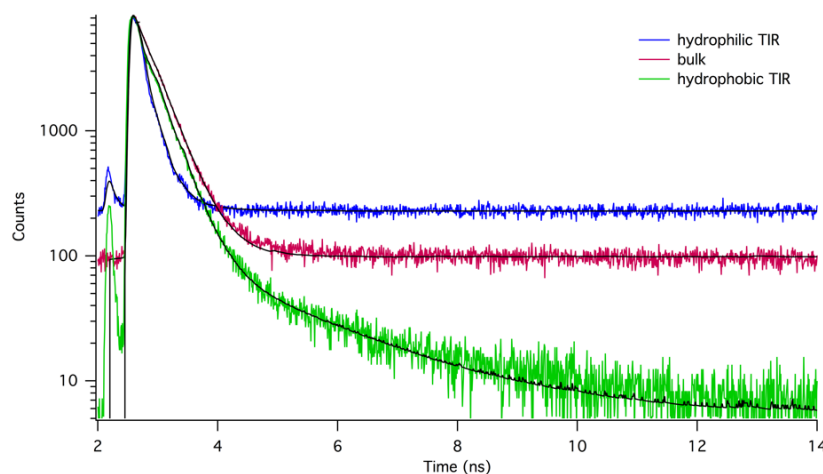
Figure 4.8 TIR-TCSPC spectrum of DMABN at the hydrophobic water-silica interface

4.4 Discussion

From the SHG and TIR-TCSPC results presented above, three important findings need to

be addressed:

1. DMABN solutes adsorbed at the hydrophilic water-silica interface are unable to

isomerize into their excited TICT state.

2. The silica-water interface appears polar based on the solvatochromic shifts of

the DMABN's electronic resonances in SHG spectra at the water-silica interface.

3. DMABN adsorption to the silica substrate enables the enable the S_0—S_1 transition to acquire significant intensity in the resonant SHG spectrum. Rendering the substrate hydrophobic suppresses intensity from the long wavelength S_0—S_1 transition.

4.4.1 Strong associations across the silica-aqueous interface impedes DMABN photoisomerization.

Assessing the ability of strong solvent-substrate associations to restrict solute isomerization was the primary goal of these studies. The time-resolved fluorescence results presented in Figure 4.4 strongly support the conclusion that adsorption to strongly associating water-silica interface prevents DMABN isomerization to a TICT state. In nonpolar solvents where a TICT state cannot be stabilized, DMABN fluorescence is faster than can be resolved clearly with our TCSPC assembly. (Table 4.1 and Figure 4.3) The same behavior is observed for DMABN adsorbed to the silica-aqueous interface. (Table 4.2 and Figure 4.4) In bulk aqueous solution, emission from the TICT state has a 0.31 ns lifetime and that lifetime only lengthens in other, less polar solvents. Previous reports have attributed slower isomerization rates at strongly associating interfaces to surface-induced changes in local solvent viscosity.[5-7] At silica-aqueous interfaces surface specific vibrational spectra show that strong hydrogen bonding between the water and the surface silanols groups leads to an ice-like structure in the adjacent solvent.[54] If the lone pair of adsorbed DMABN's amine serves as a hydrogen bond acceptor *and* if the hydrogen bond network at the surface is both strong and rigid, then one would reasonably expect TICT state formation from photoexcited DMABN to be slowed and correspondingly fast relaxation from the LE state. Disrupting this strong, surface induced

hydrogen bonding by rendering the surface hydrophobic enables DMABN solvation to

return to bulk solution limits, even for those solutes directly influenced by interfacial

anisotropy. These results lead us to propose that adsorbates adsorbed to the planar

silica/aqueous interface behave as if they were in confinement.

4.4.2 The silica-aqueous interface sampled by
<u>DMABN is more polar than bulk water.</u>

DMABN exhibits bathochromic behavior, with an (S_0—S_2) absorbance

wavelength that shifts from 283 to 293 nm as solvent polarity increases from that of

alkanes ($\varepsilon = 2$) to that of water ($\varepsilon = 80$). (Table 4.1, Figure 4.2) This behavior is common

for dipolar solutes having a larger dipole in the excited state than in the ground state. A

solute's solvatochromic properties have been used in SHG measurements to examine

interfacial solvent polarity as a function of solvent structure and substrate composition.[2, 8]

DMABN has a measured ground state dipole moment of 6.2 D and a calculated excited

TICT state dipole of 16.5 D.[152] While resonance-enhanced SHG intensity depends on

DMABN's hyperpolarizability and not its linear absorption cross section, for aromatic

solutes having a combination of "push-pull" ligands, these two properties have been

shown to track each other.[153-155] Despite the solvatochromic evidence for a polar

interface, we do not observe the expected corresponding behavior in the SHG intensities

for the S_1 and S_2 resonances.

As noted above, numerous studies have shown how surface-induced anisotropic

solvent structure changes solvent polarity from bulk solution limits. The details of these

changes depend upon solvent structure and substrate-solvent interactions. For example,

hydrogen bonding between silica and alcohols creates an alkane-like interfacial polarity,

even when the solvent is methanol. In contrast, the local polarity at both silica-cyclohexane and silica-acetonitrile interfaces is greater than bulk solution limits.

Recent discoveries imply that the local interfacial dielectric environment at the silica-aqueous interface depends sensitively on the details of substrate-solvent interactions.[156] DMABN data support this conclusion. The main feature in every bulk solution absorption spectrum of DMABN, regardless of polarity, is the $S_0 \rightarrow S_2$ transition, seen at ~290 nm. In less polar solutions, the $S_0 \rightarrow S_1$ peak is also clearly evident – albeit weakly – between 317 and 321 nm depending on solvent polarity.[148] Most calculations and experiments[135, 157] have supported the hypothesis that the $S_0 \rightarrow S_2$ transition proceeds along the charge transfer pathway, so in bulk solution, the intensity of the $S_0 \rightarrow S_1$ peak decreases with increased solvent polarity as the S_2 transition becomes more and more stabilized and represents a larger percentage of the absorption spectrum's total integrated intensity. Furthermore, the S_0—S_1 transition that is not observable in absorption or 1-photon fluorescence excitation spectroscopy is expected to appear at ~320 nm in polar solvents. SHG data show this wavelength to be 342 nm for DMABN adsorbed to the silica aqueous interface. Wavelengths for both transitions of adsorbed DMABN, S_0—S_1 and S_0—S_2, are redshifted from bulk aqueous limits leading us to conclude that the local polarity experienced by adsorbed solutes is more polar than bulk aqueous solution.

An interesting effect to consider is the role that surface charge may play in controlling the local environment. Several reports show that the static polarity of ices are greater than that of water.[96, 158-160] However, at the experimental pH (pH = 5.8), silica carries a partial negative charge. Over the short distances intrinsic to an interface, this

charge together with a polar solvent can create strong electric fields on the order of ~10^6

V/cm and higher. Semi-empirical calculations show that the S_0—S_1 and S_0—S_2 transition

wavelengths are affected both by local electric fields and by conformational distortions.

(*Vide infra.*) Table 4.3 reports how calculated S_0—S_1 and S_0—S_2 wavelengths change as

a function of local electric field. Given these considerations – surface-induced ice-like

structure in the solvent and strong local electric fields created by the partially charged

Field Strength	Twist Angle	λ_1	F_{01}	λ_2	F_{02}
0	0°	295	.027	274	.596
	30°	295	.024	280	.511
	45°	293	.019	286	.387
	60°	293	.216	289	.012
	90°	300	0	277	.002
-5.14x10^6	0°	296	.028	278	.601
	30°	296	.025	284	.511
	45°	295	.020	291	.382
	60°	299	.209	290	.013
	90°	310	0	277	.002
-2.57x10^7	0°	301	.032	293	.620
	30°	303	.030	302	.516
	45°	313	.372	302	.025
	60°	328	.192	299	.017
	90°	349	0	280	.001

Table 4.3. Calculated transition wavelengths (in nm) and oscillator strengths (in a.u.) for the S_1 and S_2 transitions in DMABN at different local field strengths (in V/cm) and ground state amine twist angle.

surface – we have several plausible mechanisms that can explain the observed

solvatochromic shifts observed in DMABN's SHG spectrum. The fact that only one of

these transitions returns to more bulk-like limits when the surface is rendered

hydrophobic implies that surface charge plays less of a role in creating the high polarity

solvation environment at the silica/aqueous interface.

4.4.3 A combination of surface charge and
amino twist are responsible for enhanced SHG
intensity in the S_0–S_1 transition.

A previous report has proposed that DMABN may already assume partial charge

transfer character in its solvated ground state.[161] When the amine on DMABN is in its

gas phase equilibrium structure (with both methyl groups 60˚ below the ring plane), F_{01}

and F_{02}, the oscillator strengths for the S_1 and S_2 transitions, respectively, are calculated

to be .027 and .596 using ZINDO. As the amine group begins to rotate around the ring

carbon-N axis however, F_{02} diminishes monotonically, while F_{01} first increases and then

decreases. (Table 4.3)

Furthermore, changes in rotation angle are accompanied by pronounced changes

in the permanent dipole. Table 4.4 summarizes these effects for the zero external field

condition. Changes in oscillator strengths and excitation wavelengths become even more

pronounced in the presence of an external field. With a static field of -5.14x10^7 V/cm,

the S_0—S_1 transition wavelength red-shifts more than 100 nm with changing twist angle.

These changes in dipole also lead to changes in S_0–S_1 and S_0–S_2 transition

wavelengths. With surface potentials at the silica-aqueous interface estimated to be on the

order of 30-50 mV (at a pH of 6.0)[47] and with surface charge effects converging to bulk

Twist Angle	ΔDipole (D)
0°	-5.79
10°	-5.89
20°	-6.20
30°	-6.71
40°	-7.42
50°	-8.29
60°	-2.06
70°	-1.56
80°	-0.56
90°	0.22

Table 4.4: Calculated changes in permanent dipole strength in DMABN at 0 field strength for primary S_2 transition around 290 nm

solution (neutral) limits on the order of 1-2 nm, local electric fields can be $\geq 10^6$ V/cm. Consequently, we anticipate that local gradients in interfacial potential are capable of significantly affecting adsorbed DMABN's ground and excited state electronic structure. While the effects of local potential and geometric deformation cannot be decoupled from one another, we expect that both play a role in DMABN's unexpected nonlinear susceptibility.

4.5 Conclusions

Second harmonic and surface fluorescence spectra of DMABN at the water-silica interface show that DMABN molecules adsorbed at this interface experience an environment that prevents them from accessing their excited TICT state which has dramatic effects on its surface spectra. When the silica surface is modified by the addition of a hydrophobic silane layer, the effects seen at a surface capable of hydrogen bond donation modulate to resemble those seen when DMABN is dissolved in a polar organic

solvent. Energy structure calculations show that surface potential and twisting of the amine group in DMABN may contribute to the unique second harmonic spectrum of DMABN at both the hydrophobic and hydrophilic silica interfaces.

4.6 References

1.   Zenasni, O.; Marquez, M. D.; Jamison, A. C.; Lee, H. J.; Czader, A.; Lee, T. R., Inverted Surface Dipoles in Fluorinated Self-Assembled Monolayers. *Chem Mater* **2015,** *27* (21), 7433-7446.

2.   Steel, W. H.; Walker, R. A., Measuring dipolar width across liquid-liquid interfaces with 'molecular rulers'. *Nature* **2003,** *424* (6946), 296-299.

3.   Zhang, X. Y.; Esenturk, O.; Walker, R. A., Reduced polarity in protic solvents near hydrophobic solid surfaces. *J Am Chem Soc* **2001,** *123* (43), 10768-10769.

4.   Zhong, J.; Carignano, M. A.; Kais, S.; Zeng, X. C.; Francisco, J. S.; Gladich, I., Tuning the Stereoselectivity and Solvation Selectivity at Interfacial and Bulk Environments by Changing Solvent Polarity: Isomerization of Glyoxal in Different Solvent Environments. *J Am Chem Soc* **2018,** *140* (16), 5535-5543.

5.   Gobrogge, E. A.; Walker, R. A., Binary Solvent Organization at Silica/Liquid Interfaces: Preferential Ordering in Acetonitrile-Methanol Mixtures. *J Phys Chem Lett* **2014,** *5* (15), 2688-2693.

6.   Gobrogge, E. A.; Woods, B. L.; Walker, R. A., Liquid organization and solvation properties at polar solid/liquid interfaces. *Faraday Discuss* **2013,** *167*, 309-327.

7.   Roy, D.; Liu, S. L.; Woods, B. L.; Siler, A. R.; Fourkas, J. T.; Weeks, J. D.; Walker, R. A., Nonpolar Adsorption at the Silica/Methanol Interface: Surface Mediated Polarity and Solvent Density across a Strongly Associating Solid/Liquid Boundary. *J Phys Chem C* **2013,** *117* (51), 27052-27061.

8.   Woods, B. L.; Walker, R. A., pH Effects on Molecular Adsorption and Solvation of p-Nitrophenol at Silica/Aqueous Interfaces. *J Phys Chem A* **2013,** *117* (29), 6224-6233.

9.   Woods, B. L.; George, J. K.; Sherman, A. M.; Callis, P. R.; Walker, R. A., Adsorption and Aggregation at Silica/Methanol Interfaces: The Role of Solute Structure. *J Phys Chem C* **2015,** *119* (25), 14230-14238.

10.   Beniwal, V.; Manna, A.; Kumar, A., Spectacular Rate Enhancement of the Diels-Alder Reaction at the Ionic Liquid/n-Hexane Interface. *Chemphyschem* **2016,** *17* (13), 1969-1972.

11.   Dong, R. H.; Zhang, T.; Feng, X. L., Interface-Assisted Synthesis of 2D Materials: Trend and Challenges. *Chem Rev* **2018,** *118* (13), 6189-6235.

12.   Arnold, W. A.; Roberts, A. L., Pathways and kinetics of chlorinated ethylene and chlorinated acetylene reaction with Fe(O) particles. *Environ Sci Technol* **2000,** *34* (9), 1794-1805.

13.   Tseng, T. C.; Urban, C.; Wang, Y.; Otero, R.; Tait, S. L.; Alcami, M.; Ecija, D.; Trelka, M.; Gallego, J. M.; Lin, N.; Konuma, M.; Starke, U.; Nefedov, A.; Langner, A.; Woll, C.; Herranz, M. A.; Martin, F.; Martin, N.; Kern, K.; Miranda, R., Charge-transfer-induced structural rearrangements at both sides of organic/metal interfaces. *Nat Chem* **2010,** *2* (5), 374-379.

14.   Munninghoff, J. A. W.; Elemans, J. A. A. W., Chemistry at the square nanometer: reactivity at liquid/solid interfaces revealed with an STM. *Chem Commun* **2017,** *53* (11), 1769-1788.

15.   Shibukawa, M.; Miyake, A.; Eda, S.; Saito, S., Determination of the cis-trans lsomerization Barriers of L-Alanyl-L-proline in Aqueous Solutions and at Water/Hydrophobic Interfaces by On-Line Temperature-Jump Relaxation HPLC and Dynamic On-Column Reaction HPLC. *Anal Chem* **2015,** *87* (18), 9280-9287.

16.   Chen, H.; Zou, H. B.; Hao, Y. J.; Yang, H. Q., Flow Pickering Emulsion Interfaces Enhance Catalysis Efficiency and Selectivity for Cyclization of Citronellal. *Chemsuschem* **2017,** *10* (9), 1989-1995.

17.   Guo, L. W.; Cesari, S.; de Guillen, K.; Chalvon, V.; Mammri, L.; Ma, M. Q.; Meusnier, I.; Bonnot, F.; Padilla, A.; Peng, Y. L.; Liu, J. F.; Kroj, T., Specific recognition of two MAX effectors by integrated HMA domains in plant immune receptors involves distinct binding surfaces. *P Natl Acad Sci USA* **2018,** *115* (45), 11637-11642.

18.   Fukuda, T., Biological recognition at interfaces involving dendritic molecules. *Polym J* **2019,** *51* (6), 535-546.

19.   Neal, J. F.; Zhao, W.; Grooms, A. J.; Smeltzer, M. A.; Shook, B. M.; Flood, A. H.; Allen, H. C., Interfacial Supramolecular Structures of Amphiphilic Receptors Drive Aqueous Phosphate Recognition. *J Am Chem Soc* **2019,** *141* (19), 7876-7886.

20.   Dubacheva, G. V.; Curk, T.; Frenkel, D.; Richter, R. P., Multivalent Recognition at Fluid Surfaces: The Interplay of Receptor Clustering and Superselectivity. *J Am Chem Soc* **2019,** *141* (6), 2577-2588.

21.   Lin, J. F.; Liu, Y.; Liu, Y. P.; Huang, C.; Liu, W. H.; Mi, X. H.; Fan, D. Y.; Fan, F. T.; Lu, H. D.; Chen, X. B., SnS2 Nanosheets/H-TiO2 Nanotube Arrays as a Type II Heterojunctioned Photoanode for Photoelectrochemical Water Splitting. *Chemsuschem* **2019,** *12* (5), 961-967.

22.   Zang, S. H.; Zhang, G. G.; Lan, Z. A.; Zheng, D. D.; Wang, X. C., Enhancement of photocatalytic H-2 evolution on pyrene-based polymer promoted by MoS2 and visible light. *Appl Catal B-Environ* **2019,** *251*, 102-111.

23.   Urban, C.; Wang, Y.; Rodriguez-Fernandez, J.; Garcia, R.; Herranz, M. A.; Alcami, M.; Martin, N.; Martin, F.; Gallego, J. M.; Miranda, R.; Otero, R., Charge transfer-assisted self-limited decyanation reaction of TCNQ-type electron acceptors on Cu(100). *Chem Commun* **2014,** *50* (7), 833-835.

24.   Zhang, X.; Steel, W. H.; Walker, R. A., Probing solvent polarity across strongly associating solid/liquid interfaces using molecular rulers. *J Phys Chem B* **2003,** *107* (16), 3829-3836.

25.   Karnes, J. J.; Gobrogge, E. A.; Walker, R. A.; Benjamin, I., Unusual Structure and Dynamics at Silica/Methanol and Silica/Ethanol Interfaces-A Molecular Dynamics and Nonlinear Optical Study. *J Phys Chem B* **2016,** *120* (8), 1569-1578.

27.   Ding, F.; Hu, Z. H.; Zhong, Q.; Manfred, K.; Gattass, R. R.; Brindza, M. R.; Fourkas, J. T.; Walker, R. A.; Weeks, J. D., Interfacial Organization of Acetonitrile: Simulation and Experiment. *J Phys Chem C* **2010,** *114* (41), 17651-17659.

36.   Moad, A. J.; Simpson, G. J., A unified treatment of selection rules and symmetry relations for sum-frequency and second harmonic spectroscopies. *J Phys Chem B* **2004,** *108* (11), 3548-3562.

47.   Ong, S. W.; Zhao, X. L.; Eisenthal, K. B., Polarization of Water-Molecules at a Charged Interface - 2nd Harmonic Studies of the Silica Water Interface. *Chem Phys Lett* **1992,** *191* (3-4), 327-335.

51.   Sulpizi, M.; Gaigeot, M. P.; Sprik, M., The Silica-Water Interface: How the Silanols Determine the Surface Acidity and Modulate the Water Properties. *J Chem Theory Comput* **2012,** *8* (3), 1037-1047.

54.   Shen, Y. R.; Ostroverkhov, V., Sum-frequency vibrational spectroscopy on water interfaces: Polar orientation of water molecules at interfaces. *Chem Rev* **2006,** *106* (4), 1140-1154.

59.   Grabowski, Z. R.; Rotkiewicz, K.; Rettig, W., Structural changes accompanying intramolecular electron transfer: Focus on twisted intramolecular charge-transfer states and structures. *Chem Rev* **2003,** *103* (10), 3899-4031.

61.   Visser, R. J.; Varma, C. A. G. O., Source of Anomalous Fluorescence from Solutions of 4-N,N-Dimethylaminobenzonitrile in Polar-Solvents. *J Chem Soc Farad T 2* **1980,** *76*, 453-471.

62.   Chandross, E. A.; Thomas, H. T., The interaction of amine-hydrocarbon exciplexes with small dipolar molecules - stoichiometric complex formation. *Chem Phys Lett* **1971,** *9* (5), 397-400.

63.   Khalil, O. S., Excimer Model of N,N-Dialkyl-Para-Cyanoanilines Fluorescence in Polar-Solvents. *Chem Phys Lett* **1975,** *35* (2), 172-174.

64.   Zachariasse, K. A., Comment on "Pseudo-Jahn-Teller and TICT-models: a photophysical comparison of meta-and para-DMABN derivatives" [Chem. Phys. Lett. 305(1999)8] - The PICT model for dual fluorescence of aminobenzonitriles. *Chem Phys Lett* **2000,** *320* (1-2), 8-13.

65.   Zachariasse, K. A.; Grobys, M.; vonderHaar, T.; Hebecker, A.; Ilichev, Y. V.; Morawski, O.; Ruckert, I.; Kuhnle, W., Photoinduced intramolecular charge transfer and internal conversion in molecules with a small energy gap between S-1 and S-2. Dynamics and structure. *J Photoch Photobio A* **1997,** *105* (2-3), 373-383.

66.   Lewis, F. D.; Holman, B., Singlet-States of Benzonitrile and Para-Dimethylaminobenzonitrile. *J Phys Chem-Us* **1980,** *84* (18), 2326-2328.

67.   Sobolewski, A. L.; Domcke, W., Promotion of intramolecular charge transfer in dimethylamino derivatives: Twisting versus acceptor-group rehybridization. *Chem Phys Lett* **1996,** *259* (1-2), 119-127.

68.   Sobolewski, A. L.; Domcke, W., Charge transfer in aminobenzonitriles: Do they twist? *Chem Phys Lett* **1996,** *250* (3-4), 428-436.

69.   Rotkiewicz, K.; Grellmann, K. H.; Grabowski, Z. R., Reinterpretation of Anomalous Fluorescence of "Para-N,N-Dimethylamino-Benzonitrile. *Chem Phys Lett* **1973,** *19* (3), 315-318.

73.   Nad, S.; Kumbhakar, M.; Pal, H., Photophysical properties of coumarin-152 and coumarin-481 dyes: Unusual behavior in nonpolar and in higher polarity solvents. *Journal of Physical Chemistry A* **2003,** *107* (24), 4808-4816.

76.   Cave, R. J.; Burke, K.; Castner, E. W., Theoretical Investigation of the Ground and Excited States of Coumarin 151 and Coumarin 120. *The Journal of Physical Chemistry A* **2002,** *106* (40), 9294-9305.

77.   Cave, R. J.; Castner, E. W., Time-Dependent Density Functional Theory Investigation of the Ground and Excited States of Coumarins 102, 152, 153, and 343. *The Journal of Physical Chemistry A* **2002,** *106* (50), 12117-12123.

85.   Shang, X. M.; Benderskii, A. V.; Eisenthal, K. B., Ultrafast solvation dynamics at silica/liquid interfaces probed by time-resolved second harmonic generation (vol 150B, pg 11578, 2001). *J Phys Chem B* **2001,** *105* (47), 11928-11928.

96.   Johari, G. P.; Whalley, E., The Dielectric-Properties of Ice Ih in the Range 272-133-K. *J Chem Phys* **1981,** *75* (3), 1333-1340.

104.   Brindza, M. R.; Walker, R. A., Differentiating Solvation Mechanisms at Polar Solid/Liquid Interfaces. *J Am Chem Soc* **2009,** *131* (17), 6207-6214.

108.   Purnell, G. E.; Walker, R. A., Hindered Isomerization at the Silica/Aqueous Interface: Surface Polarity or Restricted Solvation? *Langmuir* **2018,** *34* (34), 9946-9949.

114.   Ohno, P. E.; Wang, H. F.; Geiger, F. M., Second-order spectral lineshapes from charged interfaces. *Nat Commun* **2017,** *8*.

115.   Ohno, P. E.; Saslow, S. A.; Wang, H. F.; Geiger, F. M.; Eisenthal, K. B., Phase-referenced nonlinear spectroscopy of the alpha-quartz/water interface. *Nat Commun* **2016,** *7*.

119.   Horng, P.; Brindza, M. R.; Walker, R. A.; Fourkas, J. T., Behavior of Organic Liquids at Bare and Modified Silica Interfaces. *J Phys Chem C* **2010,** *114* (1), 394-402.

124.   del Junco, C.; Vaikuntanathan, S., Interface height fluctuations and surface tension of driven liquids with time-dependent dynamics. *J Chem Phys* **2019,** *150* (9).

125.   Liu, J. C.; Li, X.; Hou, J.; Li, X.; Lu, Z., The Influence of Sodium Iodide Salt on the Interfacial Properties of Aqueous Methanol Solution by a Combined Molecular Simulation and Sum Frequency Generation Vibrational Spectroscopy Study. *Langmuir* **2019,** *35* (21), 7050-7059.

126.   Shibaev, V.; Bobrovsky, A.; Boiko, N., Photoactive liquid crystalline polymer systems with light-controllable structure and optical properties. *Prog Polym Sci* **2003,** *28* (5), 729-836.

127.   Shen, X. Y.; Wang, Y. J.; Zhao, E. G.; Yuan, W. Z.; Liu, Y.; Lu, P.; Qin, A. J.; Ma, Y. G.; Sun, J. Z.; Tang, B. Z., Effects of Substitution with Donor-Acceptor Groups on the Properties of Tetraphenylethene Trimer: Aggregation-Induced Emission, Solvatochromism, and Mechanochromism. *J Phys Chem C* **2013,** *117* (14), 7334-7347.

128.   Velema, W. A.; Szymanski, W.; Feringa, B. L., Photopharmacology: Beyond Proof of Principle. *J Am Chem Soc* **2014,** *136* (6), 2178-2191.

129.   Charpentier, T.; Kroll, P.; Mauri, F., First-Principles Nuclear Magnetic Resonance Structural Analysis of Vitreous Silica. *J Phys Chem C* **2009,** *113* (18), 7917-7929.

130.   Snyder, L. R.; Ward, J. W., Surface Structure of Porous Silicas. *J Phys Chem-Us* **1966,** *70* (12), 3941-&.

131.   Mcdonald, R. S., Surface Functionality of Amorphous Silica by Infrared Spectroscopy. *J Phys Chem-Us* **1958,** *62* (10), 1168-1178.

132.   Darlington, A. M.; Jarisz, T. A.; DeWalt-Kerian, E. L.; Roy, S.; Kim, S.; Azam, M. S.; Hore, D. K.; Gibbs, J. M., Separating the pH-Dependent Behavior of Water in the Stern and Diffuse Layers with Varying Salt Concentration. *J Phys Chem C* **2017,** *121* (37), 20229-20241.

133.   Purnell, G. E.; Walker, R. A., Surface solvation and hindered isomerization at the water/silica interface explored with second harmonic generation. *The Journal of Chemical Physics* **2019,** *150* (19), 194701.

134.   Lippert, E., Lüder, W., Boos, H., Fluoreszenzspektrum und Frank-Condon-Prinzip in Lösungen aroma-tischer Verbindungen. In *Advances in Molecular Spectroscopy*, Mangini, A., Ed. Pergamon Press: Oxford, 1962; Vol. 1, pp 442-456.

135.   Zachariasse, K. A.; Vonderhaar, T.; Hebecker, A.; Leinhos, U.; Kuhnle, W., Intramolecular Charge-Transfer in Aminobenzonitriles - Requirements for Dual Fluorescence. *Pure Appl Chem* **1993,** *65* (8), 1745-1750.

136.   Schuddeboom, W.; Jonker, S. A.; Warman, J. M.; Leinhos, U.; Kuhnle, W.; Zachariasse, K. A., Excited-State Dipole-Moments of Dual Fluorescent 4-(Dialkylamino)Benzonitriles - Influence of Alkyl Chain-Length and Effective Solvent Polarity. *J Phys Chem-Us* **1992,** *96* (26), 10809-10819.

137.   Rettig, W., Charge Separation in Excited-States of Decoupled Systems - Tict Compounds and Implications Regarding the Development of New Laser-Dyes and the Primary Processes of Vision and Photosynthesis. *Angew Chem Int Edit* **1986,** *25* (11), 971-988.

138.   Grabowski, Z. R.; Dobkowski, J., Twisted Intramolecular Charge-Transfer (Tict) Excited-States - Energy and Molecular-Structure. *Pure Appl Chem* **1983,** *55* (2), 245-252.

139.   Bajzer, E.; Moncrieffe, M. C.; Penzar, I.; Prendergast, F. G., Complex homogeneous and heterogeneous fluorescence anisotropy decays: Enhancing analysis accuracy. *Biophys J* **2001,** *81* (3), 1765-1775.

140.   Ridley, J.; Zerner, M., Intermediate Neglect of Differential Overlap Technique for Spectroscopy - Pyrrole and Azines. *Theor Chim Acta* **1973,** *32* (2), 111-134.

141.   Theiste, D.; Callis, P. R.; Woody, R. W., Effects of the Crystal-Field on Transition Moments in 9-Ethylguanine. *J Am Chem Soc* **1991,** *113* (9), 3260-3267.

142.   Sreerama, N.; Woody, R. W.; Callis, P. R., Theoretical-Study of the Crystal-Field Effects on the Transition Dipole-Moments in Methylated Adenines. *J Phys Chem-Us* **1994,** *98* (41), 10397-10407.

143.   Biesso, A.; Xu, J. H.; Muino, P. L.; Callis, P. R.; Knutson, J. R., Charge Invariant Protein-Water Relaxation in GB1 via Ultrafast Tryptophan Fluorescence. *J Am Chem Soc* **2014,** *136* (7), 2739-2747.

144.   Liu, T. Q.; Callis, P. R.; Hesp, B. H.; de Groot, M.; Buma, W. J.; Broos, J., Ionization potentials of fluoroindoles and the origin of nonexponential tryptophan fluorescence decay in proteins. *J Am Chem Soc* **2005,** *127* (11), 4104-4113.

145.   M. J. Frisch, G. W. T., H. B. Schlegel, G. E. Scuseria, M. A. Robb, J. R. Cheeseman, G. Scalmani, V. Barone, G. A. Petersson, H. Nakatsuji, X. Li, M. Caricato, A. Marenich, J. Bloino, B. G. Janesko, R. Gomperts, B. Mennucci, H. P. Hratchian, J. V. Ortiz, A. F. Izmaylov, J. L. Sonnenberg, D. Williams-Young, F. Ding, F. Lipparini, F. Egidi, J. Goings, B. Peng, A. Petrone, T. Henderson, D. Ranasinghe, V. G. Zakrzewski, J. Gao, N. Rega, G. Zheng, W. Liang, M. Hada, M. Ehara, K. Toyota, R. Fukuda, J. Hasegawa, M. Ishida, T. Nakajima, Y. Honda, O. Kitao, H. Nakai, T. Vreven, K. Throssell, J. A. Montgomery, Jr., J. E. Peralta, F. Ogliaro, M. Bearpark, J. J. Heyd, E. Brothers, K. N. Kudin, V. N. Staroverov, T. Keith, R. Kobayashi, J. Normand, K. Raghavachari, A. Rendell, J. C. Burant, S. S. Iyengar, J. Tomasi, M. Cossi, J. M. Millam, M. Klene, C. Adamo, R. Cammi, J. W. Ochterski, R. L. Martin, K. Morokuma, O. Farkas, J. B. Foresman, and D. J. Fox *Gaussian 09, Revision A.02*, Wallingford CT, 2016.

146.   Hoffmann, K.; Marlow, F.; Caro, J.; Dähne, S., Modification of fluorescence of p-N,N-dimethylaminobenzonitrile by adsorption in molecular sieves. *Zeolites* **1996,** *16* (2), 138-141.

147.   Rettig, W.; Wermuth, G.; Lippert, E., Photophysical Primary Processes in Solutions of P-Substituted Dialkylanilines. *Ber Bunsen Phys Chem* **1979,** *83* (7), 692-697.

148.   Galievsky, V. A.; Zachariasse, K. A., Intramolecular charge transfer with N,N-Dialkyl-4-(trifluoromethyl)anilines and 4-(dimethylamino)benzonitrile in polar solvents. Investigation of the excitation wavelength dependence of the reaction pathway. *Acta Phys Pol A* **2007,** *112*, S39-S56.

149.   Tyrode, E.; Liljeblad, J. F. D., Water Structure Next to Ordered and Disordered Hydrophobic Silane Monolayers: A Vibrational Sum Frequency Spectroscopy Study. *The Journal of Physical Chemistry C* **2013,** *117* (4), 1780-1790.

150.   Heinz, T. F., Second-Order Nonlinear Optical Effects at Surfaces and Interfaces. In *Nonlinear Surface Electromagnetic Phenomena*, Ponath, H.-E.; Stegeman, G. I., Eds. Elsevier Science Publishers: 1991.

151.   Higgins, D. A.; Byerly, S. K.; Abrams, M. B.; Corn, R. M., 2nd Harmonic-Generation Studies of Methylene-Blue Orientation at Silica Surfaces. *J Phys Chem-Us* **1991,** *95* (18), 6984-6990.

152.   Baumann, W.; Bischof, H.; Frohling, J. C.; Brittinger, C.; Rettig, W.; Rotkiewicz, K., Considerations on the Dipole-Moment of Molecules Forming the Twisted Intramolecular Charge-Transfer State. *J Photoch Photobio A* **1992,** *64* (1), 49-72.

153.   Bhalekar, S.; Avhad, K.; Sekar, N., Synthesis, photophysical, viscosity and DFT study of solid state fluorescent molecular rotors. *Journal of Photochemistry and Photobiology A: Chemistry* **2019,** *371*, 223-237.

154.   Moran, A. M.; Delbecque, C.; Kelley, A. M., Solvent effects on ground and excited electronic state structures of the push-pull chromophore julolidinyl-n-N,N '-diethylthiobarbituric acid. *J Phys Chem A* **2001,** *105* (45), 10208-10219.

155.   Erande, Y.; Kothavale, S.; Sreenath, M. C.; Chitrambalam, S.; Joe, I. H.; Sekar, N., NLOphoric multichromophoric auxiliary methoxy aided triphenylamine D-pi-A chromophores - Spectroscopic and computational studies. *Opt Mater* **2017,** *73*, 602-616.

156.   Singappuli-Arachchige, D.; Manzano, J. S.; Sherman, L. M.; Slowing, I. I., Polarity Control at Interfaces: Quantifying Pseudo-solvent Effects in Nano-confined Systems. *Chemphyschem* **2016,** *17* (19), 2982-2986.

157.   Druzhinin, S. I.; Mayer, P.; Stalke, D.; von Bulow, R.; Noltemeyer, M.; Zachariasse, K. A., Intramolecular Charge Transfer with 1-tert-Butyl-6-cyano-1,2,3,4-tetrahydroquinoline (NTC6) and Other Aminobenzonitriles. A Comparison of Experimental Vapor Phase Spectra and Crystal Structures with Calculations. *J Am Chem Soc* **2010,** *132* (22), 7730-7744.

158.   Aragones, J. L.; MacDowell, L. G.; Vega, C., Dielectric Constant of Ices and Water: A Lesson about Water Interactions. *The Journal of Physical Chemistry A* **2011,** *115* (23), 5745-5758.

159.   Whalley, E.; Heath, J. B. R.; Davidson, D. W., Ice 9 - an Antiferroelectric Phase Related to Ice 3. *J Chem Phys* **1968,** *48* (5), 2362-&.

160.   Johari, G. P.; Lavergne, A.; Whalley, E., Dielectric Properties of Ice Vii and Viii and Phase Boundary between Ice Vi and Vii. *J Chem Phys* **1974,** *61* (10), 4292-4300.

161.   Catalan, J., Can the dipolarity of the medium induce the formation of charge transfer structures? An unexpected finding in the photophysics of DMABN. *Phys Chem Chem Phys* **2014,** *16* (17), 7734-7740.

CHAPTER FIVE

ISOMERIZATION AT AQUEOUS-SILICA INTERFACES

AND THE ROLE OF SOLUTE STRUCTURE

<u>Contribution of Authors and Co-Authors</u>

Manuscript in Chapter 5:

Author: Grace E. Purnell

Contributions: Collected and analyzed experimental data and authored manuscript

Author: Marshall T. McNally

Contributions: Collected second harmonic data

Co-Author: Robert A. Walker

Contributions: Assisted with data analysis and edited manuscript

Manuscript Information

Grace E. Purnell, Marshall T. McNally, and Robert A. Walker

Chemical Physics Letters

Status of Manuscript:
_X_ Prepared for submission to a peer-reviewed journal
____ Officially submitted to a peer-reviewed journal
____ Accepted by a peer-reviewed journal
____ Published in a peer-reviewed journal

Publisher: Elsevier

CHAPTER FIVE

ISOMERIZATION AT AQUEOUS-SILICA INTERFACES

AND THE ROLE OF SOLUTE STRUCTURE

5.1 Introduction

Isomerization reactions are among the simplest chemical transformations that involve structural and bond rearrangements. Isomerization serves as the simplest model for RRKM (Rice-Ramsperger-Kassel-Marcus) descriptions of molecular reaction pathways[162-163] and encompasses a variety of changes to molecular structure. Common isomerization reactions include cis-trans isomerization about a double bond, molecular rearrangements and intramolecular charge transfer reactions. In the limit that isomerization leads to intramolecular charge separation, reaction rates depend sensitively on the solute's local environment. In higher polarity solvents that can stabilize the charge separation, this reaction proceeds as much as 10x faster than in nonpolar media.[164]

Another factor that can affect isomerization is confinement. Reactions such as cis-trans trans isomerization or twisted intramolecular charge transfer (TICT) state formation involve a reorientation of functional groups about a bond. Such large amplitude motions in solution require that a solute's surrounding solvation shell be sufficiently mobile to accommodate significant solute volume changes, especially at the solute's transition state. Confinement restricts solute motion so that even if local polarity is likely to stabilize isomerization in the excited state, steric constraints restrict isomer formation. A study looking at confined catalysts showed that confinement can be used to

discriminate by polarity of adsorbate, allowing reactions that occur at confined catalytic

sites to be selective by the polarity of the substrate.[165] In experiments that have studied

isomerization in confinement, longer emissive lifetimes and broader absorption bands

have been observed from molecules that undergo cis-trans isomerizations, such as

stilbenes[166] and some organic dye molecules.[167-168]
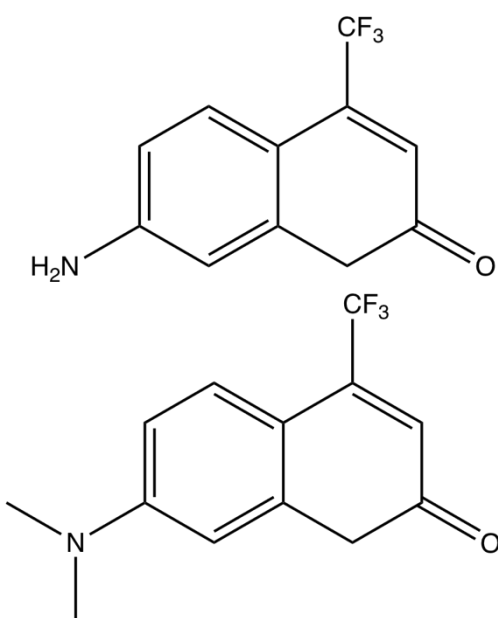
Figure 5.1: Coumarin 151 (top) and Coumarin 152 (bottom)

Recently, several reports[108, 133] have shown that solute isomerization at the

strongly associating, planar aqueous-silica interface is restricted with adsorbed solutes

behaving *as if* they experience confinement. Specifically, time resolved emission from

two different solutes known to form TICT states upon photo excitation in polar solvents

behave as if they were in nonpolar environments when adsorbed to aqueous-silica

boundaries. The two solutes, Coumarin 152 (C152) and 4-dimethylaminobenzonitrile

(DMABN), have well characterized photophysical properties that depend sensitively on

the local dielectric properties, and only polar solvents can stabilize the charge separation found in the TICT isomer. For DMABN adsorbed to the aqueous-silica interface, time resolved fluorescence shows emission out of the non-TICT or locally excited state, even though independent resonant enhanced second harmonic generation experiments show that the interface is measurably more polar than even bulk aqueous solution.

The experiments described below were designed to explore further the effects that strong associations between a substrate and solvent have on adsorbed solute isomerization. Specifically, a solute was chosen that *does not* require a large change in solvation volume as it forms its photoexcited isomer. 7-aminocoumarins with alkyl substituents on the amino group, i.e. Coumarin 152 (C152), have a radiationless deactivation pathway in polar solvents not seen in coumarins with a primary amine in the 7-position, such as Coumarin 151 (C151) (Figure 5.1).[79, 169] This radiationless deexcitation pathway is attributed to TICT state formation,[72-73, 78-79] where a charge from the amino group is transferred to the C=O moiety on the pyrone ring and the alkyl amino group twists 90° relative to the plane defined by the benzopyrone rings. This phenomenon is only possible due to the electron donating alkyl amine groups and is therefore not observed from aminocoumarin dyes with primary amines.[59, 170] Coumarin 151 is closely related to C152, but has a primary rather than a tertiary amine in the 7-position. C151 and C152 share several similarities: both show strong solvatochromic behavior due to the large (positive) change in dipole that occurs upon photoexcitation (+2.81 D for C151, +4.13 for C152)[73, 170] and both have time dependent emission behavior that is extremely sensitive to both solvent polarity and hydrogen bonding.

However, whereas C152 forms a TICT isomer in polar, protic solvents following photoexcitation, C151 simply isomerizes to a planar ICT state where the excited solute has both amine protons in the plane of the molecule and the amine nitrogen assumes sp^2 hybridization character. These differences lead to very different time-resolved emission from these two solutes that serves as a sensitive indicator of local solvation behavior.

In order to more specifically understand solute isomerization behavior at the interface, we examined the photophysical behavior of Coumarin 151 at the aqueous-silica interface. ICT formation *does not* require large amplitude, intramolecular motion nor does it require extensive solvent rearrangement. Given the hypothesis that strong solvent-substrate interactions restrict solute dynamics and impede solute photoisomerization, C151 should show very little change in its photophysical behavior relative to bulk aqueous solution when adsorbed to aqueous-silica interfaces. Time resolved emission experiments presented below support this hypothesis. Fluorescence lifetimes of C151 adsorbed to an aqueous-silica interface differ very little from C151 lifetimes in bulk aqueous solution. Independent SHG measurements show the aqueous-silica interface to still be very polar, similar to what has been reported in the C152 and DMABN studies.[108, 171] Model calculations performed to estimate solute volume in its ground state structure, transition state geometry and excited state structure support the hypothesis that a flexible solute solvation volume is just as critical to promoting isomerization reactions as the local dielectric environment.

Results from these and prior studies provide clear benchmarks for emerging models seeking to describe chemical reactivity at buried interfaces.[172-174] Strong,

anisotropic forces in between two phases strongly influence some reactions (e.g. TICT formation) but appear to have very little effect on others (e.g. planar ICT formation). We anticipate that these findings will provide grist for the mill in the general area of condensed phase theory and surface science for years to come.

5.2 Experimental

Laser grade Coumarin 151 was purchased and used as received from Aldrich. Water used in the experiments was nanopure, from a Millipore filtration system, resistivity of 18.2 MΩ. Silica slides and experimental assemblies were rinsed with methanol and DI water then soaked in a bath of 50/50 sulfuric/nitric acid for no less than one hour, and rinsed with DI water and dried under nitrogen before use. Experiments described in this work used saturated solutions of Coumarin 151 in water, that were made by combining excess C151 and water and allowing the solution to equilibrate with stirring overnight at 50°C. The solutions were filtered to remove excess dye before use. At room temperature, the concentration of C151 in a saturated aqueous solution is approximately 6 μM. SHG spectra were collected from Kel-F sample chambers containing saturated C151 solution in contact with fused silica slides (Structure Probe, Inc.). For TIR-TCSPC measurements, a custom-built assembly was made from Kel-F sample chambers containing saturated aqueous C151 solution in contact with fused silica prisms (ISP Optics, Inc.), which allowed the excitation pulse to irradiate the interface formed between a hemispherical prism and an aqueous solution at angles greater than the critical angle (61° at 400 nm). Sample chambers, coumarin

solutions, silica slides and prisms were allowed to equilibrate for at least an hour before being used in experiments.

Silica slides (Structure Probe, Inc.) and prisms (ISP Optics, Inc.) were functionalized with a solution of dimethyldichlorosilane in THF to create hydrophobic surfaces. Silica substrates were cleaned as described above and allowed to sit in the silane solution at 30°C for 36 hours. Once removed from the silane solution, silica slides and prisms were first washed with toluene, then methanol and finally tested with water to verify that the surface was hydrophobic.

To collect TIR-TCSPC spectra, the output of a Ti:Sapphire oscillator (Chameleon, Coherent) was frequency doubled (APE Autotracker) and the 80 MHz repetition rate was attenuated to 4 MHz using an electro-optic modulator (Conoptics Model 350-105). Fluorescence emission was collected using a Picoquant 200 time-to-amplitude converter and the instrument response function (IRF) was measured using a non-emissive Ludox scattering solution. Emission was detected at 90° relative to the silica-aqueous interface. The TIR assembly's IRF was ~200 ps. For every experiment, the IRF was deconvoluted from the time-resolved emission histogram and the resulting trace was then fit to one or more single exponential decays. The minimum number of lifetimes required to accurately fit the data was determined using the Akaike information criterion.

In order to collect SHG signal from surface molecules, the coherent output from a tunable, amplified Ti:sapphire pumped optical parametric amplifier (OPA) at frequency ω is focused on the surface and creates a polarization of the surface

molecules at 2ω. The intensity of the collected second harmonic signal is proportional to the square of the second order polarizability, denoted as $P^{(2)}$:

$$I(2\omega) \propto \left| P^{(2)}(2\omega) \right|^2 \tag{5.1}$$

where $P^{(2)} = \left| \chi^{(2)} E(\omega_1) E(\omega_2) \right|$. In the case of second harmonic generation, the incident beam is of a single frequency and $\omega_1 = \omega_2$. The surface specificity of SHG, along with all second order nonlinear optical techniques, derives from $\chi^{(2)}$, the second order nonlinear susceptibility. $\chi^{(2)}$ is a rank 3 tensor consisting of 27 matrix elements; in centrosymmetric systems, the requirement that $\chi_{i,j,k}^{(2)} = \chi_{-i,-j,-k}^{(2)}$ means that no second harmonic response will originate from an isotropic solution within the electric dipole approximation. At an interface where symmetry is broken, elements of the $\chi^{(2)}$ tensor can take on non-zero values, dependent on the identity of the molecules at the interface. $\chi^{(2)}$ is composed of a non-resonant (NR) piece and a resonant (R) piece:

$$\chi^{(2)} = \chi_{NR}^{(2)} + \chi_R^{(2)} \tag{5.2}$$

The non-resonant portion of the $\chi^{(2)}$ tensor is usually simple and can be fit to a single value whereas the resonant contribution is more complicated. The resonant portion of $\chi^{(2)}$ is equal to the number of molecules on the surface multiplied by the orientational average over the molecular hyperpolarizability (β) of the adsorbed molecules:

$$\chi_R^{(2)} = N \langle \beta_{i,j,k} \rangle, \text{ where } \beta \text{ is given by: } \beta = \frac{A}{\omega_0 - \omega - i\Gamma} \tag{5.3}$$

111

In this expression for β, A is a constant related to the transition dipole moment of the electronic resonance being examined, ω_0 is the resonant frequency of the transition, ω is the frequency of the incident light, and Γ is the linewidth associated with the transition.

In cases where the interface under investigation carries a surface charge, the second harmonic spectral lineshape can be influenced by some non-resonant elements of the $\chi^{(3)}$ tensor, which makes equation (5.2) take the form

$$\chi^{(2)}_{total} \propto \chi^{(2)} + (\chi^{(3)}_1 + i\chi^{(3)}_2)\Phi(0) \tag{5.4}$$

where $\Phi(0)$ is the interfacial potential and both elements of the $\chi^{(3)}$ tensor are purely real.[114-115] Collected second harmonic spectra are fit with equations (5.2), (5.3) and (5.4) to determine the linewidth and the center of the resonant peak.

Resonance-enhanced SHG spectra were acquired from an experimental assembly that has been described previously.[8-9] Briefly, ~3.3W from a Ti:Sapphire regenerative amplifier (Libra-HE, Coherent, 85 fs pulses, 1 kHz repetition rate, 801 nm) was coupled to a visible optical parametric amplifier (Coherent OPerA Solo, fwhm 10 nm) and focused on the sample. If necessary, incident visible light was attenuated to below 4 mW with neutral density filters before it reached the sample. Second harmonic signal was collected using a photomultiplier tube and photon counting electronics. Data from each individual wavelength was collected over 3-5 separate 10s intervals, background corrected and then averaged. Typically, up to 300 counts were measured on resonance during a 10 sec. acquisition.

5.3 Results and Discussion

C151 emission in solution depends sensitively on solvent polarity. Figure 5.2 shows TCSPC traces from C151 dissolved in solvents selected to represent a range of static dielectric constants as well as both polar protic (methanol) and polar aprotic (acetonitrile) limits. Table 5.1 shows lifetimes and amplitudes from the traces displayed in Figure 5.2. C151 decay in nonpolar solvents can be fit to two lifetimes, 1.05 ns and 1.62 ns. In every other non-aqueous polar solvent C151 decays with single lifetimes between 5.2 and 5.3 ns. In water, C151 decays with a single lifetime of 4.57 ns. These lifetimes agree with data previously reported by Nad and Pal.[170] The long lifetimes observed in polar solvents has been attributed to ICT formation following photoexcitation. Nonpolar solvents cannot stabilize the ICT isomer.
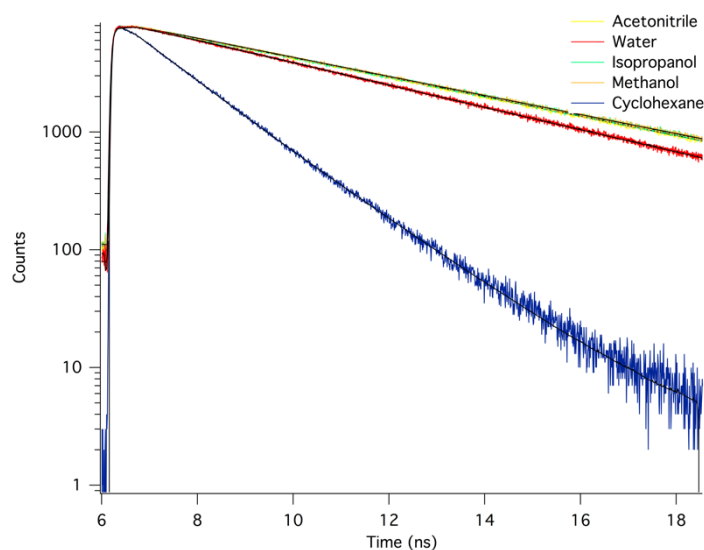
Figure 5.2: TCSPC decay traces of C151 dissolved in various bulk solvents

An important point to note when assessing data in Table 5.1 is the extreme lifetime difference between C151 in aqueous solution and in cyclohexane. If C151 motion at the

	A_1	τ_1 (ns)	A_2	τ_2 (ns)	χ^2	ε
Cyclohexane	.59	1.620	.41	1.047	1.008	2.02
Isopropanol	1	5.323			1.101	17.9
Acetonitrile	1	5.244			1.020	37.5
Methanol	1	5.332			1.029	32.7
Water	1	4.566			1.082	80.1

Table 5.1: Lifetimes and amplitudes from C151 fluorescence decay in bulk solvents

aqueous-silica interface were restricted, one would expect to observe a faster

fluorescence decay from C151 in the TIR data. Figure 5.3 shows TIR emission from

C151 adsorbed to the aqueous-silica interface. Adsorbed C151 decays with a single

lifetime of 4.51 ns, unchanged from its bulk water lifetime within the error of the

instrument (Figure 5.3). This result stands in marked contrast to previously reported data

from C152 and DMABN where adsorption to the aqueous-silica introduces a new decay

pathway consistent with the adsorbed solute's *inability* to isomerize.
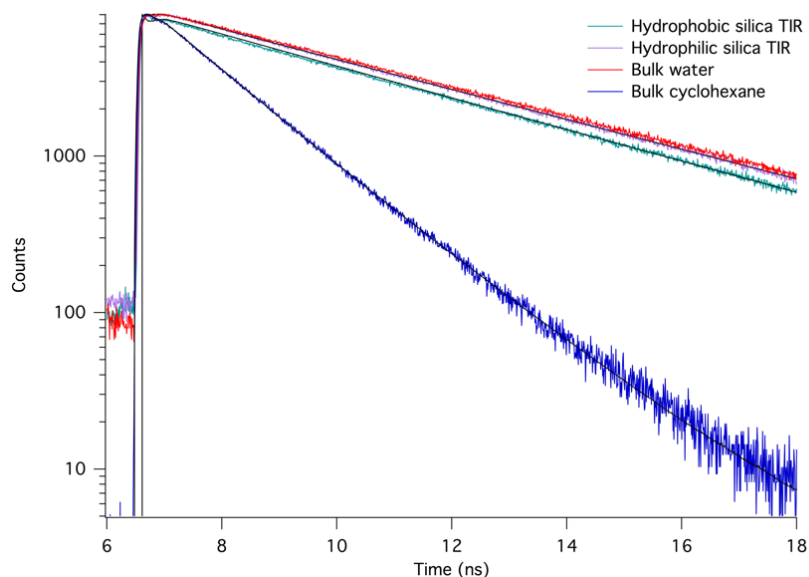
Figure 5.3: Fluorescence decay traces of C151 at the aqueous-silica interface with relevant bulk traces also shown

In prior work, disrupting the strong hydrogen bonding interactions between interfacial water molecules and surface silanol groups enabled adsorbed solutes to behave more like they were in bulk solution. To test what effects – if any – water-silica interactions have on C151 isomerization, the silica prism used in the TIR-TCSPC experiments was functionalized with a dichlorodimethylsilane layer to create a non-polar methyl layer at the silica-aqueous interface. C151 adsorbed to the aqueous-hydrophobic silica interface showed 2 emission lifetimes, one attributed to molecules in contact with the hydrophobic methyl layer and the other to C151 solutes dissolved in the bulk solution. The bulk lifetime, comprising 72% of the decay amplitude, is consistent with bulk solution measurements at 4.55 ns. The second lifetime was 3.51 ns. This shorter lifetime is difficult to interpret, as it does not correspond to C151 fluorescence decay in any known solvent, regardless of solvent polarity, viscosity, or hydrogen bonding. We propose that this lifetime originates from a local environment that affects C151 ICT formation without changing the interfacial polarity. Importantly, this result emphasizes the dangers of assuming that interfacial solvation and reactivity can be represented as a weighted average of two limiting behaviors.

	A_1	τ_1 (ns)	A_2	τ_2 (ns)	χ^2
Hydrophilic silica TIR	1	4.513			0.972
Hydrophobic silica TIR	.72	4.548	.28	3.509	1.204

Table 5.2: Lifetimes and amplitudes of C151 fluorescence decay at various silica-aqueous interfaces

The resonance-enhanced second harmonic generation (SHG) spectrum taken of C151 at the aqueous-silica interface aligns well with the absorbance spectrum of C151 in bulk water (Figure 5.4). The peak of the SHG spectrum is at 364 nm; the peak absorbance in bulk water is at 367 nm. To within experimental uncertainty, these numbers are functionally equivalent. The SHG spectrum has a much narrower linewidth than the bulk absorbance spectrum—27 nm vs 63 nm—a result consistent with other reported SHG spectra[108]. The resonant SHG spectrum illustrates that C151 adsorbed to the aqueous-silica interface experiences a polar, strong hydrogen bonding solvation environment very similar to bulk water.
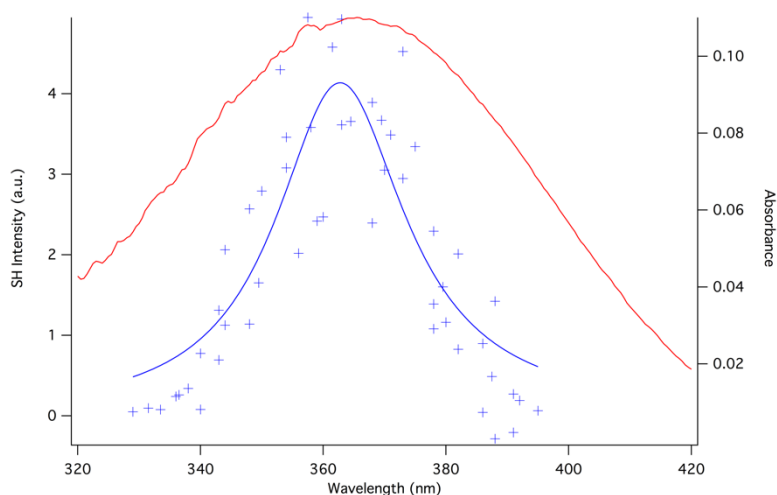
Figure 5.4: SHG spectrum (left ordinate, blue crosses) at the silica-aqueous interface and aqueous absorbance (right ordinate, red line) of Coumarin 151

Given similarities in both the SHG and TCSPC data between C151 adsorbed to the aqueous-silica interface and in bulk solution, we also measured the resonantly enhanced SHG spectrum of C151 adsorbed to the aqueous-hydrophobic silica interface. As described above, TCSPC data from this system showed an unusual 3.51 ns lifetime that did not correspond to any known lifetime from bulk solution measurements raising

the question about the local polarity sampled by C151 at this surface. SHG data are shown in Figure 5.5. Superimposed on the C151 SHG spectrum at the aqueous-hydrophobic silica interface is the C151 spectrum from the aqueous-hydrophilic silica interface (reproduced from Figure 5.4). At the hydrophobic silica interface, C151 shows a maximum in its SHG spectrum at 366 nm, virtually unchanged from hydrophilic silica result. The only significant difference between the spectra at the hydrophobic and hydrophilic silica interfaces is the linewidth—32 nm at the hydrophobic interface, 5 nm wider than at the hydrophilic interface. This result suggests more inhomogeneous broadening at the aqueous-hydrophobic silica interface. We expect that in the absence of strong, directional hydrogen bonding opportunities provided by the surface silanol groups, correspondingly greater disorder in the interfacial water organization will lead to more heterogeneity in adsorbed C151's environment. This difference in linewidth notwithstanding, the important result from the SHG measurements is that the polarity experienced by C151 at the aqueous-hydrophilic silica and aqueous-hydrophobic silica interfaces is effectively the same, meaning that differences observed in the TIR-TCSPC data likely owe their origins to differences in solvation dynamics.

Collectively, both the TIR-TCSPC and SHG results of C151 at the silica-aqueous interface suggest that despite any ordering of the water due to hydrogen bonding to the silica surface, C151 solutes at the interface do not experience a significantly different environment than in bulk water solution. These findings support the hypothesis that isomerization reactions requiring very small intramolecular structural rearrangements are
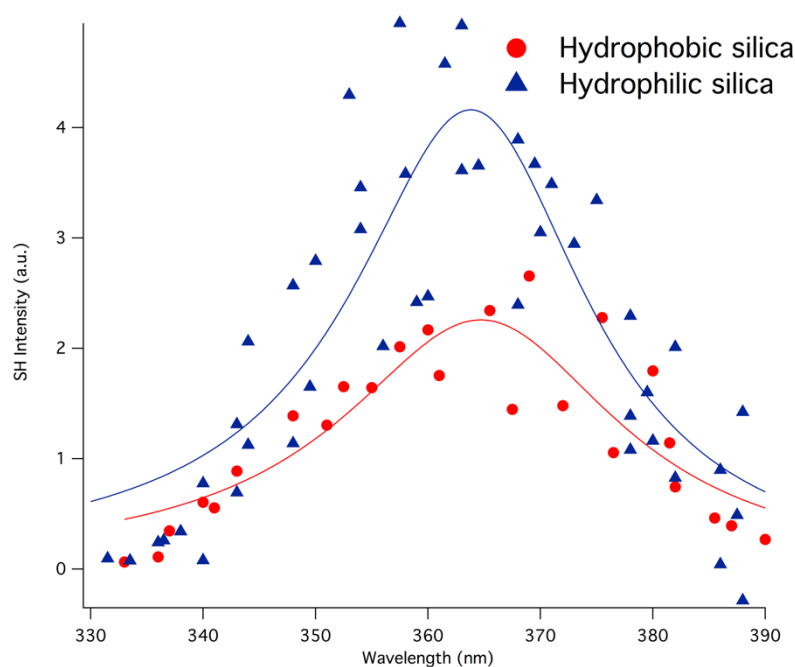
Figure 5.5: SHG spectra of C151 taken at the unmodified hydrophilic and the hydrophobic silica interfaces

largely insensitive to structural constraints imposed by the surrounding environment. Results also stand in stark contrast to the behavior of Coumarin 151's tertiary amine analog, Coumarin 152, that experiences significant restriction in its ability to isomerize at the interface, resulting in dramatic spectral differences between solutes dissolved at the aqueous-silica interface and in bulk water.[108, 171] We believe that this difference between these otherwise similar molecules has to do with the reaction coordinate required for each to form its excited state isomer. C152 isomerizes into a TICT state upon photoexcitation, where C151, not having the electron donating ability on its primary amine to form a TICT state, isomerizes into a planar ICT excited state. C151's isomerization from pyramidal amine to one in the plane of the rest of the molecule requires a much smaller solvent volume than the TICT isomerization, where C152's alkyl amine group goes from pyramidal in the ground state to a 90° twist relative to the molecular plane. Because of

the significant solvent ordering due to hydrogen bonding between the water molecules and the silanols at the interface, C152 is unable to complete this isomerization at the aqueous-silica interface due to strong geometric restriction. C151, with its much smaller excited state isomerization, is not restricted by solvent organization at the interface, and therefore displays the same solvation behavior at the silica-aqueous interface as it does in bulk solution.

5.4 Conclusions

Coumarin 151 solutes at the aqueous-silica interface do not experience a solvation environment significantly different than in bulk water. This result is in contrast to that of the closely-related Coumarin 152, where molecules adsorbed at the interface show time resolved fluorescence that implies a nonpolar environment. This result is attributed to the difference in excited state isomerization behavior between C151 and C152. C152 isomerizes into an excited TICT state, an isomerization that requires significant free solvent volume. In contrast, C151 isomerizes into a planar ICT state upon photoexcitation, a change that does not require as significant solvent volume as the isomerization in C152. This difference in isomerization behavior, the result of replacing the primary amine in C151 with the tertiary amine in C152, causes different behavior in the spectra of the two molecules at the aqueous-silica interface.

119

5.5 References

8.   Woods, B. L.; Walker, R. A., pH Effects on Molecular Adsorption and Solvation of p-Nitrophenol at Silica/Aqueous Interfaces. *J Phys Chem A* **2013,** *117* (29), 6224-6233.

9.   Woods, B. L.; George, J. K.; Sherman, A. M.; Callis, P. R.; Walker, R. A., Adsorption and Aggregation at Silica/Methanol Interfaces: The Role of Solute Structure. *J Phys Chem C* **2015,** *119* (25), 14230-14238.

59.   Grabowski, Z. R.; Rotkiewicz, K.; Rettig, W., Structural changes accompanying intramolecular electron transfer: Focus on twisted intramolecular charge-transfer states and structures. *Chem Rev* **2003,** *103* (10), 3899-4031.

72.   Dahiya, P.; Kumbhakar, M.; Mukherjee, T.; Pal, H., Effect of protic solvents on twisted intramolecular charge transfer state formation in coumarin-152 and coumarin-481 dyes. *Chem Phys Lett* **2005,** *414* (1-3), 148-154.

73.   Nad, S.; Kumbhakar, M.; Pal, H., Photophysical properties of coumarin-152 and coumarin-481 dyes: Unusual behavior in nonpolar and in higher polarity solvents. *Journal of Physical Chemistry A* **2003,** *107* (24), 4808-4816.

78.   Rettig, W.; Klock, A., Intramolecular Fluorescence Quenching in Aminocoumarines - Identification of an Excited-State with Full Charge Separation. *Can J Chem* **1985,** *63* (7), 1649-1653.

79.   Rechthaler, K.; Kohler, G., Excited-State Properties and Deactivation Pathways of 7-Aminocoumarins. *Chem Phys* **1994,** *189* (1), 99-116.

108.   Purnell, G. E.; Walker, R. A., Hindered Isomerization at the Silica/Aqueous Interface: Surface Polarity or Restricted Solvation? *Langmuir* **2018,** *34* (34), 9946-9949.

114.   Ohno, P. E.; Wang, H. F.; Geiger, F. M., Second-order spectral lineshapes from charged interfaces. *Nat Commun* **2017,** *8*.

115.   Ohno, P. E.; Saslow, S. A.; Wang, H. F.; Geiger, F. M.; Eisenthal, K. B., Phase-referenced nonlinear spectroscopy of the alpha-quartz/water interface. *Nat Commun* **2016,** *7*.

133.   Purnell, G. E.; Walker, R. A., Surface solvation and hindered isomerization at the water/silica interface explored with second harmonic generation. *The Journal of Chemical Physics* **2019,** *150* (19), 194701.

162. Di Giacomo, F., A Short Account of RRKM Theory of Unimolecular Reactions and of Marcus Theory of Electron Transfer in a Historical Perspective. *J Chem Educ* **2015,** *92* (3), 476-481.

163. Wardlaw, D. M.; Marcus, R. A., Rrkm Reaction-Rate Theory for Transition-States of Any Looseness. *Chem Phys Lett* **1984,** *110* (3), 230-234.

164. Shaikh, M.; Mohanty, J.; Singh, P. K.; Bhasikuttan, A. C.; Rajule, R. N.; Satam, V. S.; Bendre, S. R.; Kanetkar, V. R.; Pal, H., Contrasting Solvent Polarity Effect on the Photophysical Properties of Two Newly Synthesized Aminostyryl Dyes in the Lower and in the Higher Solvent Polarity Regions. *J Phys Chem A* **2010,** *114* (13), 4507-4519.

165. Bates, J. S.; Gounder, R., Influence of confining environment polarity on ethanol dehydration catalysis by Lewis acid zeolites. *J Catal* **2018,** *365*, 213-226.

166. Otolski, C. J.; Raj, A. M.; Sharma, G.; Prabhakar, R.; Ramamurthy, V.; Elles, C. G., Ultrafast trans -> cis Photoisomerization Dynamics of Alkyl-Substituted Stilbenes in a Supramolecular Capsule. *J Phys Chem A* **2019,** *123* (24), 5061-5071.

167. Otolski, C. J.; Raj, A. M.; Ramamurthy, V.; Elles, C. G., Ultrafast Dynamics of Encapsulated Molecules Reveals New Insight on the Photoisomerization Mechanism for Azobenzenes. *J Phys Chem Lett* **2019,** *10* (1), 121-127.

168. Douhal, A.; Sanz, M.; Tormo, L., Femtochemistry of orange II in solution and in chemical and biological nanocavities. *P Natl Acad Sci USA* **2005,** *102* (52), 18807-18812.

169. Jones, G.; Jackson, W. R.; Kanoktanaporn, S.; Halpern, A. M., Solvent Effects on Photophysical Parameters for Coumarin Laser-Dyes. *Opt Commun* **1980,** *33* (3), 315-320.

170. Nad, S.; Pal, H., Unusual photophysical properties of coumarin-151. *J Phys Chem A* **2001,** *105* (7), 1097-1106.

171. Purnell, G. E.; Walker, R. A., Surface solvation and hindered isomerization at the water/silica interface explored with second harmonic generation. *J Chem Phys* **2019,** *150* (19).

172. Onabuta, Y.; Kunimoto, M.; Nakai, H.; Homma, T., First-principle study of the oxidation mechanism of formaldehyde and hypophosphite for copper and nickel electroless deposition process. *Electrochim Acta* **2019,** *307*, 536-542.

173. Sievers, C.; Noda, Y.; Qi, L.; Albuquerque, E. M.; Rioux, R. M.; Scott, S. L., Phenomena Affecting Catalytic Reactions at Solid-Liquid Interfaces. *Acs Catal* **2016,** *6* (12), 8286-8307.

174. Okuno, Y.; Ushirogata, K.; Sodeyama, K.; Tateyama, Y., Decomposition of the fluoroethylene carbonate additive and the glue effect of lithium fluoride products for the

solid electrolyte interphase: an ab initio study. *Phys Chem Chem Phys* **2016,** *18* (12), 8643-8653.

CHAPTER SIX

CONCLUSIONS AND FUTURE DIRECTIONS

6.1 Summary

Work presented in this thesis examined how adsorption at the strongly associating silica-aqueous interface impacted the ability of several organic molecules to isomerize in their excited states. Several linear and nonlinear electronic spectroscopic techniques were utilized to understand the interfacial environment in which these molecules were adsorbed, and from there, infer information about the excited state dynamics of the adsorbed solutes and give insight into solvent structure and dynamics at the silica-aqueous interface.

Initial studies focused on time-resolved fluorescence spectra of Coumarin 152 (C152) adsorbed to the aqueous-silica interface. These spectra showed that C152 at this interface shows fluorescence behavior very similar to solutes that are dissolved in bulk nonpolar solutions. These results were interpreted in light of the strong association between the silica and the water molecules at the interface which imposes a geometric order on the surface-associated water molecules. This solvent order at the interface means that the surface waters are unable to reorganize to stabilize the twisted intramolecular charge transfer (TICT) state after photoexcitation and that this order imposes a limited solvent volume for the solute to isomerize. This hypothesis about solvent structure and association preventing solutes from isomerizing following photoexcitation was supported by fluorescence studies of C152 inside an ice matrix. Inside a structured ice matrix, C152

solutes also show a fluorescence lifetime similar to that seen in bulk nonpolar solution and at the silica-aqueous interface.

Chapter 3 used second harmonic generation (SHG) to confirm that the silica-aqueous interface is indeed polar. Given that confirmation, we functionalized a silica surface to remove its ability to hydrogen bond by adding a dichlorodimethylsilane monolayer to that surface. When C152 is adsorbed to this hydrophobic silica-aqueous interface, its fluorescence signature once again shows that it can access its excited TICT state. This result supports the hypothesis that strong hydrogen bonding and water ordering is responsible for C152's inability to isomerize at the aqueous-silica interface. At the hydrophilic silica-aqueous interface, there is a marked distinction between ground and excited state behavior, which is caused by C152's inability to isomerize following photoexcitation when water molecules are strongly ordered by the interface. When we disrupt the ability of the silica surface to order the water molecules adjacent to it by removing its ability to hydrogen bond, the environment indicated by both ground and excited state behavior merges to a similar intermediate polarity limit.

Chapter 4 describes the studies done on 4-dimethylaminobenzonitrile (DMABN) in order to expand the hypotheses formulated to explain the behavior of C152 at the silica-aqueous interface to a more general class of organic molecules with large-amplitude excited state isomerizations. DMABN is the oldest and most well-known example of TICT chemistry, with dual emissive states, so we took SHG and TIR-TCSPC spectra of it at the aqueous silica-interface. Its time-resolved fluorescence at the surface is missing any evidence of TICT formation, as the results from prior studies with C152

would suggest. The TICT emission returns when hydrogen bonding is disrupted by adhering a hydrophobic monolayer to the silica surface, which is also predicted from the C152 studies. Unexpectedly, the SHG spectrum of DMABN at the aqueous-silica interface shows a second electronic resonance that is not immediately evident in bulk absorption spectra of the molecule. This second peak is rationalized with the help of semi-empirical calculations that show that strong electric fields caused by the surface can enhance the intensity of the S_0—S_1 transition dramatically, giving the spectrum seen from DMABN adsorbed to the aqueous-silica interface.

Chapter 5 describes the studies done on another molecule in the 7-aminocoumarin family, Coumarin 151 (C151). C151 is structurally similar to C152, but with a primary amine in the 7-position where C152 has a tertiary dimethyl amine group. This structural difference means that C151 does not form a TICT state upon photoexcitation, rather, it forms a planar intramolecular charge transfer (ICT) state. The same sets of SHG and TIR-TCSPC experiments were performed on C151 as on C152 and DMABN to examine the effect of the surface on a much smaller amplitude isomerization event. C151 shows nearly identical spectroscopic behavior at the aqueous-silica surface as in bulk aqueous solution, indicating that only large amplitude isomerizations are restricted at the interface.

Together the experiments described in this thesis represent a detailed investigation of how surface properties can influence molecular isomerization behavior, which has a significant impact on those molecules' reactivity at that interface. Since the surface restricts the formation of excited states with a significant geometric change from the ground state, these results were interpreted as a form of chemistry in confinement, similar

to that which might occur inside a zeolite or molecular pore. Understanding how the

reactivity of molecules is changed by adsorption to an interface is important for many

areas of chemistry from chromatography to environmental geochemistry.

6.2 Future Directions

While these experiments represent new and important discoveries into the surface

chemistry of organic molecules, there remain several avenues of investigation prompted

by the results in this thesis that have not yet been investigated. The remaining questions

inspired by this work fall into 3 general areas: other solutes, other solvents, and effect of

pH.

6.2.1 Other Solutes

The work in this thesis examined coumarin dyes and a substituted aniline

molecule, but there are several other classes of organic molecules that are also capable of

large amplitude isomerizations. A particularly interesting example of TICT chemistry is

Rhodamine B (Figure 6.1). Rhodamine B has a closed-ring spirolactone that can be

opened by hydrogen ions. In its closed form, it exists in a TICT state that is colorless and

nonfluorescent. When it is opened by acid, conjugation extends over the whole molecule,

and it turns bright pink and highly fluorescent. Given the propensity of the surface to

inhibit TICT formation, an interesting application of the results of this thesis would be to

place a basic (colorless, TICT) solution of Rhodamine B adjacent to the silica surface and

see if and to what extent the surface rejects the TICT state and makes the molecules

adhered to the surface fluorescent again. This concept is supported by an offhanded
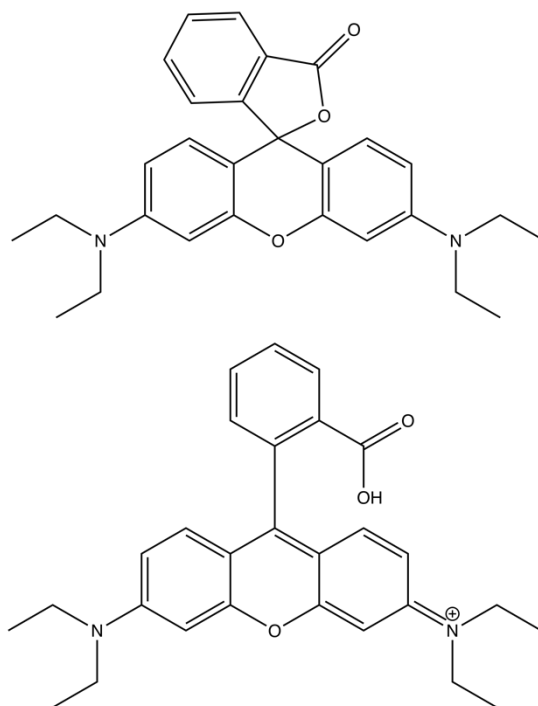
Figure 6.1 Rhodamine B in its closed-ring spirolactone form (top) and its open, conjugated, fluorescent form (bottom)

mention in a paper from 1982, which stated that their rhodamine solutions could not be left in their silica cuvettes for long before taking a spectrum, as contact with the walls of the cuvette tended to turn the solution pink.[175]

6.2.2 Other Solvents

The work described in this thesis is concerned only with the aqueous-silica interface but there are many other solvents that have interesting interactions with silica surfaces that warrant examination. It is known that the strong association of alcohols to the silica surface creates a nonpolar region adjacent to the interface where the hydrogen bonded hydroxyl groups align the attached alkyl tails.[6, 25, 104, 119] In this thesis, we look at the effect of creating a hydrophobic surface to prevent association with water, but to my

knowledge, this surface has not been explored in terms of the solvation of organic solutes in solvents other than water. In particular, do alcoholic solvents adjacent to a hydrophobic silica surface also align with their alkyl tails attracted to the silica and their hydroxyl groups forming an ordered, high polarity region adjacent to the interface, or do they interact by another means? Understanding how different solvents interact with the silica surface and what that means for molecules solvated therein is important particularly for chemical separations and chromatography.

6.2.3 pH Studies

Most of the earliest work examining water structure at silica-aqueous interfaces noted that the spectral peaks corresponding to ordered (i.e. ice-like) and disordered water changed their relative intensities as an effect of changing the pH of the water solution.[37] Specifically, in low and high pH solutions that create a more strongly charged silica surface, the intensity of the ordered, ice-like peak was larger than in the solutions of more neutral pH. Given that the central premise of this thesis is that ordering of water molecules as a result of association with the silica surface interferes with molecular isomerization, investigation of surfaces with different degrees and structures of water ordering is an obvious next step. Additionally, changing the pH of the water solution in contact with the silica surface will also affect the surface charge and corresponding electric field on the silica surface. The computational results presented in chapter 4 attest to the importance of the surface field in determining molecular reactivity at the interface, so a systematic study of the effect of the pH of the aqueous solution provides a convenient way to experimentally test those computational conclusions.

6.3 References

6.   Gobrogge, E. A.; Woods, B. L.; Walker, R. A., Liquid organization and solvation properties at polar solid/liquid interfaces. *Faraday Discuss* **2013,** *167*, 309-327.

25.   Karnes, J. J.; Gobrogge, E. A.; Walker, R. A.; Benjamin, I., Unusual Structure and Dynamics at Silica/Methanol and Silica/Ethanol Interfaces-A Molecular Dynamics and Nonlinear Optical Study. *J Phys Chem B* **2016,** *120* (8), 1569-1578.

37.   Du, Q.; Freysz, E.; Shen, Y. R., Vibrational-Spectra of Water-Molecules at Quartz Water Interfaces. *Phys Rev Lett* **1994,** *72* (2), 238-241.

104.   Brindza, M. R.; Walker, R. A., Differentiating Solvation Mechanisms at Polar Solid/Liquid Interfaces. *J Am Chem Soc* **2009,** *131* (17), 6207-6214.

119.   Horng, P.; Brindza, M. R.; Walker, R. A.; Fourkas, J. T., Behavior of Organic Liquids at Bare and Modified Silica Interfaces. *J Phys Chem C* **2010,** *114* (1), 394-402.

175.   Snare, M. J.; Treloar, F. E.; Ghiggino, K. P.; Thistlethwaite, P. J., The Photophysics of Rhodamine-B. *J Photochem* **1982,** *18* (4), 335-346.

129

REFERENCES CITED

1.   Zenasni, O.; Marquez, M. D.; Jamison, A. C.; Lee, H. J.; Czader, A.; Lee, T. R., Inverted Surface Dipoles in Fluorinated Self-Assembled Monolayers. *Chem Mater* **2015,** *27* (21), 7433-7446.

2.   Steel, W. H.; Walker, R. A., Measuring dipolar width across liquid-liquid interfaces with 'molecular rulers'. *Nature* **2003,** *424* (6946), 296-299.

3.   Zhang, X. Y.; Esenturk, O.; Walker, R. A., Reduced polarity in protic solvents near hydrophobic solid surfaces. *J Am Chem Soc* **2001,** *123* (43), 10768-10769.

4.   Zhong, J.; Carignano, M. A.; Kais, S.; Zeng, X. C.; Francisco, J. S.; Gladich, I., Tuning the Stereoselectivity and Solvation Selectivity at Interfacial and Bulk Environments by Changing Solvent Polarity: Isomerization of Glyoxal in Different Solvent Environments. *J Am Chem Soc* **2018,** *140* (16), 5535-5543.

5.   Gobrogge, E. A.; Walker, R. A., Binary Solvent Organization at Silica/Liquid Interfaces: Preferential Ordering in Acetonitrile-Methanol Mixtures. *J Phys Chem Lett* **2014,** *5* (15), 2688-2693.

6.   Gobrogge, E. A.; Woods, B. L.; Walker, R. A., Liquid organization and solvation properties at polar solid/liquid interfaces. *Faraday Discuss* **2013,** *167*, 309-327.

7.   Roy, D.; Liu, S. L.; Woods, B. L.; Siler, A. R.; Fourkas, J. T.; Weeks, J. D.; Walker, R. A., Nonpolar Adsorption at the Silica/Methanol Interface: Surface Mediated Polarity and Solvent Density across a Strongly Associating Solid/Liquid Boundary. *J Phys Chem C* **2013,** *117* (51), 27052-27061.

8.   Woods, B. L.; Walker, R. A., pH Effects on Molecular Adsorption and Solvation of p-Nitrophenol at Silica/Aqueous Interfaces. *J Phys Chem A* **2013,** *117* (29), 6224-6233.

9.   Woods, B. L.; George, J. K.; Sherman, A. M.; Callis, P. R.; Walker, R. A., Adsorption and Aggregation at Silica/Methanol Interfaces: The Role of Solute Structure. *J Phys Chem C* **2015,** *119* (25), 14230-14238.

10.   Beniwal, V.; Manna, A.; Kumar, A., Spectacular Rate Enhancement of the Diels-Alder Reaction at the Ionic Liquid/n-Hexane Interface. *Chemphyschem* **2016,** *17* (13), 1969-1972.

11.   Dong, R. H.; Zhang, T.; Feng, X. L., Interface-Assisted Synthesis of 2D Materials: Trend and Challenges. *Chem Rev* **2018,** *118* (13), 6189-6235.

12.   Arnold, W. A.; Roberts, A. L., Pathways and kinetics of chlorinated ethylene and chlorinated acetylene reaction with Fe(O) particles. *Environ Sci Technol* **2000,** *34* (9), 1794-1805.

13.   Tseng, T. C.; Urban, C.; Wang, Y.; Otero, R.; Tait, S. L.; Alcami, M.; Ecija, D.; Trelka, M.; Gallego, J. M.; Lin, N.; Konuma, M.; Starke, U.; Nefedov, A.; Langner, A.; Woll, C.; Herranz, M. A.; Martin, F.; Martin, N.; Kern, K.; Miranda, R., Charge-transfer-induced structural rearrangements at both sides of organic/metal interfaces. *Nat Chem* **2010,** *2* (5), 374-379.

14.   Munninghoff, J. A. W.; Elemans, J. A. A. W., Chemistry at the square nanometer: reactivity at liquid/solid interfaces revealed with an STM. *Chem Commun* **2017,** *53* (11), 1769-1788.

15.   Shibukawa, M.; Miyake, A.; Eda, S.; Saito, S., Determination of the cis-trans lsomerization Barriers of L-Alanyl-L-proline in Aqueous Solutions and at Water/Hydrophobic Interfaces by On-Line Temperature-Jump Relaxation HPLC and Dynamic On-Column Reaction HPLC. *Anal Chem* **2015,** *87* (18), 9280-9287.

16.   Chen, H.; Zou, H. B.; Hao, Y. J.; Yang, H. Q., Flow Pickering Emulsion Interfaces Enhance Catalysis Efficiency and Selectivity for Cyclization of Citronellal. *Chemsuschem* **2017,** *10* (9), 1989-1995.

17.   Guo, L. W.; Cesari, S.; de Guillen, K.; Chalvon, V.; Mammri, L.; Ma, M. Q.; Meusnier, I.; Bonnot, F.; Padilla, A.; Peng, Y. L.; Liu, J. F.; Kroj, T., Specific recognition of two MAX effectors by integrated HMA domains in plant immune receptors involves distinct binding surfaces. *P Natl Acad Sci USA* **2018,** *115* (45), 11637-11642.

18.   Fukuda, T., Biological recognition at interfaces involving dendritic molecules. *Polym J* **2019,** *51* (6), 535-546.

19.   Neal, J. F.; Zhao, W.; Grooms, A. J.; Smeltzer, M. A.; Shook, B. M.; Flood, A. H.; Allen, H. C., Interfacial Supramolecular Structures of Amphiphilic Receptors Drive Aqueous Phosphate Recognition. *J Am Chem Soc* **2019,** *141* (19), 7876-7886.

20.   Dubacheva, G. V.; Curk, T.; Frenkel, D.; Richter, R. P., Multivalent Recognition at Fluid Surfaces: The Interplay of Receptor Clustering and Superselectivity. *J Am Chem Soc* **2019,** *141* (6), 2577-2588.

21.   Lin, J. F.; Liu, Y.; Liu, Y. P.; Huang, C.; Liu, W. H.; Mi, X. H.; Fan, D. Y.; Fan, F. T.; Lu, H. D.; Chen, X. B., SnS2 Nanosheets/H-TiO2 Nanotube Arrays as a Type II Heterojunctioned Photoanode for Photoelectrochemical Water Splitting. *Chemsuschem* **2019,** *12* (5), 961-967.

22.   Zang, S. H.; Zhang, G. G.; Lan, Z. A.; Zheng, D. D.; Wang, X. C., Enhancement of photocatalytic H-2 evolution on pyrene-based polymer promoted by MoS2 and visible light. *Appl Catal B-Environ* **2019,** *251*, 102-111.

23.   Urban, C.; Wang, Y.; Rodriguez-Fernandez, J.; Garcia, R.; Herranz, M. A.; Alcami, M.; Martin, N.; Martin, F.; Gallego, J. M.; Miranda, R.; Otero, R., Charge

transfer-assisted self-limited decyanation reaction of TCNQ-type electron acceptors on Cu(100). *Chem Commun* **2014,** *50* (7), 833-835.

24.   Zhang, X.; Steel, W. H.; Walker, R. A., Probing solvent polarity across strongly associating solid/liquid interfaces using molecular rulers. *J Phys Chem B* **2003,** *107* (16), 3829-3836.

25.   Karnes, J. J.; Gobrogge, E. A.; Walker, R. A.; Benjamin, I., Unusual Structure and Dynamics at Silica/Methanol and Silica/Ethanol Interfaces-A Molecular Dynamics and Nonlinear Optical Study. *J Phys Chem B* **2016,** *120* (8), 1569-1578.

26.   Shang, X. M.; Benderskii, A. V.; Eisenthal, K. B., Ultrafast solvation dynamics at silica/liquid interfaces probed by time-resolved second harmonic generation. *J Phys Chem B* **2001,** *105* (47), 11578-11585.

27.   Ding, F.; Hu, Z. H.; Zhong, Q.; Manfred, K.; Gattass, R. R.; Brindza, M. R.; Fourkas, J. T.; Walker, R. A.; Weeks, J. D., Interfacial Organization of Acetonitrile: Simulation and Experiment. *J Phys Chem C* **2010,** *114* (41), 17651-17659.

28.   Kirkwood, J. G., The dielectric polarization of polar liquids. *J Chem Phys* **1939,** *7* (10), 911-919.

29.   Axelrod, D.; Burghardt, T. P.; Thompson, N. L., Total Internal-Reflection Fluorescence. *Annu Rev Biophys Bio* **1984,** *13*, 247-268.

30.   Hecht, E., *Optics*. Fourth ed.; Addison Wesley: San Francisco, CA, 2002.

31.   Martin-Fernandez, M. L.; Tynan, C. J.; Webb, S. E. D., A 'pocket guide' to total internal reflection fluorescence. *J Microsc-Oxford* **2013,** *252* (1), 16-22.

32.   Birch, D. J. S.; Imhof, R. E., Time-Domain Fluorescence Spectroscopy Using Time-Correlated Single-Photon Counting. In *Topics in Fluorescence Spectroscopy, Volume 1: Techniques*, Lakowicz, J. R., Ed. Plenum Press: New York, 1991.

33.   Franken, P. A.; Weinreich, G.; Peters, C. W.; Hill, A. E., Generation of Optical Harmonics. *Phys Rev Lett* **1961,** *7* (4), 118-&.

34.   Boyd, R. W., Nonlinear Optics, 3rd Edition. *Nonlinear Optics, 3rd Edition* **2008**, 1-613.

35.   He, G. S., *Nonlinear Optics and Photonics*. First ed.; Oxford University Press: Oxford, UK, 2015.

36.   Moad, A. J.; Simpson, G. J., A unified treatment of selection rules and symmetry relations for sum-frequency and second harmonic spectroscopies. *J Phys Chem B* **2004,** *108* (11), 3548-3562.

37.   Du, Q.; Freysz, E.; Shen, Y. R., Vibrational-Spectra of Water-Molecules at Quartz Water Interfaces. *Phys Rev Lett* **1994,** *72* (2), 238-241.

38.   Klier, K.; Zettlemoyer, A. C., Water at Interfaces - Molecular-Structure and Dynamics. *J Colloid Interf Sci* **1977,** *58* (2), 216-229.

39.   Sovago, M.; Campen, R. K.; Bakker, H. J.; Bonn, M., Hydrogen bonding strength of interfacial water determined with surface sum-frequency generation. *Chem Phys Lett* **2009,** *470* (1-3), 7-12.

40.   Sovago, M.; Campen, R. K.; Wurpel, G. W. H.; Muller, M.; Bakker, H. J.; Bonn, M., Vibrational response of hydrogen-bonded interfacial water is dominated by intramolecular coupling. *Phys Rev Lett* **2008,** *100* (17).

41.   Nihonyanagi, S.; Yamaguchi, S.; Tahara, T., Water Hydrogen Bond Structure near Highly Charged Interfaces Is Not Like Ice. *J Am Chem Soc* **2010,** *132* (20), 6867-+.

42.   Tian, C. S.; Shen, Y. R., Comment on "Vibrational Response of Hydrogen-Bonded Interfacial Water is Dominated by Intramolecular Coupling". *Phys Rev Lett* **2008,** *101* (13).

43.   Sovago, M.; Campen, R. K.; Wurpel, G. W. H.; Muller, M.; Bakker, H. J.; Bonn, M., Comment on "Vibrational Response of Hydrogen-Bonded Interfacial Water is Dominated by Intramolecular Coupling" - Reply. *Phys Rev Lett* **2008,** *101* (13).

44.   Nihonyanagi, S.; Mondal, J. A.; Yamaguchi, S.; Tahara, T., Structure and Dynamics of Interfacial Water Studied by Heterodyne-Detected Vibrational Sum-Frequency Generation. *Annu Rev Phys Chem* **2013,** *64*, 579-603.

45.   de Beer, A. G. F.; Roke, S., What interactions can distort the orientational distribution of interfacial water molecules as probed by second harmonic and sum frequency generation? *J Chem Phys* **2016,** *145* (4).

46.   Gupta, P. K.; Meuwly, M., Dynamics and vibrational spectroscopy of water at hydroxylated silica surfaces. *Faraday Discuss* **2013,** *167*, 329-346.

47.   Ong, S. W.; Zhao, X. L.; Eisenthal, K. B., Polarization of Water-Molecules at a Charged Interface - 2nd Harmonic Studies of the Silica Water Interface. *Chem Phys Lett* **1992,** *191* (3-4), 327-335.

48.   Zhuravlev, L. T., Concentration of Hydroxyl-Groups on the Surface of Amorphous Silicas. *Langmuir* **1987,** *3* (3), 316-318.

49.   Iler, R. K., *Chemistry of Silica*. John Wiley & Sons: 1979.

50.   Yeganeh, M. S.; Dougal, S. M.; Pink, H. S., Vibrational spectroscopy of water at liquid/solid interfaces: Crossing the isoelectric point of a solid surface. *Phys Rev Lett* **1999,** *83* (6), 1179-1182.

51.   Sulpizi, M.; Gaigeot, M. P.; Sprik, M., The Silica-Water Interface: How the Silanols Determine the Surface Acidity and Modulate the Water Properties. *J Chem Theory Comput* **2012,** *8* (3), 1037-1047.

52.   Argyris, D.; Cole, D. R.; Striolo, A., Dynamic Behavior of Interfacial Water at the Silica Surface. *J Phys Chem C* **2009,** *113* (45), 19591-19600.

53.   Kjellander, R.; Marcelja, S., Perturbation of Hydrogen-Bonding in Water near Polar Surfaces. *Chem Phys Lett* **1985,** *120* (4-5), 393-396.

54.   Shen, Y. R.; Ostroverkhov, V., Sum-frequency vibrational spectroscopy on water interfaces: Polar orientation of water molecules at interfaces. *Chem Rev* **2006,** *106* (4), 1140-1154.

55.   Shi, X.; Borguet, E.; Tarnovsky, A. N.; Eisenthal, K. B., Ultrafast dynamics and structure at aqueous interfaces by second harmonic generation. *Chem Phys* **1996,** *205* (1-2), 167-178.

56.   Shirota, H.; Castner, E. W., Solvation in highly nonideal solutions: A study of aqueous 1-propanol using the coumarin 153 probe. *J Chem Phys* **2000,** *112* (5), 2367-2376.

57.   Barbara, P. F., Ultrafast Studies on Intramolecular Charge-Transfer and Solvation. *Springer Series Chem* **1990,** *53*, 393-396.

58.   Nagarajan, V.; Brearley, A. M.; Kang, T. J.; Barbara, P. F., Time-Resolved Spectroscopic Measurements on Microscopic Solvation Dynamics. *J Chem Phys* **1987,** *86* (6), 3183-3196.

59.   Grabowski, Z. R.; Rotkiewicz, K.; Rettig, W., Structural changes accompanying intramolecular electron transfer: Focus on twisted intramolecular charge-transfer states and structures. *Chem Rev* **2003,** *103* (10), 3899-4031.

60.   Lippert, E.; Lüder, W.; Boos, H., Fluoreszenzspektrum und Frank-Condon-Prinzip in Lösungen aroma-tischer Verbindungen. In *Advances in Molecular Spectroscopy*, Mangini, A., Ed. Pergamon Press: Oxford, 1962; Vol. 1, pp 442-456.

61.   Visser, R. J.; Varma, C. A. G. O., Source of Anomalous Fluorescence from Solutions of 4-N,N-Dimethylaminobenzonitrile in Polar-Solvents. *J Chem Soc Farad T 2* **1980,** *76*, 453-471.

62.   Chandross, E. A.; Thomas, H. T., The interaction of amine-hydrocarbon exciplexes with small dipolar molecules - stoichiometric complex formation. *Chem Phys Lett* **1971,** *9* (5), 397-400.

63.   Khalil, O. S., Excimer Model of N,N-Dialkyl-Para-Cyanoanilines Fluorescence in Polar-Solvents. *Chem Phys Lett* **1975,** *35* (2), 172-174.

64.   Zachariasse, K. A., Comment on "Pseudo-Jahn-Teller and TICT-models: a photophysical comparison of meta-and para-DMABN derivatives" [Chem. Phys. Lett. 305(1999)8] - The PICT model for dual fluorescence of aminobenzonitriles. *Chem Phys Lett* **2000,** *320* (1-2), 8-13.

65.   Zachariasse, K. A.; Grobys, M.; vonderHaar, T.; Hebecker, A.; Ilichev, Y. V.; Morawski, O.; Ruckert, I.; Kuhnle, W., Photoinduced intramolecular charge transfer and internal conversion in molecules with a small energy gap between S-1 and S-2. Dynamics and structure. *J Photoch Photobio A* **1997,** *105* (2-3), 373-383.

66.   Lewis, F. D.; Holman, B., Singlet-States of Benzonitrile and Para-Dimethylaminobenzonitrile. *J Phys Chem-Us* **1980,** *84* (18), 2326-2328.

67.   Sobolewski, A. L.; Domcke, W., Promotion of intramolecular charge transfer in dimethylamino derivatives: Twisting versus acceptor-group rehybridization. *Chem Phys Lett* **1996,** *259* (1-2), 119-127.

68.   Sobolewski, A. L.; Domcke, W., Charge transfer in aminobenzonitriles: Do they twist? *Chem Phys Lett* **1996,** *250* (3-4), 428-436.

69.   Rotkiewicz, K.; Grellmann, K. H.; Grabowski, Z. R., Reinterpretation of Anomalous Fluorescence of "Para-N,N-Dimethylamino-Benzonitrile. *Chem Phys Lett* **1973,** *19* (3), 315-318.

70.   Siemiarczuk, A.; Grabowski, Z. R.; Krowczynski, A., 2 Emitting States of Excited Para-(9-Anthryl)-N,N-Dimethylaniline Derivatives in Polar-Solvents. *Chem Phys Lett* **1977,** *51* (2), 315-320.

71.   Grabowski, Z. R.; Rotkiewicz, K.; Siemiarczuk, A., Dual Fluorescence of Donor-Acceptor Molecules and the Twisted Intra-Molecular Charge-Transfer (Tict) States. *J Lumin* **1979,** *18-9* (Jan), 420-424.

72.   Dahiya, P.; Kumbhakar, M.; Mukherjee, T.; Pal, H., Effect of protic solvents on twisted intramolecular charge transfer state formation in coumarin-152 and coumarin-481 dyes. *Chem Phys Lett* **2005,** *414* (1-3), 148-154.

73.   Nad, S.; Kumbhakar, M.; Pal, H., Photophysical properties of coumarin-152 and coumarin-481 dyes: Unusual behavior in nonpolar and in higher polarity solvents. *Journal of Physical Chemistry A* **2003,** *107* (24), 4808-4816.

74.   Arbeloa, T. L.; Arbeloa, F. L.; Estevez, M. J. T.; Arbeloa, I. L., Binary Solvent Effects on the Absorption and Emission of 7-Aminocoumarins. *J Lumin* **1994,** *59* (6), 369-375.

75.   Arbeloa, T. L.; Arbeloa, F. L.; Tapia, M. J.; Arbeloa, I. L., Hydrogen-Bonding Effect on the Photophysical Properties of 7-Aminocoumarin Derivatives. *J Phys Chem-Us* **1993,** *97* (18), 4704-4707.

76.   Cave, R. J.; Burke, K.; Castner, E. W., Theoretical Investigation of the Ground and Excited States of Coumarin 151 and Coumarin 120. *The Journal of Physical Chemistry A* **2002,** *106* (40), 9294-9305.

77.   Cave, R. J.; Castner, E. W., Time-Dependent Density Functional Theory Investigation of the Ground and Excited States of Coumarins 102, 152, 153, and 343. *The Journal of Physical Chemistry A* **2002,** *106* (50), 12117-12123.

78.   Rettig, W.; Klock, A., Intramolecular Fluorescence Quenching in Aminocoumarines - Identification of an Excited-State with Full Charge Separation. *Can J Chem* **1985,** *63* (7), 1649-1653.

79.   Rechthaler, K.; Kohler, G., Excited-State Properties and Deactivation Pathways of 7-Aminocoumarins. *Chem Phys* **1994,** *189* (1), 99-116.

80.   Corrie, J. E. T.; Munasinghe, V. R. N.; Rettig, W., Synthesis and fluorescence properties of substituted 7-aminocoumarin-3-carboxylate derivatives. *J Heterocyclic Chem* **2000,** *37* (6), 1447-1455.

81.   Du, Q.; Superfine, R.; Freysz, E.; Shen, Y. R., Vibrational Spectroscopy of Water at the Vapor Water Interface. *Phys Rev Lett* **1993,** *70* (15), 2313-2316.

82.   Richmond, G. L., Molecular bonding and interactions at aqueous surfaces as probed by vibrational sum frequency spectroscopy. *Chem Rev* **2002,** *102* (8), 2693-2724.

83.   Mondal, J. A.; Nihonyanagi, S.; Yamaguchi, S.; Tahara, T., Structure and Orientation of Water at Charged Lipid Monolayer/Water Interfaces Probed by Heterodyne-Detected Vibrational Sum Frequency Generation Spectroscopy. *J Am Chem Soc* **2010,** *132* (31), 10656-10657.

84.   Leung, K.; Nielsen, I. M. B.; Criscenti, L., Elucidating the bimodal acid-base behavior of the water-silica interface from first principles. *Geochim Cosmochim Ac* **2010,** *74* (12), A584-A584.

85.   Shang, X. M.; Benderskii, A. V.; Eisenthal, K. B., Ultrafast solvation dynamics at silica/liquid interfaces probed by time-resolved second harmonic generation (vol 150B, pg 11578, 2001). *J Phys Chem B* **2001,** *105* (47), 11928-11928.

86. Wang, H. F.; Borguet, E.; Eisenthal, K. B., Polarity of liquid interfaces by second harmonic generation spectroscopy. *J Phys Chem A* **1997,** *101* (4), 713-718.

87. Steel, W. H.; Beildeck, C. L.; Walker, R. A., Solvent polarity across strongly associating interfaces. *J Phys Chem B* **2004,** *108* (41), 16107-16116.

88. Cave, R. J.; Castner, E. W., Time-dependent density functional theory investigation of the ground and excited states of coumarins 102, 152, 153, and 343. *Journal of Physical Chemistry A* **2002,** *106* (50), 12117-12123.

89. Boamah, M. D.; Ohno, P. E.; Geiger, F. M.; Eisenthal, K. B., Relative permittivity in the electrical double layer from nonlinear optics. *J Chem Phys* **2018,** *148* (22).

90. Fumagalli, L.; Esfandiar, A.; Fabregas, R.; Hu, S.; Ares, P.; Janardanan, A.; Yang, Q.; Radha, B.; Taniguchi, T.; Watanabe, K.; Gomila, G.; Novoselov, K. S.; Geim, A. K., Anomalously low dielectric constant of confined water. *Science* **2018,** *360* (6395), 1339-+.

91. Skelton, A. A.; Fenter, P.; Kubicki, J. D.; Wesolowski, D. J.; Cummings, P. T., Simulations of the Quartz(10(1)over-bar1)/Water Interface: A Comparison of Classical Force Fields, Ab Initio Molecular Dynamics, and X-ray Reflectivity Experiments. *J Phys Chem C* **2011,** *115* (5), 2076-2088.

92. Scales, P. J.; Grieser, F.; Healy, T. W.; White, L. R.; Chan, D. Y. C., Electrokinetics of the Silica Solution Interface - a Flat-Plate Streaming Potential Study. *Langmuir* **1992,** *8* (3), 965-974.

93. Horiuchi, H.; Nikolov, A.; Wasan, D. T., Calculation of the surface potential and surface charge density by measurement of the three-phase contact angle. *J Colloid Interf Sci* **2012,** *385*, 218-224.

94. Shishkin, I.; Alon, T.; Dagan, R.; Ginzburg, P., Temperature and Phase Transition Sensing in Liquids with Fluorescent Probes. *Mrs Adv* **2017,** *2* (44), 2391-2399.

95. Rick, S. W.; Haymet, A. D. J., Dielectric constant and proton order and disorder in ice Ih: Monte Carlo computer simulations. *J Chem Phys* **2003,** *118* (20), 9291-9296.

96. Johari, G. P.; Whalley, E., The Dielectric-Properties of Ice Ih in the Range 272-133-K. *J Chem Phys* **1981,** *75* (3), 1333-1340.

97. Eftekhari-Bafrooei, A.; Borguet, E., Effect of Electric Fields on the Ultrafast Vibrational Relaxation of Water at a Charged Solid-Liquid Interface as Probed by Vibrational Sum Frequency Generation. *J Phys Chem Lett* **2011,** *2* (12), 1353-1358.

98.   Reymond, F.; Fermin, D.; Lee, H. J.; Girault, H. H., Electrochemistry at liquid/liquid interfaces: methodology and potential applications. *Electrochim Acta* **2000,** *45* (15-16), 2647-2662.

99.   Zhang, X. Y.; Walker, R. A., Discrete partitioning of solvent permittivity at liquid-solid interfaces. *Langmuir* **2001,** *17* (15), 4486-4489.

100.   Berne, B. J.; Fourkas, J. T.; Walker, R. A.; Weeks, J. D., Nitriles at Silica Interfaces Resemble Supported Lipid Bilayers. *Accounts Chem Res* **2016,** *49* (9), 1605-1613.

101.   Leung, K.; Nielsen, I. M. B.; Criscenti, L. J., Elucidating the Bimodal Acid-Base Behavior of the Water-Silica Interface from First Principles. *Journal of the American Chemical Society* **2009,** *131* (51), 18358-18365.

102.   Dalstein, L.; Potapova, E.; Tyrode, E., The elusive silica/water interface: isolated silanols under water as revealed by vibrational sum frequency spectroscopy. *Phys Chem Chem Phys* **2017,** *19* (16), 10343-10349.

103.   Isaienko, O.; Borguet, E., Hydrophobicity of Hydroxylated Amorphous Fused Silica Surfaces. *Langmuir* **2013,** *29* (25), 7885-7895.

104.   Brindza, M. R.; Walker, R. A., Differentiating Solvation Mechanisms at Polar Solid/Liquid Interfaces. *J Am Chem Soc* **2009,** *131* (17), 6207-6214.

105.   Shin, S.; Willard, A. P., Water's Interfacial Hydrogen Bonding Structure Reveals the Effective Strength of Surface-Water Interactions. *Journal of Physical Chemistry B* **2018,** *122* (26), 6781-6789.

106.   Zaera, F., Probing Liquid/Solid Interfaces at the Molecular Level. *Chem Rev* **2012,** *112* (5), 2920-2986.

107.   Sohrabpour, Z.; Kearns, P. M.; Massari, A. M., Vibrational Sum Frequency Generation Spectroscopy of Fullerene at Dielectric Interfaces. *J Phys Chem C* **2016,** *120* (3), 1666-1672.

108.   Purnell, G. E.; Walker, R. A., Hindered Isomerization at the Silica/Aqueous Interface: Surface Polarity or Restricted Solvation? *Langmuir* **2018,** *34* (34), 9946-9949.

109.   Milischuk, A. A.; Ladanyi, B. M., Structure and dynamics of water confined in silica nanopores. *J Chem Phys* **2011,** *135* (17).

110.   Warne, M. R.; Allan, N. L.; Cosgrove, T., Computer simulation of water molecules at kaolinite and silica surfaces. *Phys Chem Chem Phys* **2000,** *2* (16), 3663-3668.

111.   Bloembergen, N., 2nd Harmonic Reflected Light. *Opt Acta* **1966,** *13* (4), 311-+.

112.   Eisenthal, K. B., Second harmonic spectroscopy of aqueous nano- and microparticle interfaces. *Chem Rev* **2006,** *106* (4), 1462-1477.

113.   Heinz, T. F.; Chen, C. K.; Ricard, D.; Shen, Y. R., Spectroscopy of Molecular Monolayers by Resonant 2nd-Harmonic Generation. *Phys Rev Lett* **1982,** *48* (7), 478-481.

114.   Ohno, P. E.; Wang, H. F.; Geiger, F. M., Second-order spectral lineshapes from charged interfaces. *Nat Commun* **2017,** *8*.

115.   Ohno, P. E.; Saslow, S. A.; Wang, H. F.; Geiger, F. M.; Eisenthal, K. B., Phase-referenced nonlinear spectroscopy of the alpha-quartz/water interface. *Nat Commun* **2016,** *7*.

116.   Lowe, B. M.; Skylaris, C. K.; Green, N. G.; Shibuta, Y.; Sakata, T., Calculation of surface potentials at the silica-water interface using molecular dynamics: Challenges and opportunities. *Jpn J Appl Phys* **2018,** *57* (4).

117.   Aragones, J. L.; MacDowell, L. G.; Vega, C., Dielectric Constant of Ices and Water: A Lesson about Water Interactions. *Journal of Physical Chemistry A* **2011,** *115* (23), 5745-5758.

118.   Bouhadja, M.; Skelton, A. A., Dynamical Properties of Water and Ions at the Quartz (101)-Water Interface at a Range of Solution Conditions: A Classical Molecular Dynamics Study. *J Phys Chem C* **2018,** *122* (3), 1535-1546.

119.   Horng, P.; Brindza, M. R.; Walker, R. A.; Fourkas, J. T., Behavior of Organic Liquids at Bare and Modified Silica Interfaces. *J Phys Chem C* **2010,** *114* (1), 394-402.

120.   Wang, H. F.; Borguet, E.; Eisenthal, K. B., Generalized interface polarity scale based on second harmonic spectroscopy. *J Phys Chem B* **1998,** *102* (25), 4927-4932.

121.   Benjamin, I., Inhomogeneous broadening of electronic spectra at liquid interfaces. *Chem Phys Lett* **2011,** *515* (1-3), 56-61.

122.   Tyrode, E.; Liljeblad, J. F. D., Water Structure Next to Ordered and Disordered Hydrophobic Silane Monolayers: A Vibrational Sum Frequency Spectroscopy Study. *J Phys Chem C* **2013,** *117* (4), 1780-1790.

123.   Lee, S. H.; Rossky, P. J., A Comparison of the Structure and Dynamics of Liquid Water at Hydrophobic and Hydrophilic Surfaces - a Molecular-Dynamics Simulation Study. *J Chem Phys* **1994,** *100* (4), 3334-3345.

124.   del Junco, C.; Vaikuntanathan, S., Interface height fluctuations and surface tension of driven liquids with time-dependent dynamics. *J Chem Phys* **2019,** *150* (9).

125.   Liu, J. C.; Li, X.; Hou, J.; Li, X.; Lu, Z., The Influence of Sodium Iodide Salt on the Interfacial Properties of Aqueous Methanol Solution by a Combined Molecular Simulation and Sum Frequency Generation Vibrational Spectroscopy Study. *Langmuir* **2019,** *35* (21), 7050-7059.

126.   Shibaev, V.; Bobrovsky, A.; Boiko, N., Photoactive liquid crystalline polymer systems with light-controllable structure and optical properties. *Prog Polym Sci* **2003,** *28* (5), 729-836.

127.   Shen, X. Y.; Wang, Y. J.; Zhao, E. G.; Yuan, W. Z.; Liu, Y.; Lu, P.; Qin, A. J.; Ma, Y. G.; Sun, J. Z.; Tang, B. Z., Effects of Substitution with Donor-Acceptor Groups on the Properties of Tetraphenylethene Trimer: Aggregation-Induced Emission, Solvatochromism, and Mechanochromism. *J Phys Chem C* **2013,** *117* (14), 7334-7347.

128.   Velema, W. A.; Szymanski, W.; Feringa, B. L., Photopharmacology: Beyond Proof of Principle. *J Am Chem Soc* **2014,** *136* (6), 2178-2191.

129.   Charpentier, T.; Kroll, P.; Mauri, F., First-Principles Nuclear Magnetic Resonance Structural Analysis of Vitreous Silica. *J Phys Chem C* **2009,** *113* (18), 7917-7929.

130.   Snyder, L. R.; Ward, J. W., Surface Structure of Porous Silicas. *J Phys Chem-Us* **1966,** *70* (12), 3941-&.

131.   Mcdonald, R. S., Surface Functionality of Amorphous Silica by Infrared Spectroscopy. *J Phys Chem-Us* **1958,** *62* (10), 1168-1178.

132.   Darlington, A. M.; Jarisz, T. A.; DeWalt-Kerian, E. L.; Roy, S.; Kim, S.; Azam, M. S.; Hore, D. K.; Gibbs, J. M., Separating the pH-Dependent Behavior of Water in the Stern and Diffuse Layers with Varying Salt Concentration. *J Phys Chem C* **2017,** *121* (37), 20229-20241.

133.   Purnell, G. E.; Walker, R. A., Surface solvation and hindered isomerization at the water/silica interface explored with second harmonic generation. *The Journal of Chemical Physics* **2019,** *150* (19), 194701.

134.   Lippert, E., Lüder, W., Boos, H., Fluoreszenzspektrum und Frank-Condon-Prinzip in Lösungen aroma-tischer Verbindungen. In *Advances in Molecular Spectroscopy*, Mangini, A., Ed. Pergamon Press: Oxford, 1962; Vol. 1, pp 442-456.

135.   Zachariasse, K. A.; Vonderhaar, T.; Hebecker, A.; Leinhos, U.; Kuhnle, W., Intramolecular Charge-Transfer in Aminobenzonitriles - Requirements for Dual Fluorescence. *Pure Appl Chem* **1993,** *65* (8), 1745-1750.

136.   Schuddeboom, W.; Jonker, S. A.; Warman, J. M.; Leinhos, U.; Kuhnle, W.; Zachariasse, K. A., Excited-State Dipole-Moments of Dual Fluorescent 4-(Dialkylamino)Benzonitriles - Influence of Alkyl Chain-Length and Effective Solvent Polarity. *J Phys Chem-Us* **1992,** *96* (26), 10809-10819.

137.   Rettig, W., Charge Separation in Excited-States of Decoupled Systems - Tict Compounds and Implications Regarding the Development of New Laser-Dyes and the Primary Processes of Vision and Photosynthesis. *Angew Chem Int Edit* **1986,** *25* (11), 971-988.

138.   Grabowski, Z. R.; Dobkowski, J., Twisted Intramolecular Charge-Transfer (Tict) Excited-States - Energy and Molecular-Structure. *Pure Appl Chem* **1983,** *55* (2), 245-252.

139.   Bajzer, E.; Moncrieffe, M. C.; Penzar, I.; Prendergast, F. G., Complex homogeneous and heterogeneous fluorescence anisotropy decays: Enhancing analysis accuracy. *Biophys J* **2001,** *81* (3), 1765-1775.

140.   Ridley, J.; Zerner, M., Intermediate Neglect of Differential Overlap Technique for Spectroscopy - Pyrrole and Azines. *Theor Chim Acta* **1973,** *32* (2), 111-134.

141.   Theiste, D.; Callis, P. R.; Woody, R. W., Effects of the Crystal-Field on Transition Moments in 9-Ethylguanine. *J Am Chem Soc* **1991,** *113* (9), 3260-3267.

142.   Sreerama, N.; Woody, R. W.; Callis, P. R., Theoretical-Study of the Crystal-Field Effects on the Transition Dipole-Moments in Methylated Adenines. *J Phys Chem-Us* **1994,** *98* (41), 10397-10407.

143.   Biesso, A.; Xu, J. H.; Muino, P. L.; Callis, P. R.; Knutson, J. R., Charge Invariant Protein-Water Relaxation in GB1 via Ultrafast Tryptophan Fluorescence. *J Am Chem Soc* **2014,** *136* (7), 2739-2747.

144.   Liu, T. Q.; Callis, P. R.; Hesp, B. H.; de Groot, M.; Buma, W. J.; Broos, J., Ionization potentials of fluoroindoles and the origin of nonexponential tryptophan fluorescence decay in proteins. *J Am Chem Soc* **2005,** *127* (11), 4104-4113.

145.   M. J. Frisch, G. W. T., H. B. Schlegel, G. E. Scuseria, M. A. Robb, J. R. Cheeseman, G. Scalmani, V. Barone, G. A. Petersson, H. Nakatsuji, X. Li, M. Caricato, A. Marenich, J. Bloino, B. G. Janesko, R. Gomperts, B. Mennucci, H. P. Hratchian, J. V. Ortiz, A. F. Izmaylov, J. L. Sonnenberg, D. Williams-Young, F. Ding, F. Lipparini, F. Egidi, J. Goings, B. Peng, A. Petrone, T. Henderson, D. Ranasinghe, V. G. Zakrzewski, J. Gao, N. Rega, G. Zheng, W. Liang, M. Hada, M. Ehara, K. Toyota, R. Fukuda, J. Hasegawa, M. Ishida, T. Nakajima, Y. Honda, O. Kitao, H. Nakai, T. Vreven, K. Throssell, J. A. Montgomery, Jr., J. E. Peralta, F. Ogliaro, M. Bearpark, J. J. Heyd, E. Brothers, K. N. Kudin, V. N. Staroverov, T. Keith, R. Kobayashi, J. Normand, K. Raghavachari, A. Rendell, J. C. Burant, S. S. Iyengar, J. Tomasi, M. Cossi, J. M. Millam, M. Klene, C. Adamo, R. Cammi, J. W. Ochterski, R. L. Martin, K. Morokuma, O.

Farkas, J. B. Foresman, and D. J. Fox *Gaussian 09, Revision A.02*, Wallingford CT, 2016.

146.   Hoffmann, K.; Marlow, F.; Caro, J.; Dähne, S., Modification of fluorescence of p-N,N-dimethylaminobenzonitrile by adsorption in molecular sieves. *Zeolites* **1996,** *16* (2), 138-141.

147.   Rettig, W.; Wermuth, G.; Lippert, E., Photophysical Primary Processes in Solutions of P-Substituted Dialkylanilines. *Ber Bunsen Phys Chem* **1979,** *83* (7), 692-697.

148.   Galievsky, V. A.; Zachariasse, K. A., Intramolecular charge transfer with N,N-Dialkyl-4-(trifluoromethyl)anilines and 4-(dimethylamino)benzonitrile in polar solvents. Investigation of the excitation wavelength dependence of the reaction pathway. *Acta Phys Pol A* **2007,** *112,* S39-S56.

149.   Tyrode, E.; Liljeblad, J. F. D., Water Structure Next to Ordered and Disordered Hydrophobic Silane Monolayers: A Vibrational Sum Frequency Spectroscopy Study. *The Journal of Physical Chemistry C* **2013,** *117* (4), 1780-1790.

150.   Heinz, T. F., Second-Order Nonlinear Optical Effects at Surfaces and Interfaces. In *Nonlinear Surface Electromagnetic Phenomena*, Ponath, H.-E.; Stegeman, G. I., Eds. Elsevier Science Publishers: 1991.

151.   Higgins, D. A.; Byerly, S. K.; Abrams, M. B.; Corn, R. M., 2nd Harmonic-Generation Studies of Methylene-Blue Orientation at Silica Surfaces. *J Phys Chem-Us* **1991,** *95* (18), 6984-6990.

152.   Baumann, W.; Bischof, H.; Frohling, J. C.; Brittinger, C.; Rettig, W.; Rotkiewicz, K., Considerations on the Dipole-Moment of Molecules Forming the Twisted Intramolecular Charge-Transfer State. *J Photoch Photobio A* **1992,** *64* (1), 49-72.

153.   Bhalekar, S.; Avhad, K.; Sekar, N., Synthesis, photophysical, viscosity and DFT study of solid state fluorescent molecular rotors. *Journal of Photochemistry and Photobiology A: Chemistry* **2019,** *371*, 223-237.

154.   Moran, A. M.; Delbecque, C.; Kelley, A. M., Solvent effects on ground and excited electronic state structures of the push-pull chromophore julolidinyl-n-N,N '-diethylthiobarbituric acid. *J Phys Chem A* **2001,** *105* (45), 10208-10219.

155.   Erande, Y.; Kothavale, S.; Sreenath, M. C.; Chitrambalam, S.; Joe, I. H.; Sekar, N., NLOphoric multichromophoric auxiliary methoxy aided triphenylamine D-pi-A chromophores - Spectroscopic and computational studies. *Opt Mater* **2017,** *73*, 602-616.

156.   Singappuli-Arachchige, D.; Manzano, J. S.; Sherman, L. M.; Slowing, I. I., Polarity Control at Interfaces: Quantifying Pseudo-solvent Effects in Nano-confined Systems. *Chemphyschem* **2016,** *17* (19), 2982-2986.

157.   Druzhinin, S. I.; Mayer, P.; Stalke, D.; von Bulow, R.; Noltemeyer, M.; Zachariasse, K. A., Intramolecular Charge Transfer with 1-tert-Butyl-6-cyano-1,2,3,4-tetrahydroquinoline (NTC6) and Other Aminobenzonitriles. A Comparison of Experimental Vapor Phase Spectra and Crystal Structures with Calculations. *J Am Chem Soc* **2010,** *132* (22), 7730-7744.

158.   Aragones, J. L.; MacDowell, L. G.; Vega, C., Dielectric Constant of Ices and Water: A Lesson about Water Interactions. *The Journal of Physical Chemistry A* **2011,** *115* (23), 5745-5758.

159.   Whalley, E.; Heath, J. B. R.; Davidson, D. W., Ice 9 - an Antiferroelectric Phase Related to Ice 3. *J Chem Phys* **1968,** *48* (5), 2362-&.

160.   Johari, G. P.; Lavergne, A.; Whalley, E., Dielectric Properties of Ice Vii and Viii and Phase Boundary between Ice Vi and Vii. *J Chem Phys* **1974,** *61* (10), 4292-4300.

161.   Catalan, J., Can the dipolarity of the medium induce the formation of charge transfer structures? An unexpected finding in the photophysics of DMABN. *Phys Chem Chem Phys* **2014,** *16* (17), 7734-7740.

162.   Di Giacomo, F., A Short Account of RRKM Theory of Unimolecular Reactions and of Marcus Theory of Electron Transfer in a Historical Perspective. *J Chem Educ* **2015,** *92* (3), 476-481.

163.   Wardlaw, D. M.; Marcus, R. A., Rrkm Reaction-Rate Theory for Transition-States of Any Looseness. *Chem Phys Lett* **1984,** *110* (3), 230-234.

164.   Shaikh, M.; Mohanty, J.; Singh, P. K.; Bhasikuttan, A. C.; Rajule, R. N.; Satam, V. S.; Bendre, S. R.; Kanetkar, V. R.; Pal, H., Contrasting Solvent Polarity Effect on the Photophysical Properties of Two Newly Synthesized Aminostyryl Dyes in the Lower and in the Higher Solvent Polarity Regions. *J Phys Chem A* **2010,** *114* (13), 4507-4519.

165.   Bates, J. S.; Gounder, R., Influence of confining environment polarity on ethanol dehydration catalysis by Lewis acid zeolites. *J Catal* **2018,** *365*, 213-226.

166.   Otolski, C. J.; Raj, A. M.; Sharma, G.; Prabhakar, R.; Ramamurthy, V.; Elles, C. G., Ultrafast trans -> cis Photoisomerization Dynamics of Alkyl-Substituted Stilbenes in a Supramolecular Capsule. *J Phys Chem A* **2019,** *123* (24), 5061-5071.

167.   Otolski, C. J.; Raj, A. M.; Ramamurthy, V.; Elles, C. G., Ultrafast Dynamics of Encapsulated Molecules Reveals New Insight on the Photoisomerization Mechanism for Azobenzenes. *J Phys Chem Lett* **2019,** *10* (1), 121-127.

144

168.	Douhal, A.; Sanz, M.; Tormo, L., Femtochemistry of orange II in solution and in chemical and biological nanocavities. *P Natl Acad Sci USA* **2005,** *102* (52), 18807-18812.

169.	Jones, G.; Jackson, W. R.; Kanoktanaporn, S.; Halpern, A. M., Solvent Effects on Photophysical Parameters for Coumarin Laser-Dyes. *Opt Commun* **1980,** *33* (3), 315-320.

170.	Nad, S.; Pal, H., Unusual photophysical properties of coumarin-151. *J Phys Chem A* **2001,** *105* (7), 1097-1106.

171.	Purnell, G. E.; Walker, R. A., Surface solvation and hindered isomerization at the water/silica interface explored with second harmonic generation. *J Chem Phys* **2019,** *150* (19).

172.	Onabuta, Y.; Kunimoto, M.; Nakai, H.; Homma, T., First-principle study of the oxidation mechanism of formaldehyde and hypophosphite for copper and nickel electroless deposition process. *Electrochim Acta* **2019,** *307*, 536-542.

173.	Sievers, C.; Noda, Y.; Qi, L.; Albuquerque, E. M.; Rioux, R. M.; Scott, S. L., Phenomena Affecting Catalytic Reactions at Solid-Liquid Interfaces. *Acs Catal* **2016,** *6* (12), 8286-8307.

174.	Okuno, Y.; Ushirogata, K.; Sodeyama, K.; Tateyama, Y., Decomposition of the fluoroethylene carbonate additive and the glue effect of lithium fluoride products for the solid electrolyte interphase: an ab initio study. *Phys Chem Chem Phys* **2016,** *18* (12), 8643-8653.

175.	Snare, M. J.; Treloar, F. E.; Ghiggino, K. P.; Thistlethwaite, P. J., The Photophysics of Rhodamine-B. *J Photochem* **1982,** *18* (4), 335-346.